

Novel Framework for Nonlinear HRV Analysis and its Physiological Interpretation



Universidad Zaragoza



Instituto Universitario de Investigación
de Ingeniería de Aragón
Universidad Zaragoza

Juan R. Bolea Bolea

Advisor: Dr. Raquel Bailón Luesma

Dr. Esther Pueyo Paules

Biomedical Signal Interpretation and
Computational Simulation (BSICoS) Group
Instituto de Investigación en Ingeniería de Aragón (I3A)
University of Zaragoza

Dissertation submitted for the degree of
Doctor of Philosophy on Biomedical Engineering

University of Zaragoza

April 2018

A mi familia

A Eva

Acknowledgements

This PhD thesis entitled "Novel framework for nonlinear HRV analysis and its physiological interpretation" has been developed in the frame of the following scientific projects:

- "Investigación computacional de arritmias cardíacas y efecto de fármacos: de los canales iónicos al electrocardiograma de superficie" (TEC2010-191410, Ministerio de Ciencia e Innovación, Gobierno de España)
- "Procesado multimodal de señales biomédicas para el análisis y la caracterización fisiológica de afecciones cardiovasculares, respiratorias y autonómicas" (TEC2010-21703-C03-02, Ministerio de Ciencia e Innovación, Gobierno de España)
- "Predicción de la hipotensión del bloqueo espinal de las cesáreas mediante análisis de la actividad del sistema nervioso autónomo, y efectos de la profilaxis farmacológica de la hipotensión sobre el bienestar fetal. (PI10/02851, Instituto de Salud Carlos III, FIS)
- "Procesado de señales guiado por la fisiología para la estratificación del riesgo cardiovascular y guiado de la terapia: herramientas para mejorar la toma de decisiones" (TEC2013-42140-R, Ministerio de Economía y Competitividad, Gobierno de España)
- "El sistema nervioso autónomo como modulador de la función cardíaca: investigación integral mediante procesado de señal y modelado computacional" (TIN2013-41998-R, Ministerio de economía y competitividad, Gobierno de España; Fondos FEDER)
- "Evaluación no invasiva del sistema nervioso autónomo mediante análisis de la variabilidad de bioseñales. Aplicación a situaciones clínicas relacionadas con el estrés" (TIN2014-53567-R, Ministerio de economía y competitividad, Gobierno de España; Fondos FEDER)
- Biomedical Signal Interpretation and Computational Simulation (BSICoS) Group (Grupo consolidado T96, Gobierno de Aragón)

I would like to mention the HERMES high computational cluster from the Instituto de Investigación en Ingeniería de Aragón (I3A), Universidad de Zaragoza. It has been a privilege for me to have HERMES available that allowed parallel computing reducing significantly the computational cost of analysis.

Special thanks to my supervisors Dr. Raquel Bailón and Dr. Esther Pueyo for your support, it was essential to carry this thesis out. I am very proud of being guided by two brilliant and passionate scientists.

My acknowledgments to Dr. Pablo Laguna, Dr. Juan Pablo Martínez, and Dr. Eduardo Gil. To Arantxa Trigo, I will never forget your support, thank you very much. It is a pleasure to work with all of you. Lab-mates, Ana Mincholé, Michele Orini, Violeta Monasterio, Mariano Llamedo, Daniel Romero, Maikel Noriega, Carlos Sánchez, José Vicente (Pepo), Alejandro Alcaine, David Sampedro, Maite Valderas, without you these years would have been totally different. We have tried to fix the world problems as many times as I cannot remember. Thank you for the huge amount of good moments we shared. You have been more than lab-mates, you have become friends. I know that this is a long list but each of you deserve to be mentioned because you were part of my life. Fer, Rute and Sonia, thank you very much to be always unconditionally there even in the distance.

The BSICoS "new generation", they have already demonstrated their scientific potential. Jesús Lázaro, Julia Ramírez, David Hernando, Alba Martín, Javier Milagro, Spyros Kontaxis thank you, I have learnt many things from you.

Thanks to Augusto Navarro, Eva Rovira and Jose María Remartínez from Miguel Servet Hospital Anesthesiology division team. From the beginning I saw your will to investigate with us and the path we took led successfully to this thesis. Thank you very much for your availability, patience and for the scientific discussions that were very productive.

Gracie mile to Riccardo Barbieri and the lab-mates of Italy: Luca, Eros, Federica, Pier, Stefania... I would point out your kindness when I was there. Although you were in the third floor, there is no doubt that you are the engine of the fourth floor.

Quiero agradecer a aquellas personas que han servido de inspiración para mi en este camino, en especial a David Izquierdo e Israel Guío. A mis amig@s del grupo de los telecos, gracias por saber estar ahí.

A mis amigos de Calanda: Ruben, Fran, Almu, Jenny, Juanjo, Marcos. Sin ninguna duda hay gente que te cambia la vida como Glory. Su apoyo incondicional e infinito junto con el del Dr Ro ha sido muy gratificante todo este tiempo. Una parte muy importante de esta tesis es vuestra. Muchas gracias por estar siempre ahí. A Chema, bro, eres muy grande.

A mi familia. Ma, Pa! ¡ya está! Cuánta paciencia, cuánta comprensión y cuánto apoyo. Esto va por vosotros, gracias por haber confiado en mí en los peores momentos. Estoy muy orgulloso de todos y cada uno de vosotros, por lo que hemos vivido, por cómo hemos superado y superaremos cada prueba que la vida nos ponga. Papás, tatas, cuñados, sobrinos os tengo en mi pensamiento todos los días, aunque no haya podido compartir más tiempo con vosotros. He sentido vuestro apoyo y eso me ha llevado hasta aquí. Os quiero.

A mi cielo y estrellas, Eva. Gracias por ser cómo eres, por tu amor, por la paciencia en momentos de desesperación, por tu comprensión, por otras tantas cosas que las palabras se quedan cortas.

Abstract

Nonlinear methods applied to heart rate variability (HRV) signals have been reported to provide new insights to characterize abnormalities occurring in the context of cardiac conditions or pathologies like congestive heart failure or atrial fibrillation, to name a few. Also, alterations in the Autonomic Nervous System (ANS), which modulates heart rate, have been shown to lead to changes in nonlinear HRV patterns. Nonetheless, the still unclear mechanisms underlying physiological or pathophysiological variations in nonlinear HRV indices, in combination with the time-consuming algorithms required to estimate these indices, represent bottlenecks for their application in clinical practice.

Following an introduction to the topics of the thesis, which is covered in chapter 1, the second chapter, chapter 2, is devoted to the first major contribution of this thesis, which consists of the proposal and development of a methodology to reliably estimate a nonlinear HRV index, namely correlation dimension, while notably reducing the computational cost associated with its computation. The proposed framework is shown to be highly effective in reducing the time for calculation of short-term nonlinear HRV analysis to just a few seconds.

With regards to interpretation of nonlinear HRV analysis, it is important to note that there are a number of factors that affect its calculation and should be taken into account when comparing different studies from the literature. Characteristics of HRV time series like sampling rate as well as selection of parameter values in nonlinear methods all have an impact on nonlinear HRV results and could under some circumstances lead to misleading interpretations. A major objective of chapter 3 is to study the influence of sampling rate on nonlinear HRV indices and to propose methods to attenuate this influence. The proposed methods include, on the one hand, heart rate-correction of HRV estimates by individual- or population-based regression formulas and, on the other hand, pre-processing of HRV time series by interpolation or point-process models.

Chapter 4 focuses on investigating the effect of parameter value selection as required for calculation of certain nonlinear HRV indices (e.g. approximate entropy) and proposes a novel index independent of *a-priori* parameter value definition. This novel index is called multidimensional approximate entropy. Nonlinear HRV analysis, including the novel proposed index, is applied to the study of conditions associated with alterations in cardiac ANS modulation, like aging and congestive heart failure (CHF). All evaluated nonlinear HRV indices are found to be significantly decreased in elderly subjects with respect to young ones under resting supine conditions. Additionally, congestive heart failure patients are shown to have statistically significantly larger values of the evaluated nonlinear indices as compared to healthy subjects, in all cases analyzing the night period. Also, nonlinear HRV analysis is assessed in response to sympathetic provocations, as induced by changing from supine to standing position or by atropine administration, where a decrease in all estimated nonlinear indices is observed.

Chapter 5 is devoted to assess the performance of nonlinear HRV analysis in the triage of prophylaxis administration to prevent hypotensive episodes caused by spinal anesthesia during cesarean delivery. The study is conducted in collaboration with the Anesthesia Department of Hospital Universitario Miguel Servet (Zaragoza, Spain). Since prophylaxis may produce side effects on the fetus, the challenge is to predict normotensive outcomes for which prophylaxis could be disregarded. The hypothesis in this thesis is based on the fact that altered ANS regulation caused by the last period of pregnancy and the proximity to surgery could be reflected on nonlinear HRV indices and this could help to predict hypotensive vs normotensive outcomes with higher accuracy than when using demographic variables only. Importantly, the methodological knowhow on nonlinear HRV analysis developed in the thesis is applied to characterize other cardiovascular signals, like the pulse photoplethysmographic signal. Time series derived from this signal, including peripheral vascular information, are incorporated into a logistic regression-based classifier together with nonlinear HRV indices. The proposed classifier reaches 76.5 % sensitivity and 72.2 % accuracy in detecting normotensive outcomes, thus providing relevant objective information to support clinicians' decisions.

In Chapter 6 the main conclusions derived from the thesis are presented and future extensions of the conducted investigations are considered. Emphasis is made on the contribution of the thesis to the development of novel methodologies to more robustly characterize nonlinear HRV indices and reliably interpret corresponding results. Based on the developed methodologies, conditions or pathologies associated with altered cardiac ANS modulation are investigated and the contribution of nonlinear HRV analysis for their characterization is highlighted.

In summary, methodological objectives of this thesis include: i) proposal of a novel framework to improve reliability of correlation dimension estimation by using an algorithm with reduced computational load that facilitates its applicability in clinical practice; ii) development of alternative methods to attenuate the dependency of nonlinear heart rate variability (HRV) indices on mean heart rate (HR); iii) proposal of a novel multidimensional nonlinear HRV index independent of *a priori* parameter definition for its computation. In addition, objectives related to clinical application of the methodological contributions are: i) characterization of the effect of aging on nonlinear HRV; ii) assessment of complexity and irregularity of heart rate in congestive heart failure (CHF) patients as compared to healthy subjects; iii) improvement in the efficacy of prophylaxis administration for the prevention of hypotensive events after spinal anesthesia during programmed cesarean delivery.

Resumen y Conclusiones

La inclusión de métodos no lineales aplicados a señales de variabilidad del ritmo cardíaco (HRV, del inglés Heart Rate Variability) proporciona una nueva visión en la caracterización de anomalías en el contexto de las enfermedades cardíacas o patologías como la insuficiencia cardíaca o la fibrilación auricular, por nombrar algunas. Se ha demostrado que alteraciones en el sistema nervioso autónomo (ANS, del inglés Autonomic Nervous System), el cuál modula el ritmo cardíaco, conllevan a cambios en los patrones no lineales de la HRV. Sin embargo, la incertidumbre, todavía presente, en los mecanismos que subyacen a variaciones fisiológicas o patofisiológicas en los índices no lineales de la HRV, junto con el alto tiempo que requieren los algoritmos para la estimación de estos índices, representan el cuello de botella para su aplicación en la práctica clínica.

Después de una breve introducción sobre los temas abordados en esta tesis en el capítulo 1, el segundo capítulo, el capítulo 2, está dedicado a la primera gran contribución de esta tesis, que consiste en la propuesta y desarrollo de una metodología con el fin de reducir el coste computacional asociado a la caracterización no lineal de la HRV. El esquema propuesto es muy eficaz, reduciendo el tiempo de cálculo a unos pocos segundos para el análisis no lineal de señales de HRV de corta longitud (5 minutos).

Con respecto a la interpretación del análisis no lineal de la HRV, es importante señalar que hay una serie de factores que afectan a su cálculo y deben tenerse en cuenta al comparar diferentes estudios de la literatura. Las características de las series de HRV, como la frecuencia de muestreo, así como la selección de valores de parámetros en los métodos no lineales, tienen un impacto en los resultados de los índices no lineales de la HRV y, en algunas circunstancias, pueden dar lugar a interpretaciones erróneas. Uno de los principales objetivos del capítulo 3 es estudiar la influencia de la tasa de muestreo en los índices no lineales de la HRV y proponer alternativas para atenuar esta influencia. Los métodos propuestos incluyen, por una parte, la corrección de la frecuencia cardíaca de las estimaciones de la HRV mediante fórmulas de regresión individuales o basadas en la población y, por otra, el preprocesamiento de las series temporales de HRV mediante modelos de interpolación o de point-process.

El capítulo 4 se centra en investigar el efecto de la selección del valor de los parámetros requeridos para el cálculo de ciertos índices no lineales de la HRV (por ejemplo, la entropía aproximada) y proponiendo un nuevo índice independiente de la definición del valor de éstos parámetros *a-priori*. Este novedoso índice se denomina entropía multidimensional aproximada. El análisis no lineal de la

HRV, incluido el nuevo índice propuesto, se aplica al estudio de afecciones asociadas a alteraciones de la modulación cardiaca del ANS, como el envejecimiento y la insuficiencia cardiaca congestiva (CHF, del inglés Congestive Heart Failure). Por un lado, todos los índices no lineales de la HRV evaluados ven disminuidos significativamente sus valores en las personas mayores en comparación con los jóvenes ambos grupos en condiciones de reposo en posición de decubito supino. Por otro lado, los pacientes con insuficiencia cardiaca muestran valores más altos de los índices no lineales significativamente con respecto al grupo de sujetos sanos, en ambos casos analizando el período nocturno. Además, el análisis no lineal de la HRV es evaluada en respuesta a provocaciones simpáticas, inducidas por el cambio de la posición supina a la posición de pie o por la administración de atropina, donde se observa una disminución en todos los índices no lineales estimados.

El capítulo 5 está dedicado a la evaluación del rendimiento del análisis no lineal de la HRV en el triaje de la administración profiláctica con el fin de prevenir los episodios de hipotensión causados por la anestesia espinal durante el parto por cesárea. El estudio se realiza en colaboración con el Servicio de Anestesia del Hospital Universitario Miguel Servet (Zaragoza, España). Debido a que la profilaxis puede producir efectos secundarios en el feto, el desafío consiste en predecir los casos normotensos para los cuales se puede prescindir del tratamiento profiláctico. La hipótesis de esta tesis se basa en el hecho de que la alteración de la regulación del ANS causada por el último período de embarazo y la proximidad a la cirugía podría reflejarse en los índices no lineales de la HRV, lo que podría ayudar a predecir los casos que deriven en hipotensión y normotensión con mayor precisión que cuando se utilizan solamente variables demográficas. Es importante destacar que las propuestas metodológicas para el análisis no lineal de la HRV desarrolladas en la tesis se aplican en la caracterización de otras señales cardiovasculares, como la señal fotopletismográfica de pulso. Las series temporales derivadas de esta señal, que incluyen información del sistema vascular periférico, se incorporan en un clasificador basado en la regresión logística junto con los índices no lineales de la HRV. El clasificador propuesto alcanza un 76,5% de sensibilidad y un 72,2% de precisión en la detección de los casos normotensos, proporcionando así información pertinente y objetiva respaldando la decisión final del equipo médico.

En el capítulo 6 se presentan las principales conclusiones derivadas de la tesis y se consideran futuras ampliaciones en base a las investigaciones llevadas a cabo. Se hace hincapié en la contribución de la tesis al desarrollo de metodologías novedosas para caracterizar de manera más robusta los índices no lineales de la HRV e interpretar con fiabilidad los resultados correspondientes. Basándose en las metodologías desarrolladas, se investigan las condiciones o patologías asociadas con alteraciones en la modulación autonómica de la actividad cardiaca y se destaca la contribución del análisis no lineal de la HRV para su caracterización.

En conclusión, entre los objetivos metodológicos desarrollados en esta tesis se encuentran: i) la propuesta de un esquema de trabajo para incrementar la fiabilidad de la estimación de la dimensión de correlación, usando un algoritmo que reduce la carga computacional, facilitando su aplicabilidad en la práctica clínica; ii) el desarrollo de métodos alternativos para atenuar la dependencia de los índices no

lineales de la HRV con el ritmo cardiaco medio; iii) la propuesta de un índice no lineal de la HRV multidimensional independiente de la definición *a priori* de parámetros para su estimación. Además, los objetivos relacionados con la aplicación clínica de las contribuciones metodológicas son: i) la caracterización del efecto del envejecimiento en los índices no lineales de la HRV; ii) la evaluación de la complejidad e irregularidad del ritmo cardiaco en pacientes que sufren de insuficiencia cardiaca comparada con sujetos sanos; iii) la mejora de la eficacia de la profilaxis para la prevención de eventos de hipotensión después de anestesia espinal durante parto programado por cesárea.

Contents

List of Figures	xi
List of Tables	xiii
List of Acronyms	xv
1 Introduction	1
1.1 Motivation	2
1.2 Autonomic Nervous System Regulation of the Heart	2
1.3 Heart Rate Variability	4
1.4 Autonomic Nervous System Assessment	7
1.4.1 Time Domain Analysis	7
1.4.2 Frequency Domain Analysis	7
1.4.3 Nonlinear Domain Analysis	8
1.5 Applications of Nonlinear HRV Analysis	13
1.5.1 Aging	13
1.5.2 Congestive Heart Failure	13
1.5.3 Hypotension during Cesarean Section	13
1.6 Objectives	14
2 Correlation Dimension Estimation	17
2.1 Correlation Dimension	18
2.1.1 Mathematical Definition	18
2.1.2 Scaling Range Assessment: Sigmoid Curve Fitting	19
2.1.3 New Approaches for D_2 Assessment	22
2.1.4 Fast Computation of Correlation Sums	26
2.2 Validation Study	27
2.2.1 Lorenz Attractor	27
2.2.2 MIX(P) Processes	28
2.3 Evaluation Study on HRV Signals	28
2.4 Results	28

2.4.1	Validation on Synthetic Time Series	28
2.4.2	HRV Time Series Results	30
2.4.3	Evaluation of the Computational Load	31
2.5	Discussion	33
2.6	Conclusion	34
3	Nonlinear HRV Measurement Dependencies	37
3.1	Introduction	38
3.2	Materials	38
3.2.1	Fantasia Database	38
3.2.2	BPC Database	39
3.2.3	Simulation Study	39
3.3	Evaluation by Nonlinear Techniques	41
3.3.1	Correlation Dimension	41
3.3.2	Approximate and Sample Entropy	42
3.4	Nonlinear Indices Dependence on HR as Sampling Rate	43
3.4.1	Regression Formulas	44
3.4.2	Interpolation	45
3.4.3	Point-process	45
3.5	Statistical Analysis	47
3.6	Results	47
3.6.1	Nonlinear HRV Indices and Mean HR Reflect Body Position induced Changes	47
3.6.2	Nonlinear HRV Indices and RR Relationship by Simulation Study	47
3.6.3	Nonlinear Analysis of BPC Database	51
3.7	Discussion	53
3.7.1	Simulated Data	53
3.7.2	Real Data	55
3.8	Conclusion	57
4	Multidimensional Approximate Entropy	59
4.1	Introduction	60
4.2	Approximate Entropy-based Indices	61
4.2.1	Multidimensional Approximate Entropy	61
4.2.2	Time- and Frequency-domain HRV Indices	62
4.3	Materials	62
4.3.1	Synthetic Signals	62
4.3.2	HRV Signals	62
4.3.3	Statistical Analysis	63
4.4	Results	63

4.4.1	Synthetic Data	63
4.4.2	HRV Data	65
4.5	Discussion	71
4.6	Conclusion	73
5	Improvement in the Prevention of Hypotensive Episodes	75
5.1	Motivation	76
5.2	Materials and Methods	77
5.2.1	Programmed Cesareas Database	77
5.2.2	Methods	78
5.3	Results	82
5.4	Discussion	88
5.5	Conclusion	91
6	Conclusions and Future Lines	93
Bibliography		103

List of Figures

1.1	Innervation of the heart by autonomic nervous system.	3
1.2	Physiological phases of the heart and electrocardiograph signal representation.	4
1.3	Electrocardiographic lead chest positions and signal.	5
1.4	HRV signal representations.	6
1.5	Example of power spectral density of a HRV signal	8
1.6	Lorenz attractor representation.	9
1.7	A simplified model of HR regulation.	10
1.8	Milestones towards the nonlinear heart rate variability assessment.	11
1.9	Usage rate of most common nonlinear methods in HRV studies.	12
2.1	<i>Log-log</i> curves for a dynamic system.	20
2.2	<i>Log-log</i> curves discarding and accepting self-comparisons.	20
2.3	Sigmoid Curve Fitting	21
2.4	Proposals for correlation dimension (D_2) estimation.	23
2.5	Correlation dimension estimate from starting points.	24
2.6	SampEn surface.	25
2.7	Effect of norm selection in D_2	30
2.8	D_2 estimation over MIX(P) signals.	30
2.9	D_2 estimation over RR time series.	31
3.1	Simulated spectra from Fantasia database.	40
3.2	Simulation data scheme for Fantasia database.	41
3.3	Dependence of approximate entropy ($ApEn$) on threshold r	43
3.4	Dependence of $ApEn$ on threshold r	43
3.5	Representation of local log likelihood estimation in point-process paradigm.	46
3.6	HR-corrected nonlinear HRV indices for supine and standing.	48
3.7	Nonlinear HRV indices computed from simulation study varying mean heart period.	49
3.8	Nonlinear HRV indices computed from simulation study varying mean heart period.	50
3.9	Nonlinear HRV indices computed from synthetic point-process time series varying mean heart period.	51
3.10	Example of time-varying HRV series extracted from point-process.	53

3.11 Comparison of interpolation and point-process approach in temporal and nonlinear indices.	54
4.1 Nonlinear indices evaluated over $\text{MIX}(P)$, pink and white time series.	64
4.2 $\text{MApEn}(0.2)$ and MApEn_{max} evaluated on $\text{MIX}(P)$ processes, white, and pink noises.	65
4.3 $\text{ApEn}(2, r)$ and $\text{ApEn}(6, r)$ computed over $\text{MIX}(P)$ processes.	66
4.4 ApEn computed throughout embedding dimensions and $\text{MApEn}(r)$ for pink noise (blue) and white noise (red) using different thresholds.	66
4.5 Regularity and complexity indices comparing young vs. elderly, and healthy subjects vs. CHF patients.	67
4.6 $\text{MApEn}(0.2)$ and MApEn_{max} values computed for young, elderly, CHF, and healthy subjects.	67
4.7 ApEn values computed for thresholds set at 0.2 and $r_{max}(m)$ through embedding dimensions in young vs. elderly and healthy vs. CHF patients.	68
4.8 Regularity and complexity indices comparing healthy subjects vs. CHF patients restricted to an age range of 50 to 75 years old and healthy vs. CHF patients classified III-IV.	69
4.9 MApEn_{max} values computed for young, elderly, CHF, and healthy subjects in 4000-sample time series.	70
4.10 Time domain index values for young vs. elderly during awake and CHF patients vs. healthy subjects during the night period.	70
4.11 Frequency domain indices computed comparing young vs. elderly, and CHF patients vs. healthy subjects.	71
5.1 Cross-validation scheme combining leave-one-out with bootstrapping.	81
5.2 Time series of interest for predicting hypotension.	82
5.3 Correlation between nonlinear indices computed over RR and pulse rate (PR) time series.	84
5.4 $\text{ApEn}(m, r_{max}(m))$ vs. m and $\text{MApEn}_{max}^{PR(SD-LD)}$ computed on PR time series during lateral decubitus and supine decubitus.	84
5.5 Box-plots of features that reached best classification performance.	87

List of Tables

2.1	Correlation dimension estimation for attractors.	29
2.2	D_2 estimation for Lorenz attractor series and HRV signals.	32
2.3	ROC area for correlation dimension.	32
2.4	Computational load of correlation sums estimated varying sample length.	32
2.5	Computational load for correlation dimension estimates by all proposed approaches.	32
3.1	Correlation study of uncorrected and HR-corrected nonlinear HRV indices on mean HR.	49
3.2	Uncorrected and HR-corrected nonlinear HRV indices evaluated in the body position change (BPC) database.	52
5.1	Parturient characteristic data.	78
5.2	Relation of features for the lateral decubitus (LD)-supine decubitus (SD) cohort.	83
5.3	Classification results comparing classifiers.	85
5.4	Classification performance results for the three considered cohorts.	86
5.5	Logistic regression parameters for the different cohorts.	86

List of Acronyms

ANS	autonomic nervous system	1
ApEn	approximate entropy	xi
ARMA	autoregressive moving average	40
AUC	area under curve	90
AV	atrio-ventricular	2
BMI	body mass index	90
BP	blood pressure	88
BPC	body position change	xiii
BPM	beats per minute	6
CHF	congestive heart failure	ii
CVD	cardiovascular disease	
D₂	correlation dimension	xi
ECG	electrocardiogram	5
HF	high frequency	7
HR	heart rate	ii
HRM	heart rate mean	7
HRV	heart rate variability	ii
ICC	intraclass correlation coefficient	47
IPFM	integral pulse frequency modulation	6
LD	lateral decubitus	xiii
LF	low frequency	7
LF/HF	sympathovagal ratio	7
MO	matrix operations	26
MSE	Multiscale entropy	60

NNT	number needed to treat	76
PAT	pulse arrival time.....	76
PEP	pre-ejection period.....	78
PP	pulse-to-pulse	78
PPG	pulse photoplethysmographic signal.....	76
PR	pulse rate	xii
PRV	pulse rate variability.....	76
PTT	pulse transit time.....	76
RMSSD	the square root of the mean squared differences of successive normal heartbeat intervals	7
ROC	receiver operating characteristic	31
RP	respiration.....	39
RSA	respiratory sinus arrhythmia	88
<i>SampEn</i>	sample entropy	10
SCF	Sigmoid curve fitting	20
SA	sino-atrial	2
SD	supine decubitus	xiii
SDNN	standard deviation of consecutive normal beats	7
SP	sitting position	77

“The heart has reasons which reason does not know.”

- Blaise Pascal (1623-1662) -

1

Introduction

Summary

In this chapter, the motivation for the development of this thesis is introduced. The human body is a source of biomedical signals that can be used to characterize and identify health status and pathologies. This thesis is based on the heartbeat interval variations and their relation to the regulation of the autonomic nervous system (ANS) on the heart. The modulation of the heart rate through sympathetic and parasympathetic systems is introduced. Finally, technical approaches commonly used for assessing autonomic nervous system (ANS) activity using heart rate dynamics are presented throughout this dissertation.

1.1 Motivation

Heart rate variability is considered a non-invasive technique for assessing ANS regulation of heart rate [179]. During the last few decades, interest in this analysis has risen. Around 1600 related scientific papers were published in 2017 (data from Pubmed search engine <https://www.ncbi.nlm.nih.gov/pmc/>). Its potential is widely recognized and used. The analysis of HRV has been applied to characterize changes in ANS response due to several pathologies or habits, e.g. cardiovascular diseases (CVD), metabolic disorders, mental disorders and stress [49, 48, 136, 153, 90, 26, 72, 45, 163, 82, 128, 112]. The World Health Organization reported that 31% of all world global deaths were related to CVD, which is 17.7 million people, 422 million people worldwide have diabetes and 1.6 million deaths are directly related to this disease each year. In addition, more than 300 million people worldwide are suffering from a mental disorder (depression, bipolar affective disorder, schizophrenia, psychosis, dementia, developmental disorders). Early detection is crucial to reduce the incidence, morbidity and mortality of CVD, and metabolic disorders and to increase the efficacy of treatment for mental and stress disorders (retrieved from <http://www.who.int>).

After years of study, in 1996, the standards of measurement of heart rate variability, including physiological interpretation and clinical use, were published [179]. However, despite the huge number of studies related to HRV analysis, linear indices (referred to as time- and frequency-domain) are sometimes not enough to extract conclusive findings. The relationship between intrinsic pacemaker cells and ANS modulation expressed in HRV has been reported as nonlinear [194]. Nonlinear techniques have been highlighted as powerful tools to assess HRV for diagnosis and prognosis, pointing out the presence of nonlinearities in heart rate regulation, but further research is needed to relate these nonlinear techniques to a physiological interpretation [87, 85, 177].

During the following 20 years, many authors focused their research studies on this new branch. In 2015, the advances in HRV signal analysis were released, paying attention to these nonlinear techniques [161]. However, physiological interpretation of nonlinear indices is still unclear, since methodological aspects, such as their dependence on parameter setting, which has not been addressed in any great depth yet, may be misleading.

1.2 Autonomic Nervous System Regulation of the Heart

Cardiovascular and respiratory systems are regulated by ANS. Heart rate, lung volume and blood pressure are modulated in order to supply the body's needs. A sensor net, made up of sensory receptors, detects variations of these variables, information which is managed by regulatory systems. In this thesis, we focus our attention on the regulation of ANS on the heart. The presence of ANS innervation in the heart can be found at several locations. ANS fibers are present in the sino-atrial (SA) node, the atria, atrio-ventricular (AV) node and also in the ventricles, see figure 1.1. As with most of the body's organs, the heart is innervated by the two main subsystems of the ANS, the parasympathetic (vagal)

and the sympathetic system. These subsystems are described as antagonistic and they work together to maintain the cardiovascular homeostasis.

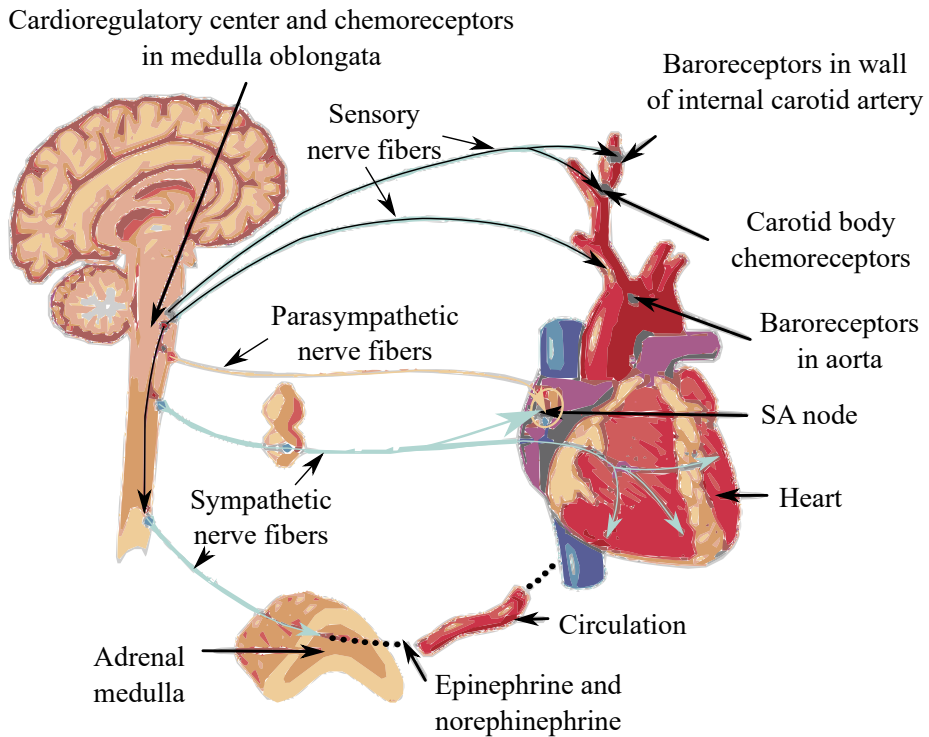


Figure 1.1 Innervation of the heart by autonomic nervous system.

The vagal system decreases heart rate and cardiac contractility (rest and digest response), while the sympathetic system acts antagonistically increasing the heart rate and cardiac contractility, and regulating the peripheral vasoconstriction (fight or flight response) [65]. The underlying mechanisms of these two subsystems present different physiological dynamics. On one hand, parasympathetic modulation acts by releasing acetylcholine into the synaptic space of the neurons, where muscarinic cholinergic receptors of cardiomyocytes are stimulated, changing properties such as ionic currents and conductances, decreasing the excitability of the cells, and then reducing the heart rate. On the other hand, sympathetic regulation stimulates the adrenal medulla, releasing adrenaline and noradrenaline into the bloodstream, which stimulates β -receptors, changing the cardiomyocyte properties, increasing the heart rate. Parasympathetic system regulation shows a faster response than the sympathetic one.

Pharmacological blockades are used for treatment of certain pathologies in which ANS response is altered, such as silent ischemia or heart failure, or to explore the subsystems behavior separately [169, 138, 96]. These drugs could stimulate or inhibit ANS subsystem activity. On one hand, the muscarinic antagonist (anticholinergic) drugs reduce the respiratory sinus arrhythmia degree, inhibiting vagal modulation, and are used in Parkinson's disease. On the other hand, β -adrenergic receptor blocker therapy plays a key role in the treatment of cardiovascular diseases due to their

antiischemic, antiarrhythmic and antihypertensive properties, and also it has been reported to be beneficial in cases of heart failure [108].

1.3 Heart Rate Variability

In normal sinus rhythm, heart rate is determined by the SA node, which receives impulses from both sympathetic and parasympathetic systems, increasing or decreasing heart rate respectively, in order to meet internal and external demands to maintain homeostasis. Heart rate variability refers to the beat-to-beat heart rate variations, and its analysis has been proposed for the assessment of ANS regulation on the heart. HRV is derived from the electrocardiogram (ECG), which describes the electrical activity of the heart, recorded by electrodes placed on the body surface.

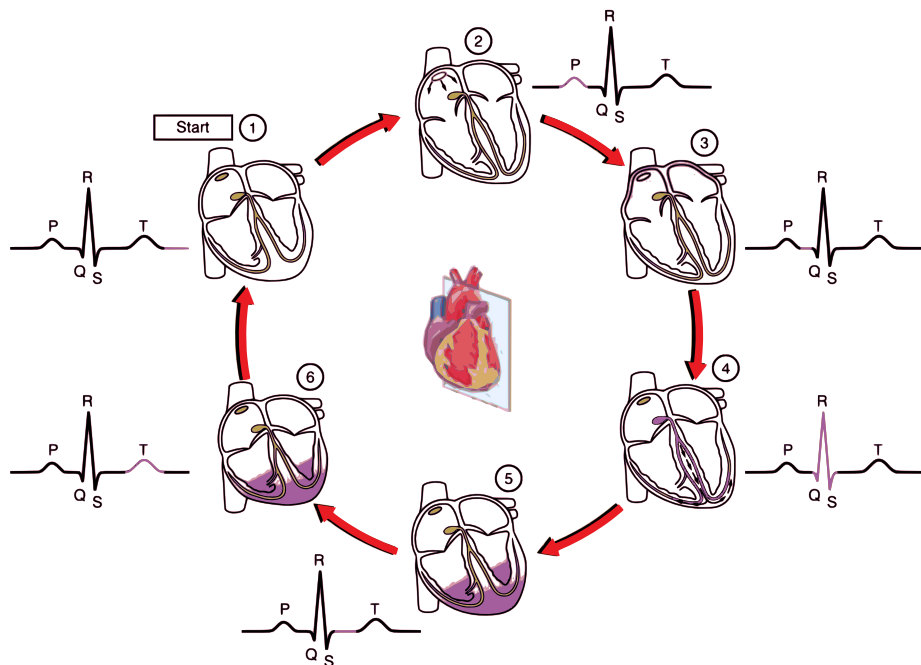


Figure 1.2 Physiological phases of the heart and electrocardiograph signal representation. 1) Pace-marker cells of SA node are ready to fire (Atrial depolarization). 2) SA cells fire and electrical activity begins (Atrial repolarization). 3) Atrium pumps blood to ventricles. 4) Electrical activity travels from atrioventricular node to Purkinje fibers to depolarize ventricles (QRS complex). 5) Ventricles begin repolarizing from endocardium to epicardium. 6) End of the ventricular repolarization and ventricles pump blood to aorta artery.

The mechanical contraction of the heart is preceded by electrical cell (cardiomyocytes) excitation, the so-called depolarization stage, while, the return to electro-mechanical relaxed condition is called repolarization. Each heartbeat generation is composed of several phases illustrated in Fig. 1.2. The cardiomyocytes belonging to the SA node present the special characteristic of being auto-activated, generating the beginning of a heartbeat. They are known as the natural pacemaker of the heart. These cells generate the stimulus to be transmitted to the rest of cardiomyocytes. First, atria are depolarized,

producing the mechanical contraction (P wave). The electrical activity travels to the atrioventricular node, where it is delayed and then, ventricles receive the electrical impulse via Purkinje fibers (QRS complex). Atria are repolarized, and ventricles start depolarizing as well as contracting (T wave). The electrocardiogram (ECG) represents the global electrical activity of the heart.

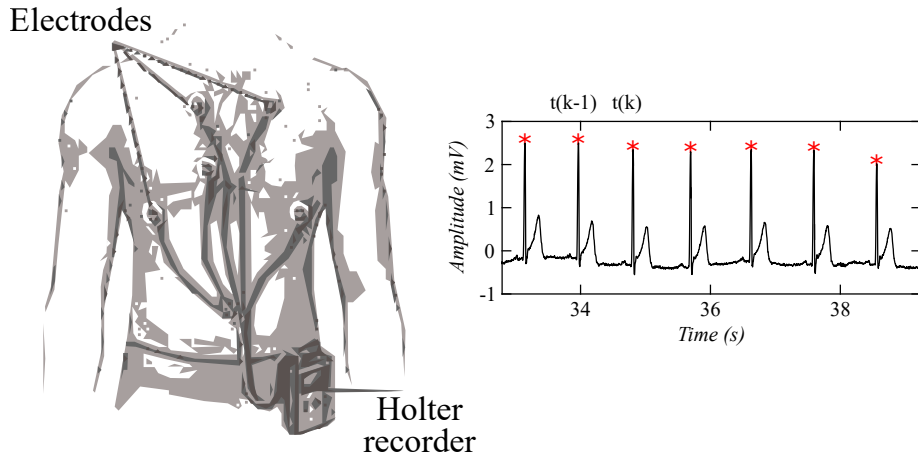


Figure 1.3 Position of electrodes placed in the chest is illustrated in the left panel. On the right, an ECG signal is shown produced by the electrical activity of each heartbeat. Asterisks represent the heartbeat location in time, $t(k)$, where k is the beat index.

To obtain HRV, the detection of each heartbeat occurrence time from the ECG is needed (see Fig. 1.3). The selection of a proper fiducial points for HRV analysis is important. The heartbeat location is commonly extracted from the R wave peak, corresponding to the fast propagation of the impulse from atria to ventricles through the AV node and the bundle of His, since it is usually the dominant wave within the QRS complex. However, in certain QRS complex morphologies, with dominant negative peak, detection of the latest would be more robust. On the other hand, switching from main positive peak to main negative peak from beat to beat would induce extra variability. Thus, in this thesis, fiducial points are selected to be either the positive or the negative QRS complex peaks, depending on which of them represent the most recurrent morphology.

Heart Rate Variability Representations

RR time Series

The tachogram or RR time series is defined as the difference between consecutive R wave peaks. Hence:

$$RR(k) = t(k) - t(k-1), \quad (1.1)$$

where $t(k)$ is the k^{th} heartbeat location in time.

Heart Rate Series

HR time series are defined as the inverse of RR time series in beats per minute (BPM) units:

$$HR(k) = \frac{60}{RR(k)} \quad (1.2)$$

These series are naturally unevenly sampled, but methods, such as interpolation, could be applied when necessary to generate evenly sampled series.

Figure 1.4 illustrates both series and their differences.

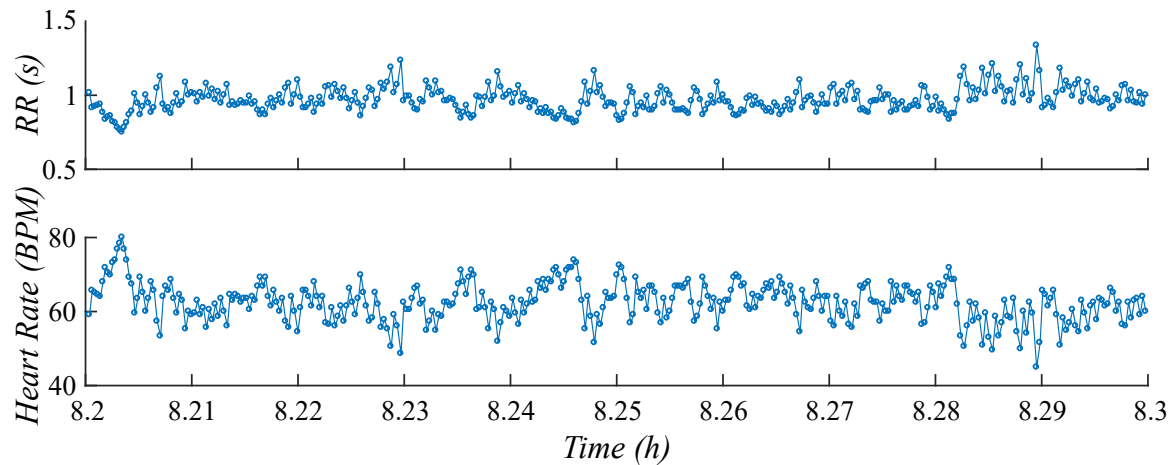


Figure 1.4 From top to bottom, RR interval and heart rate as HRV signal representations. Data extracted from a 24h Holter recording of Normal Sinus Rhythm database from www.physionet.org.

Other Alternative Representations

Alternative representations of HRV have been proposed based on physiological models.

On one hand, integrate-and-fire models such as the integral pulse frequency modulation (IPFM) model provides a physiologically plausible model for HRV representation, assuming that the ANS influence on the SA node can be described by a modulating signal, $\mathfrak{M}(t)$ [115]. The modulating signal over a DC level of 1 is integrated until reaching a threshold, which is the mean heart period, when a new heartbeat is generated and the integral is reseted.

On the other hand, models taking into account the stochasticity of the process, like the point-process model, have been also used for HRV representation. This model was firstly applied in neuroscience, analyzing the electrical activity of the brain through electroencephalogram (EEG), obtaining promising results [181]. Its application to HRV analysis provides a probability model to describe heart rate dynamics mathematically. The waiting time from one heartbeat time $t(k)$ until the next one is assumed to obey an inverse Gaussian probability density function [10].

1.4 Autonomic Nervous System Assessment

As aforementioned, HRV is considered a non-invasive technique for assessing the ANS activity related to heart regulation [179]. Approaches based on the time- frequency-domain and in terms of complexity/irregularity have been applied to HRV analysis and they are described in the following.

1.4.1 Time Domain Analysis

Time domain indices are based on statistical characteristics of HRV signals. Time domain indices give a description of the time series first moments, heart rate mean (HRM), standard deviation of consecutive normal beats (SDNN), referring to those whose origin is the SA node, and the square root of the mean squared differences of successive normal heartbeat intervals (RMSSD). In particular, SDNN and RMSSD have been related to parasympathetic activity [179].

1.4.2 Frequency Domain Analysis

In 1981, Akselrod et al. [2] characterized heart rate fluctuations in the frequency domain, describing the relation between ANS modulation (sympathetic and parasympathetic subsystems) and power spectral density content in specific bands.

The sympathetic activity was reported to contribute to low frequency (LF) band content (P_{LF} : 0.04-0.15 Hz), whereas the parasympathetic activity contribution was related to high frequency (HF) band content (P_{HF} : 0.15-0.4 Hz), but also to LF band. Figure 1.5 illustrates an exemplary spectral representation of HRV signal, corresponding to relaxed conditions. HF content was proposed as an index to estimate the parasympathetic activity . In addition, the ratio between LF and HF power spectral density band content, known as sympathovagal ratio (LF/HF), was reported to provide a measure of the balance between sympathetic and parasympathetic system regulation. The mentioned spectral band definitions are suitable for adult healthy subjects who are breathing normally. HF band definition can be modified, depending on the subject status, to ensure that parasympathetic activity is captured [9, 70], since factors such as respiratory sinus arrhythmia could be reflected in higher frequencies and thus, the pre-defined HF boundaries should be adjusted [80].

Spectral analysis can be carried out by analyzing the raw RR time series by Lomb-Scargle periodogram, since raw RR time series is unevenly sampled, or by Fourier transform on interpolated RR time series.

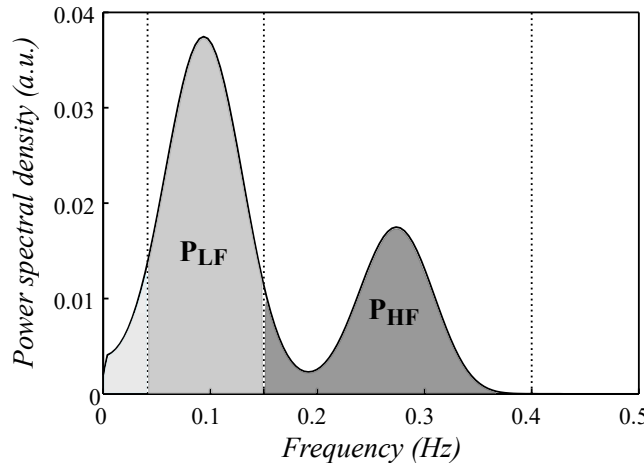


Figure 1.5 Example of power spectral density of a HRV signal (modulating signal $\mathfrak{M}(t)$) where low and high frequency contributions are illustrated.

1.4.3 Nonlinear Domain Analysis

From Deterministic to Stochastic Processes

A system can be classified as deterministic, stochastic or mixed. When an input always produces the same output, the system is said to be deterministic. Deterministic systems can be mathematically described with an unambiguous relationship between the input and the output of the system. There are deterministic systems whose response is highly influenced by initial conditions, producing a very different output depending on those conditions. Such an influence is known as the butterfly effect, as the dependence on initial conditions is represented as the beating of a butterfly's wings in California that could unleash a tornado in another part of the world. Those deterministic systems are known as chaotic. Although the output of a chaotic system could seem to be random, it is not, since it can be exactly determined. In Fig. 1.6, the Lorenz attractor, which is a chaotic system, is illustrated. This system consists of three coupled differential equations, generating three outcome signals with a randomness-like behavior (see section 2.2.1 for the Lorenz attractor mathematical description). The most widespread methods used to characterize nonlinear system dynamics are the ones based on chaos theory, where the greater the amount of information, the higher the accuracy of the measurements. In stochastic systems the output is totally random or has a certain degree of randomness.

The HRV signal could be interpreted as the observable outcome of a system containing information on cardiac ANS regulation. The HRV signal can contain information related to intrinsic physiological nonlinearities, such as changes in the gain of baro-reflex feedback loops or delays in conduction time, which might not be properly described by temporal and spectral signal characteristics [200, 6, 165]. The presence of nonlinear characteristics in HRV time series has been highlighted by surrogate data

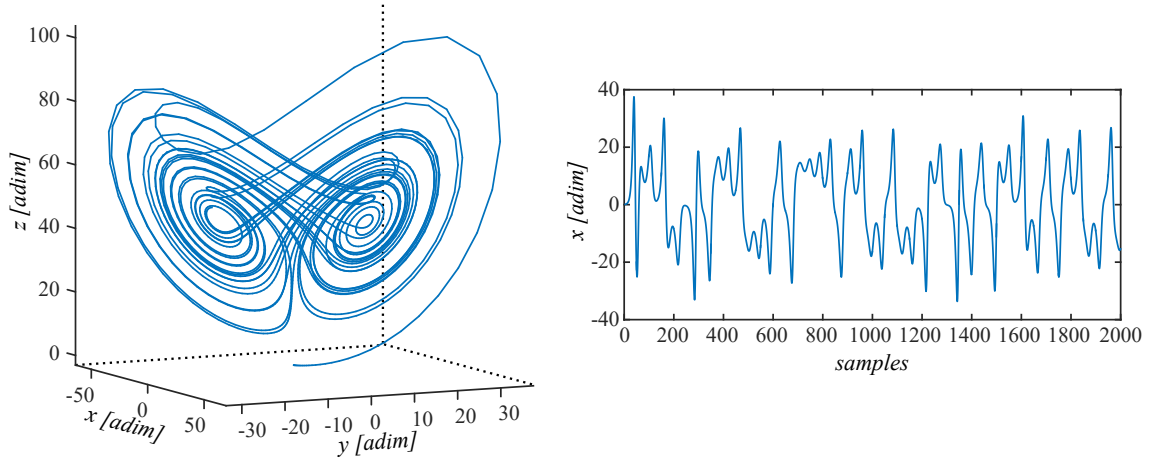


Figure 1.6 Left panel: Lorenz attractor is represented in the phase-space. Right panel: random-like behavior of one of its single outputs is illustrated.

analysis [87, 85, 177, 88]. The question of whether HRV arises from a low-dimensional attractor associated with a deterministic nonlinear dynamical system or has an stochastic origin is still unclear.

System complexity is a concept referring to dynamic richness of subsystem interconnections and feedback. In particular, HRV is known to be related to the outcomes of coupled cardiovascular and respiratory systems such as heart rate, lung volume and blood pressure, among others. Based on transfer functions and models, proposals to quantify the interaction between these variables influencing HRV have been reported [162, 187, 16, 192]. A simplified model of these interactions proposed in [187] is illustrated in Fig. 1.7. Nonlinear complexity indices have been shown to provide complementary information to linear approaches in the characterization of HRV signals [30]. Techniques based on detrended fluctuation analysis [84], Lempel-Ziv complexity [105], Lyapunov exponents [191], D_2 [145] and approximate and sample entropies [142] have been used to assess HRV complexity.

State of the Art

Availability of faster computing resources as well as development of more efficient algorithms for computation of nonlinear HRV characteristics has been crucial for the boost of these methods in research, since the associated high computational load was considered as a limitation for their applicability. Fig. 1.8 shows a timeline with relevant milestones in the characterization of HRV, both using classical and nonlinear methodologies. Some of these methodologies, like approximate entropy or detrended fluctuation analysis, have been widely applied in the last three decades, as illustrated in Fig. 1.9, which shows usage rate of nonlinear methodologies.

Nonlinear HRV indices have been highlighted as promising markers to characterize cardiovascular diseases, such as congestive heart failure, atrial fibrillation or myocardial infarction as well as risk for sudden cardiac death or other type of deaths [118, 167, 187, 40, 43, 50, 75, 173, 12, 73, 50]. Also,

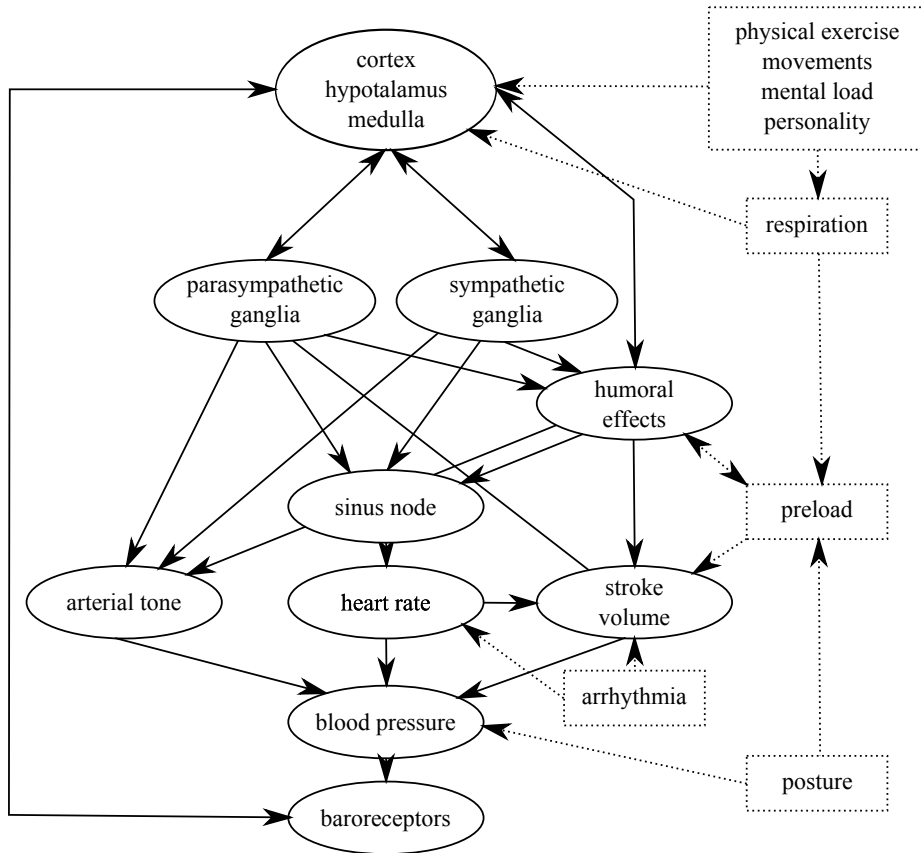


Figure 1.7 A simplified model of HR regulation, adapted from Voss et al. [187]

nonlinear HRV analysis has been applied to investigate the effects of aging [14], mental disorders [16, 122, 124] or unbalanced cardiovascular regulation [149].

According to Sassi et al. [161], nonlinear methods can be classified as: long-range correlation and fractal scaling (e.g. $1/f$ factor, DFA), short-term complexity (e.g. Poincaré plot analysis, acceleration/deceleration capacity), entropy and regularity (e.g. approximate and sample entropy), and nonlinear dynamical systems and chaotic behavior (e.g. correlation dimension, Lyapunov exponents). In this thesis, the nonlinear indices most commonly used in the literature (see Fig. 1.9), like those based on entropy and regularity (approximate and sample entropy, *ApEn* and *SampEn* respectively) and nonlinear dynamical systems and chaotic behavior (correlation dimension, D_2), have been considered.

The above mentioned nonlinear indices are based on Takens' work, which was focused on detecting strange attractors [178]. He concluded that an attractor could be properly reconstructed when the phase-space dimensionality is sufficient to unfold the attractor. He also postulated that it is possible to assess the information of a system by taking into account just one experimental output. Based on this, *ApEn*, a measure of system complexity, was introduced by Pincus [144]. Almost a decade later, Richman and Moorman introduced sample entropy (*SampEn*), an irregularity index for

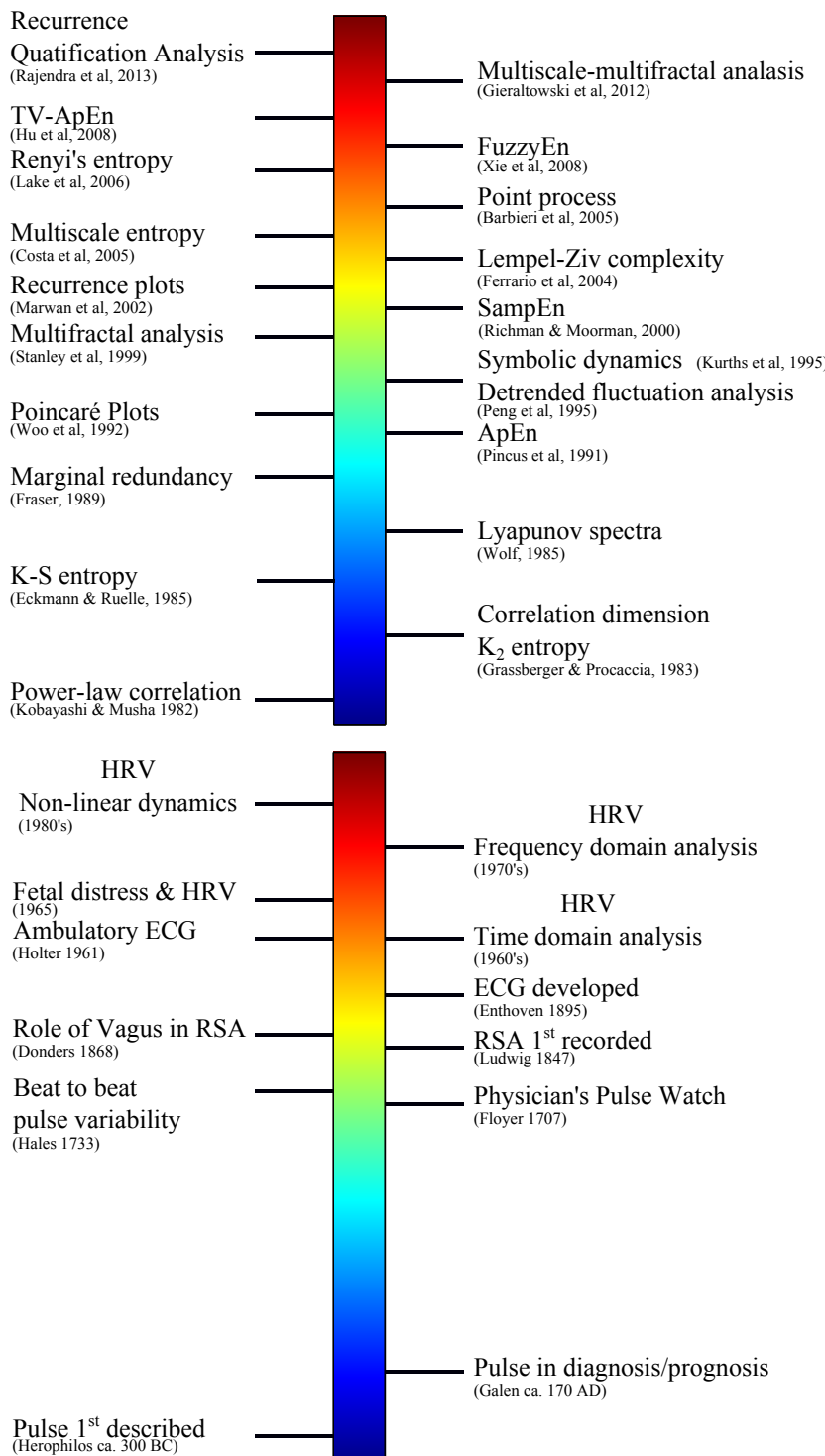


Figure 1.8 Milestones over the time towards the nonlinear heart rate variability assessment. Figure adapted from G.E. Billman (Frontiers in Physiology, 2011) [18].

which dependency on data length was attenuated with respect to *ApEn* [125]. Meanwhile, Grassberger

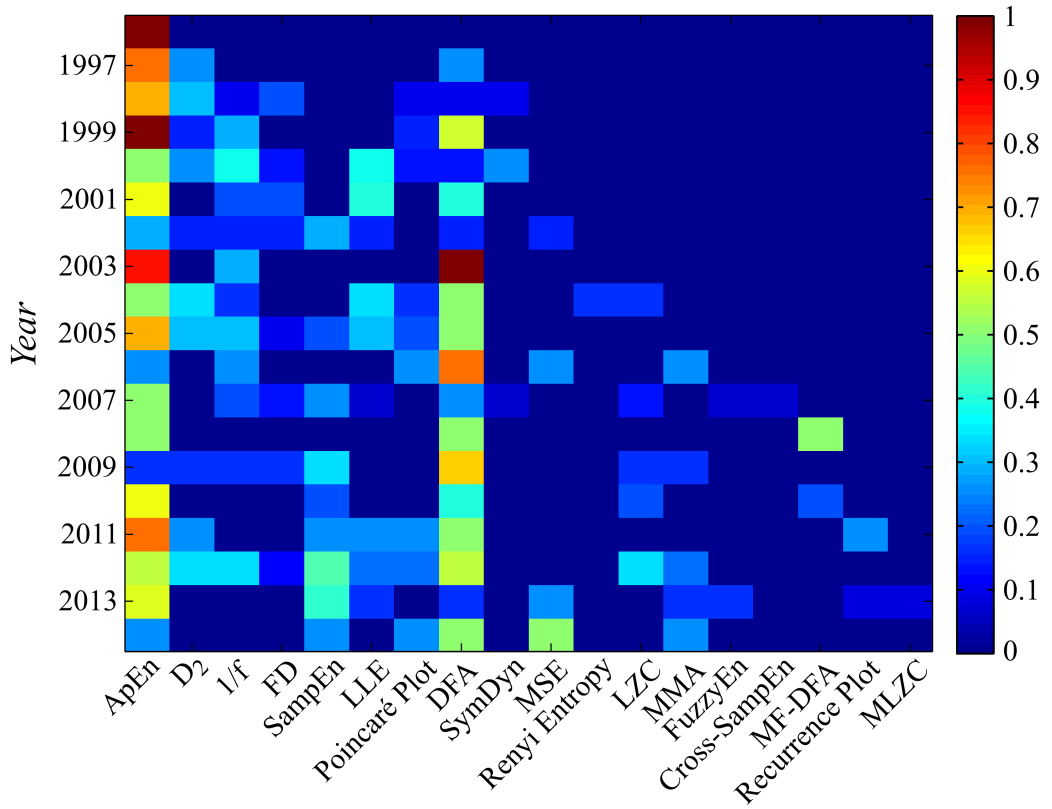


Figure 1.9 Graphical representation of usage rate of most common nonlinear methods for HRV analysis (data from Pubmed search engine e, statistical sample of two hundred studies.).

and Procaccia introduced an algorithm to estimate D_2 also based on Takens' conjecture to characterize strange attractors (chaotic systems) [60].

Shedding light into physiological interpretation of nonlinear HRV indices has been the focus of different research studies. Some studies have shown correlation between frequency-domain and nonlinear HRV indices and have postulated the role of vagal modulation in underlying nonlinear characteristics [198, 132, 75, 193]. Other studies have shown that nonlinear HRV indices are almost unaffected by postural changes known to elicit autonomic responses [172]. In contrast, a statistically significant reduction in HRV irregularity during tilt test, eliciting sympathetic activation, has been reported [75, 148]. The effect of ANS blockades on healthy subjects has been analyzed to improve physiological interpretation of HRV dynamics [135, 75, 193, 23]. Inhibition of vagal nerve activity on the heart by atropine administration revealed lower complexity in nonlinear HRV analysis, whereas no differences were found in nonlinear HRV indices following administration of the β -adrenoceptor antagonist propranolol. In response to exercise, an increase in the exercise load has been related to a decrease in the irregularity and chaos-like behavior of the HRV time series [79, 188, 64].

Nevertheless, caution is required when interpreting results obtained by using nonlinear HRV measurements. First, nonlinear HRV indices are highly influenced by values given to the parameters

involved in their definitions [118, 177, 34, 75, 20, 182, 69]. In addition, nonlinear HRV indices show a strong dependence on mean HR [202, 146, 123, 195], which should be attenuated before establishing any comparison. Standardizing the use of nonlinear HRV indices by accounting for both associated parameter definition and mean HR attenuation would be advisable if such indices are aimed to be more extensively used and interpreted.

1.5 Applications of Nonlinear HRV Analysis

The methodologies proposed in this thesis for nonlinear HRV analysis will be applied to assess cardiovascular disorders and conditions like heart failure, aging and hypotension during cesarean section.

1.5.1 Aging

Aging has been reported to be associated with a decrease in cardiac vagal modulation [24, 44, 54]. These effects have been related to a decrease in HRV, as assessed by frequency-domain indices [98]. In this thesis nonlinear HRV characteristics will be investigated in a database of healthy subjects spanning a broad range of ages.

1.5.2 Congestive Heart Failure

CHF has been associated with increased sympathetic activity and decreased peripheral response to adrenergic input [38, 63]. A decrease in the low frequency power of HRV was related to the progression of the disease in patients with severe CHF [62]. This result can be explained by: (i) a central autonomic regulatory impairment in heart failure, supported by results of muscle sympathetic nerve activity in CHF patients with absent low frequency content [186]; (ii) a decreased responsiveness to sympathetic modulation, which may reduce the capability of the heart to oscillate at this frequency [63]; and (iii) an increased chemoreceptor sensitivity, which may be related to an increase in very low frequency power (P_{VLF}) and a decrease in low frequency power in CHF patients [147]. In the case of nonlinear HRV analysis, controversial findings have been reported. While some studies report lower complexity and irregularity in CHF patients than healthy subjects [73, 107], other studies have described HRV of CHF patients as more complex and irregular than that of healthy subjects [204, 41]. In this thesis, light will be shed on potential reasons underlying these results, particularly taking into account important methodological considerations that influence nonlinear HRV analysis.

1.5.3 Hypotension during Cesarean Section

Prophylaxis treatment has become essential to prevent the development of hypotensive events after spinal anesthesia during cesarean section. However, prophylaxis administration could increase fetal distress in those cases where there is no need for it, i.e. for normotensive outcome. The combination

of symptoms caused by late pregnancy period, physiological and psychological stress and ANS disability to compensate for the drop in blood pressure induced by anesthesia could be responsible for hypotensive episodes during cesarean delivery. HRV characteristics have been found to correlate with hypotensive episodes on the day of surgery [21, 31, 66, 199]. Prediction of hypotensive episodes would benefit the wellbeing of both the mother and the fetus during the intervention, thus increasing the efficacy of prophylactics. In this thesis novel nonlinear HRV analysis will be applied to improve classification of hypotensive vs normotensive events.

1.6 Objectives

The interaction of the diverse physiological mechanisms involved in HR regulation, and how each of them is reflected by the HR dynamics, becomes an ambitious and complicated challenge to understand. Nonlinear HRV analysis was highlighted as a powerful tool to extend the description of several cardiovascular diseases, complementing the information provided by linear approaches. However, the main caveat in the nonlinear HRV analysis lies in its physiological interpretation. Searching for dependencies, such as HRM or *a priori* parameters that have to be selected for nonlinear HRV indices estimation, is of great interest in order to attenuate these influences, and clarify their physiological interpretation.

In chapter 2 alternative methodologies for more reliable estimation of nonlinear HRV indices while reducing the associated computational cost are explored. A methodological framework is initially introduced for estimation of D_2 . Based on the similarities found in the computation of approximate and sample entropy with respect to correlation dimension, the framework will be considered for the estimation of those other indices as well.

The effect of heart rate, as sampling rate of HRV signal, on nonlinear HRV indices will be investigated in chapter 3 and strategies for attenuation of this effect will be introduced. The proposed strategies will be validated in synthetic time series reproducing physiological characteristics of heart rate signals.

Nonlinear HRV indices, like approximate entropy, are to a large extent dependent on parameters which values need to be set *a priori*. In chapter 4, a nonlinear multidimensional approximate entropy-based index, independent of *a priori* parameters is proposed. Synthetic time series with different levels of randomness are used to validate the proposed index. This index, as well as other nonlinear HRV indices commonly used in the literature are applied to assess the effects of aging as well as to compare CHF patients and healthy subjects.

In chapter 5, the knowhow developed along the thesis is applied to assess a stress-related clinical problem, namely prediction of hypotensive episodes after spinal anesthesia during cesarean section. Linear and nonlinear analysis of HRV, pulse wave variability and pulse rate variability (derived

from photoplethysmographic signal) are investigated to derive combinations of indices with optical capability to classify hypotensive versus normotensive events.

Concluding remarks of this thesis are presented in chapter 6.

In summary, methodological objectives of this thesis include: i) proposal of a novel framework to improve reliability of correlation dimension estimation by using an algorithm with reduced computational load that facilitates its applicability in clinical practice; ii) development of alternative methods to attenuate the dependency of nonlinear HRV indices on mean HR; iii) proposal of a novel multidimensional nonlinear HRV index independent of *a priori* parameter definition for its computation.

Objectives related to clinical application of the methodological contributions are: i) characterization of the effect of aging on nonlinear HRV; ii) assessment of complexity and irregularity of heart rate in CHF patients as compared to healthy subjects; iii) improvement in the efficacy of prophylaxis administration for the prevention of hypotensive events after spinal anesthesia during programmed cesarean delivery.

“But the trouble was that ignorance became more interesting, especially big fascinating ignorance about huge and important things like matter and creation, and people stopped patiently building their little houses of rational sticks in the chaos of the universe and started getting interested in the chaos itself – partly because it was a lot easier to be an expert on chaos, but mostly because it made really good patterns that you could put on a t-shirt.”

- Terry Pratchett (1948-2015) -

2

Framework for Correlation Dimension Estimation

Summary

In this chapter, correlation dimension is introduced, based on that it is possible to reconstruct certain system characteristics with just considering one single system output (Takens hypothesis). The novelties, presented here, covered a new strategy to estimate the scaling region of the *log-log* curves (correlation sums vs. tolerance values), being crucial for improving reliability of correlation dimension. Besides, two proposed approaches for its estimation and an algorithm for a fast computation are introduced. The proposed framework is validated through synthetic and real data, pointing out the caveats and limitations for correlation dimension estimation.

2.1 Correlation Dimension

As mentioned in the introduction chapter, nonlinear HRV analysis measurements have been described as complementary to time- and frequency-domain indices, but some pitfalls could mislead their interpretation. One of such limitations arises from their application to time series with limited duration. In particular, D_2 estimation has shown a strong dependence on the length of the time series [60]. Alternatives to alleviate this effect were proposed in [78, 180]. In addition to this, stationarity is another requirement that a time series has to fulfill to obtain reliable results. However, these methodological constraints, regarding data length duration and stationarity, are usually difficult to satisfy at the same time [88]. Furthermore, computation of D_2 is time-consuming, increasing exponentially with data length. In this regard, several attempts have been reported trying to reduce this disadvantage, including parallel computing using MPI (Message Passing Interface) [190, 205].

In this chapter, a new methodological framework to estimate D_2 is proposed, increasing correlation dimension reliability and reducing its computational time.

2.1.1 Mathematical Definition

Let $x(n)$, $n = 1, \dots, N$, be the time series of interest, which in HRV analysis will be the *RR* interval series normalized to unit amplitude (divided by absolute maximum value), and N the total number of beats. A set of m -dimensional vectors, $\mathbf{y}_m(i)$, called reconstructed vectors, are generated [178]:

$$\mathbf{y}_i^m = [x(i), x(i + \tau), x(i + 2\tau), \dots, x(i + (m - 1)\tau)]^T \quad (2.1)$$

where τ represents the delay between consecutive samples in the reconstructed space. The amount of reconstructed vectors is $N_m = N - \tau(m - 1)$ for each embedding dimension m . The distance between each pair of reconstructed vectors, $\mathbf{y}_i^m, \mathbf{y}_j^m$, is denoted as:

$$d_{i,j}^m = d(\mathbf{y}_i^m, \mathbf{y}_j^m) \quad (2.2)$$

computed as the norm of the difference vector $\Delta\mathbf{y}_{i,j}^m = \mathbf{y}_i^m - \mathbf{y}_j^m$. In section 2.4.1, different norms and their effect on D_2 estimates from finite time series are discussed.

The self-similarity is addressed by computing the correlation sums, which represents the probability of finding similar reconstructed vectors, according to a certain threshold r . Hence, correlation sums are defined as follow:

$$\begin{aligned} C_m(r) &= \frac{1}{N_m(N_m - 1)} \sum_{i,j=1}^{N_m} H(r - d_{i,j}^m) \\ &= \frac{1}{N_m(N_m - 1)} \sum_{i=1}^{N_m} c_i^m(r) \end{aligned} \quad (2.3)$$

where $H(\cdot)$ is the Heaviside function,

$$H(x) = \begin{cases} 1 & x \geq 0 \\ 0 & x < 0 \end{cases} \quad (2.4)$$

and

$$c_i^m(r) = \sum_{j=1}^{N_m} H(r - d_{i,j}^m) \quad (2.5)$$

For deterministic systems, $C_m(r)$ decreases monotonically to 0 as r approaches 0, and it is expected that $C_m(r)$ is well approximated by $C_m(r) \approx r^{D_2^m}$. Thus, D_2^m can be defined as:

$$D_2^m = \lim_{r \rightarrow 0} \frac{\log C_m(r)}{\log(r)} \quad (2.6)$$

For increasing m , D_2^m values tend to saturate to a D_2 value, constituting the correlation dimension estimate.

2.1.2 Scaling Range Assessment: Sigmoid Curve Fitting

D_2 is estimated from Eq. (2.6), whose numerator and denominator both tend to $-\infty$ as r tends to 0. Therefore, making use of L'Hôpital's rule, the equation can be rewritten as [104]:

$$D_2^m = \lim_{r \rightarrow 0} \frac{d \log C_m(r)}{d \log(r)} \quad (2.7)$$

Since the size of the time series is finite, choosing small values of r to evaluate this limit is problematic. For values of r close to 0, very few distances contribute to the correlation sum, making the estimation unreliable. Therefore, the evaluation of this expression is usually done in a linear region in the $\log(C_m(r))$ vs $\log(r)$ representation, called the *log-log* curve, where its slope value is considered an estimate of D_2^m .

The slope of the linear region could be estimated by different approaches, e.g. searching for maximum slope can be done by directly computing the increments in the *log-log* curve, or as the maximum of the first derivative of the *log-log* curve [78]. Nevertheless, these approaches encounter some limitations, since logarithmic r values produce non-equidistant sampling. Another limitation arises in the presence of dynamic systems, whose *log-log* curves could present several linear regions, as can be seen in Fig. 2.1, where data corresponds to a RR interval series extracted from a 30-minute ECG recording. In order to estimate the slope of the linear region of the *log-log* curve, an attempt to artificially extend the linear region is made by excluding the self-comparisons ($d_{i,j}^m$) from the correlation sums (see Eq. 2.5).

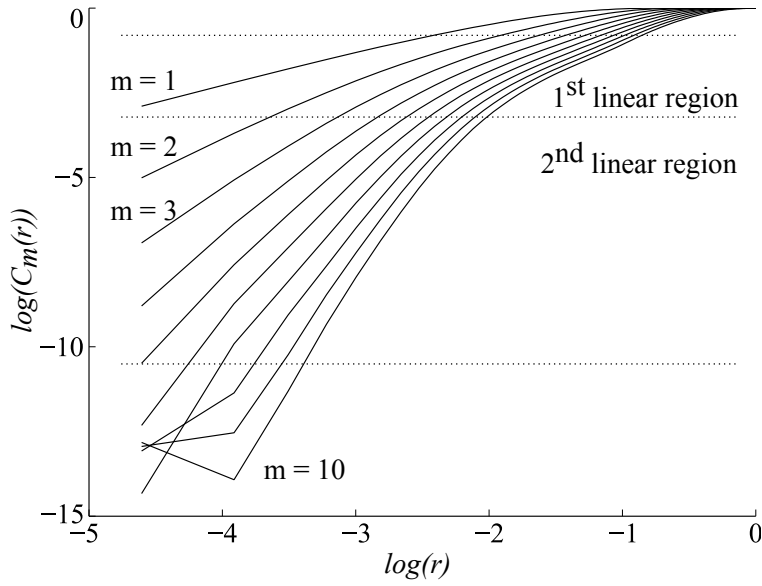


Figure 2.1 *Log-log* curves for a dynamic system. Data correspond to a RR interval series extracted from 30 mins of ECG recording.

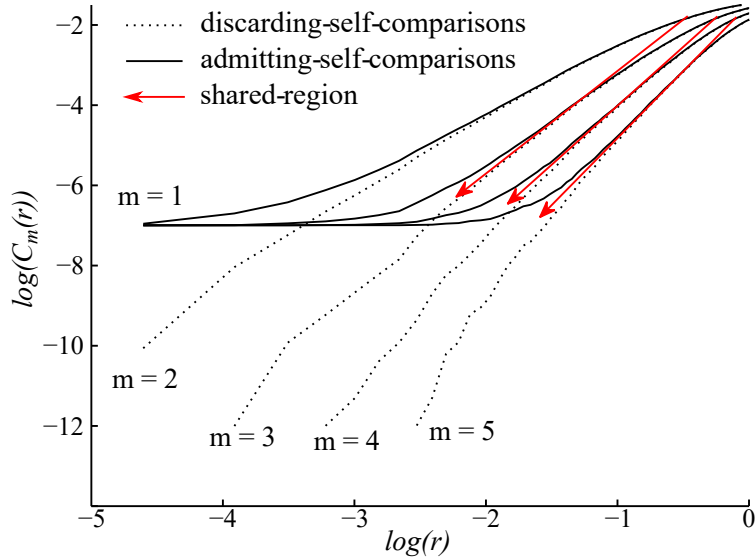


Figure 2.2 *Log-log* curves discarding and accepting self-comparisons. Arrows show the slope of the scaling range. Data correspond to a RR interval series of 300 beats.

However, the basis of the proposed approach, to improve D_2 estimation, lies in considering self-comparisons. Fig. 2.2 illustrates how *log-log* curves behave in both situations, considering or not considering self-comparisons. As shown, both share part of the linear region. Sigmoid curve

fitting (SCF) over the *log-log* curves provides an analytic function, whose maximum slope in the linear region is well defined. These *log-log* curves are reminiscent of the bi-asymptotic fractals, showing upper and lower asymptotic *log-log* values. This was studied by Rigaut [156] and Dollinger et al. in [47], where exponential fittings were proposed. The sigmoid curve fitting technique is applied to *log-log* curves, after interpolating them, in the logarithmic scale, to achieve evenly-spaced r values.

To do so, a modified Boltzmann sigmoid function was considered. This was used by Navarro et al. [130] as a model for the phase transition of smart gels:

$$f(x) = A_2 - \frac{(A_2 - A_1)}{B + e^{\frac{(-x+x_o)}{\alpha}}} \quad (2.8)$$

where A_1, A_2, α, x_o and B are the design parameters. The first derivative of $f(x)$ is:

$$\frac{df(x)}{dx} = -\frac{(A_2 - A_1)e^{\frac{(-x+x_o)}{\alpha}}}{\alpha \left(B + e^{\frac{(-x+x_o)}{\alpha}} \right)^2} \quad (2.9)$$

In this study, the sigmoid curve, $f(x)$, is fitted to each *log-log* curve. The first derivative, Eq. 2.9, is analytically determined and its maximum value constitutes the estimation of the slope of the linear region, i.e. \hat{D}_2^m , see Fig. 2.3. Note that hat notation refers the application of SCF on its estimation.

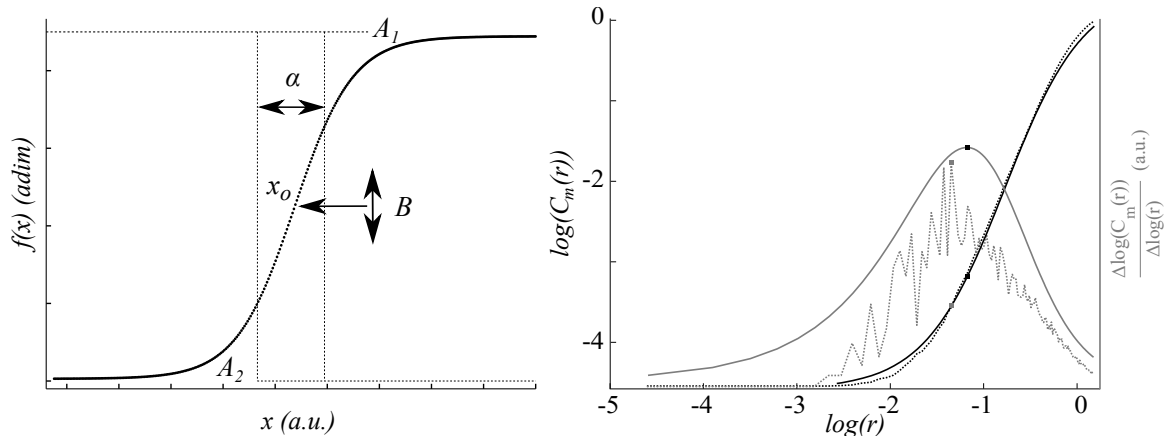


Figure 2.3 In the left panel a modified Boltzman sigmoid curve is shown where the parameters according to Eq. 2.8 are illustrated; In the right panel, an example of a *log-log* curve (black dashed line), the SCF curve obtained (black solid line). The derivative of both curves is shown in gray color, dashed and solid respectively. Maximum slope estimations are marked with dots.

In order to achieve a good fitting, the threshold values, r , have to guarantee that both upper and lower asymptotes are reached. Then, threshold values, $r \in [0.01 \ 3]$ with a step of 0.01 are considered. The upper asymptote is reached when all comparisons are above the threshold, $C_m(r) \approx 1$, and the lower asymptote when only the self-comparisons are below, $C_m(r) = \frac{1}{N_m(N_m-1)}$.

The requirement for a good fitting is to achieve a regression factor greater than 0.8 with respect to *log-log* curve values. Thus, the SCF approach is robust against erroneous D_2 estimates. In those cases, where dynamic systems exhibits *log-log* curves with more than one linear region, no estimation of D_2 is given, since the fitting is not enough satisfactory to reach the minimum necessary regression factor.

As the embedding dimension m increases, the linear regions of the *log-log* curves tend to be parallel to each other. Thus, \hat{D}_2^m estimates tend to saturate to a certain value, which is considered the \hat{D}_2 . D_2 is estimated by fitting the \hat{D}_2^m vs. m curve following a modified version of the one used by Carvajal et al. [29]:

$$D_2^m = D_2 \left(1 - Ae^{-km} \right) \quad (2.10)$$

where A , is here introduced to reach the saturation level more quickly than the previously proposed, and k is the exponential growth factor.

2.1.3 New Approaches for D_2 Assessment

In this section, new alternatives, based on (SCF) approach, to estimate D_2 are introduced. As mentioned in section 2.1.2, we chose \hat{D}_2^m as the maximum slope on each fitted sigmoid curve. Nevertheless, the linear region is composed of more than one single point. Based on this, a new approach for D_2 estimation is proposed by considering a set of points, i.e. slope estimations, extracted from these linear ranges, instead of considering only one single point per curve.

The main idea is based on selecting one point of the linear range in the SCF *log-log* curve of the lowest embedding dimension m , and moving forward to the next embedding dimension $m + 1$, selecting the point of the corresponding SCF *log-log* curve that satisfies the minimum distance to the former curve following the gradient descent technique (i.e. where an hypothetical perpendicular line starts in the m^{th} *log-log* curve and intersects the $(m + 1)^{th}$ *log-log* curve, see Fig. 2.4). Minimum distance was considered, assuming that the linear range of *log-log* curves tend to be parallel to each other. The procedure is repeated up to the maximum considered embedding dimension. Then, several sets of slopes are computed (one for each point in the linear region around the maximum slope of the SCF *log-log* curve of the lowest embedding dimension), providing a set of D_2 estimates per embedding dimension ($\hat{D}_{2(\perp),r}^m$). The dependence on r in the notation indicates that each set of D_2 estimates is linked to an r value, corresponding to the first value of each set.

Finally, Eq. 2.10 is used to estimate the final D_2 ($\hat{D}_{2(\perp),r}$) for each set of points. These ($\hat{D}_{2(\perp),r}$) estimates are linked to the $\log(r)$ value of the lowest embedding dimension. Finally, regarding the criterion in searching for the maximum slope value in the *log-log* curves, the maximum of the $\hat{D}_{2(\perp),r}$ is selected as the new D_2 estimate, called $\hat{D}_{2(\perp)}$, see Fig 2.5.

Another new approach for D_2 estimation based on *SampEn* is now presented. *SampEn* was defined by Zurek et al. [205] as:

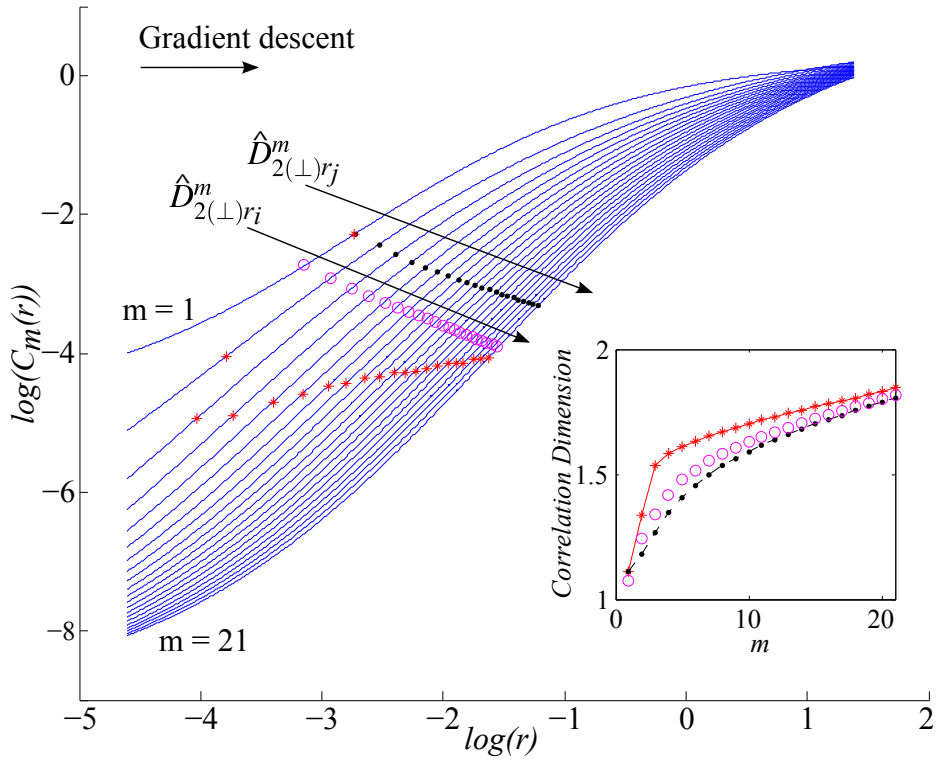


Figure 2.4 Maximum slope points are marked with crosses over fitted sigmoid curves. Points calculated using gradient descent criteria from two starting points are shown in dots and circles. r_j is the point which corresponds to the maximum slope in the lowest embedding dimension. The inset illustrates the D_2 estimation of the three sets of points.

$$\text{SampEn}(m, r) = \log(C_m(r)) - \log(C_{m+1}(r)) \quad (2.11)$$

where, in this case, $C_m(r)$ is computed as in Eq. 2.1.1, but without considering self-comparisons. Let us define $\text{SampEn}_{i=j}(m, r)$ as the sample entropy considering self-pairs, which is easily computed for all embedding dimensions m and a huge set of thresholds \mathbf{r} using the fast algorithm which will be described in section 2.1.4. We can generate a $\text{SampEn}_{i=j}(m, r)$ surface from the fitted sigmoid curves. An example of a 300-beat RR interval series extracted from one recording of the database used in [27] is shown in Fig. 2.6. For each embedding dimension, the value of r which maximizes $\text{SampEn}_{i=j}(m, r)$ is used to estimate the slope of the linear region of the SCF $\log\log$ curves, $\hat{D}_{2(max)}^m$, yielding another D_2 estimate, called in this thesis $\hat{D}_{2(max)}$.

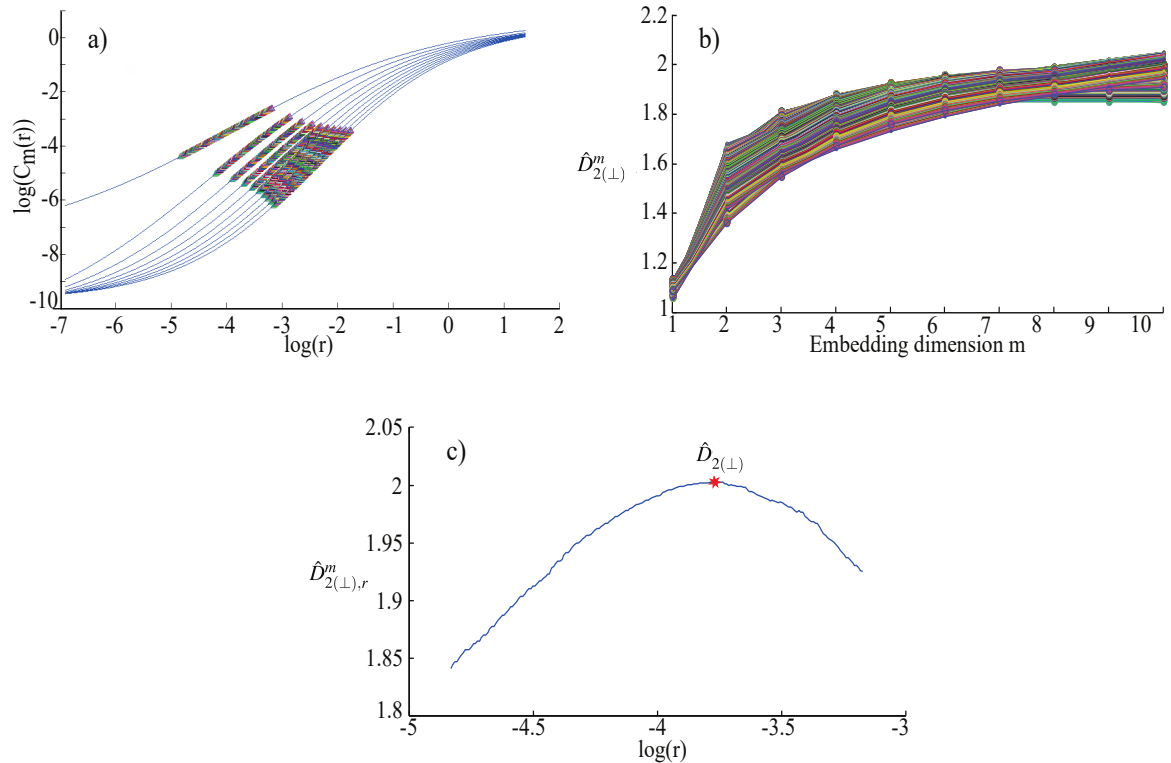


Figure 2.5 a) Set of points where slope is estimated from the fitted sigmoid curves in the approach proposed in section 2.1.3.; b) Set of $\hat{D}_{2(\perp),r}^m$ estimates for different starting points vs. embedding dimensions are fitted by the exponential Eq. 2.10; c) Correlation dimension estimate for each set corresponding to different starting points. Data extracted from Lorenz attractor of 5000 sample length.

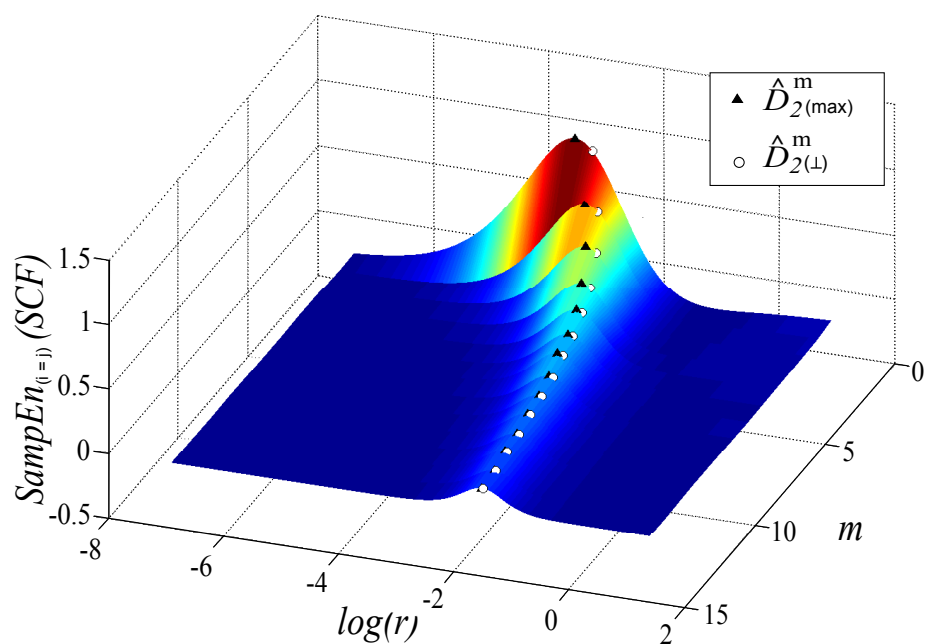


Figure 2.6 $SampEn_{i=1}(m, r)$ surface for a 300-beat RR interval series. For each embedding dimension maximum point is marked with solid triangle. Circles correspond to the r values which define $\hat{D}_{2(\perp)}$.

2.1.4 Fast Computation of Correlation Sums

One important limitation of D_2 estimation is the high computational time required, mainly due to the sequential estimation of correlation sums.

This section describes an algorithm for the fast computation of correlation sums based on matrix operations (MO). A matrix \mathbf{S} , containing the differences between all pairs of samples of $x(n)$, is computed as:

$$\mathbf{S} = \mathbf{X} - \mathbf{X}^T \quad (2.12)$$

where \mathbf{X} is the $N \times N$ matrix:

$$\mathbf{X} = \begin{pmatrix} x(1) & x(2) & \dots & x(N) \\ x(1) & x(2) & \dots & x(N) \\ x(1) & x(2) & \dots & x(N) \\ \vdots & \vdots & \ddots & \vdots \\ x(1) & x(2) & \dots & x(N) \end{pmatrix} \quad (2.13)$$

where $x_{i,j}$ symbolizes $x(i) - x(j)$. For instance, the dashed box contains the elements of the difference vector $\Delta\mathbf{y}_{i,j}^m$ for $\tau = 1$. For each embedding dimension m and the reconstructed vector i , the difference vectors $\Delta\mathbf{y}_{i,j}^m$ generates a \mathbf{S}_i^m matrix:

$$\mathbf{S} = \begin{pmatrix} x_{1,1} & \dots & x_{i,1} & x_{i+1,1} & \dots & x_{i+m-1,1} & \dots & x_{N,1} \\ \vdots & \vdots \\ x_{1,j} & \dots & x_{i,j} & x_{i+1,j} & \dots & x_{i+m-1,j} & \dots & x_{N,j} \\ x_{1,j+1} & \dots & x_{i,j+1} & x_{i+1,j+1} & \dots & x_{i+m-1,j+1} & \dots & x_{N,j+1} \\ \vdots & \vdots \\ x_{1,j+m-1} & \dots & x_{i,j+m-1} & x_{i+1,j+m-1} & \dots & x_{i+m-1,j+m-1} & \dots & x_{N,j+m-1} \\ \vdots & \vdots \\ x_{1,N} & \dots & x_{i,N} & x_{i+1,N} & \dots & x_{i+m-1,N} & \dots & x_{N,N} \end{pmatrix} \quad (2.14)$$

$$\mathbf{S}_i^m = \begin{pmatrix} x_{i,1} & x_{i+1,2} & \dots & x_{i+m-1,m} \\ \vdots & \vdots & \vdots & \vdots \\ x_{i,j} & x_{i+1,j+1} & \dots & x_{i+m-1,j+m-1} \\ \vdots & \vdots & \vdots & \vdots \\ x_{i,N_m} & x_{i+1,N_m+1} & \dots & x_{i+m-1,N} \end{pmatrix} = \begin{pmatrix} \Delta\mathbf{y}_{i,1}^m \\ \vdots \\ \Delta\mathbf{y}_{i,j}^m \\ \vdots \\ \Delta\mathbf{y}_{i,N_m}^m \end{pmatrix}^T \quad (2.15)$$

The selected norm is applied to the matrix \mathbf{S}_i^m , generating the norm vector \mathbf{d}_i^m , whose elements are distances $\mathbf{d}_{i,j}^m$.

To compute the limit described in Eq. 2.6, distances should be compared with a set of thresholds, which implies the repetition of all the process as many times as the number of thresholds. The proposed algorithm avoids this repetition, since distances in \mathbf{d}_i^m are compared with a whole set of thresholds $\mathbf{r} = [r_1, r_2, \dots, r_{N_r}]$:

$$\Gamma_i^m = \begin{pmatrix} H(r_1 - d_{i,1}^m) & H(r_2 - d_{i,1}^m) & \dots & H(r_{N_r} - d_{i,1}^m) \\ H(r_1 - d_{i,2}^m) & H(r_2 - d_{i,2}^m) & \dots & H(r_{N_r} - d_{i,2}^m) \\ \vdots & \vdots & \vdots & \vdots \\ H(r_1 - d_{i,N_m}^m) & H(r_2 - d_{i,N_m}^m) & \dots & H(r_{N_r} - d_{i,N_m}^m) \end{pmatrix} \quad (2.16)$$

where Γ_i^m is a $N_m \times N_r$ matrix, which contains ones and zeros. The summation of all elements per column of Γ_i^m represents the partial correlation sums of the i^{th} reconstructed vector for a set of thresholds r :

$$\mathbf{c}_i^m = \Gamma_i^{mT} \mathbf{1} = \begin{pmatrix} c_i^m(r_1) \\ c_i^m(r_2) \\ \vdots \\ c_i^m(r_{N_r}) \end{pmatrix} \quad (2.17)$$

where $\mathbf{1}$ is a $N_m \times 1$ vector of ones.

Finally, the procedure is repeated varying the i index N_m times to compute $C_m(r)$.

2.2 Validation Study

The selected time series chosen to validate the proposed approaches to estimate D_2 are the Lorenz attractor and the MIX(P) process.

2.2.1 Lorenz Attractor

The Lorenz attractor is a chaotic system, which is described by three coupled first order differential equations. Its evolution exhibits a chaotic behavior for certain parameter values and initial conditions.

$$\frac{dx}{dt} = \sigma(y - x), \quad (2.18)$$

$$\frac{dy}{dt} = \rho x - y - xz, \quad (2.19)$$

$$\frac{dz}{dt} = \beta z + xy \quad (2.20)$$

For parameter values $\sigma = 10$, $\rho = 28$, and $\beta = 8/3$, the theoretical D_2 value is 2.02 [109]. The Lorenz attractor was illustrated in chapter 1 Fig. 1.6.

2.2.2 MIX(P) Processes

MIX(P) is a family of stochastic processes that samples a sine for $P = 0$ and becomes more random as P increases, becoming totally random for $P = 1$. These processes were reported by Pincus et al. [145] following the expression

$$\text{MIX}(P)_j = (1 - Z_j)X_j + Z_jY_j, \quad (2.21)$$

where $X_j = \sqrt{2}\sin(2\pi j/12)$, $Y_j \equiv i.i.d.$ uniform random variables on $[-\sqrt{3}, \sqrt{3}]$, and $Z_j \equiv i.i.d.$ random variables, with $Z_j = 1$ with probability P , and $Z_j = 0$ with probability $1 - P$. MIX(P indicates a mixture of deterministic and stochastic components.

2.3 Evaluation Study on HRV Signals

The database used for evaluation was recorded at the Miguel Servet University Hospital in Zaragoza (Spain), for the prediction of hypotensive events in elective cesarean delivery [27]. It consists of ECG signals from 11 women with programmed cesarean section recorded at a 1000 Hz sampling frequency immediately before cesarean surgery. Five of them suffered from hypotension during the surgery (Hyp) and 6 did not (NoHyp). The database used in this chapter represents a subgroup of the whole database, since clinicians continued recording signals during 3 years. In chapter 5, the clinical problem will be deeply assessed. In the meantime, novel D_2 estimates were considered to evaluate their capability to track some changes in ANS modulation moments before intervention.

RR time series of 5 minutes in lateral decubitus position were analyzed. Ectopic beats as well as missed and false detections were detected and corrected [116].

2.4 Results

2.4.1 Validation on Synthetic Time Series

Lorenz attractor series were used to validate the new proposed methodologies computed using the ℓ_∞ -norm. Figure 2.5(a) displays the SCF *log-log* curves for embedding dimensions m from 1 to 10. The sets of points, where the slope was evaluated according to [88], are displayed for different starting points. For each starting point, the corresponding set of points, $\hat{D}_{2(\perp),r}^m$, was selected by gradient descent approach. Figure 2.5(b) shows the slope estimation $\hat{D}_{2(\perp),r}^m$ versus m for each starting point. Figure 2.5(c) displays the D_2 estimate $\hat{D}_{2(\perp),r}$ versus $\log(r)$ for each starting point. The maximum $\hat{D}_{2(\perp),r}$ constitutes the novel D_2 estimate, $\hat{D}_{2(\perp)}$. Tab. 2.1 illustrates D_2 estimates through the three proposed approaches presented in this chapter. The three of them led to close results to the Lorenz attractor theoretical value of D_2 , being $\hat{D}_{2(\perp)}$ the closest one. Relative errors for \hat{D}_2 and $\hat{D}_{2(max)}$ were found above 4%, while for $\hat{D}_{2(\perp)}$ was just 1%; D_2 estimated, as described in [27], was also included for comparison purposes.

Table 2.1 Correlation dimension estimates for the different proposed approaches, using different norms for Lorenz attractor series (5000 samples).

Estimates	Lorenz attractor		
	ℓ_1	ℓ_2	ℓ_∞
D_2 [27]	1.95	1.94	1.93
D_2	1.69	1.70	1.93
$D_{2(\perp)}$	1.84	1.74	2.01
$D_{2(max)}$	1.99	1.71	1.93

Use of Norms in Proposed D_2 Estimates

Although the D_2 is considered norm-invariant [180], the selection of the norm in D_2 estimates deserves further attention when applied to a finite duration time series. The norm of the difference vector, $\Delta\mathbf{y}_{i,j}^m = \mathbf{y}_i^m - \mathbf{y}_j^m$, defines the distance $d_{i,j}^m$ in Eq. 2.2. Norms from ℓ_1 ($\|\cdot\|_1$) to ℓ_∞ ($\|\cdot\|_\infty$) could be selected. Left panel in Fig. 2.7 shows norm unity for ℓ_1 and for ℓ_2 .

In Fig. 2.7, the right panel shows how different norms shifts the *log-log* curves, losing the entire linear region in some cases when a fixed range of thresholds is used. In those cases, the range of these thresholds should be long enough to ensure that the linear regions are contained therein, thus, the election of the norm is linked to the range of the thresholds.

In the SCF approach, it is particularly important that the two asymptotic regions of the *log-log* curve should be reached. Therefore, the correct selection of the norm and the range of the set of thresholds are critical to assure the goodness of the SCF approach. Tab. 2.1 shows the D_2 estimates for 5000 sample length of Lorenz attractor series. The effect of different norms is reflected in the estimates, since the set of thresholds was fixed. As shown, the usage of ℓ_∞ -norm together with the considered fixed set of thresholds achieves closest values for the novel proposed estimates with respect to the theoretical D_2 value for the Lorenz attractor, 2.01. In the case of the approach used in [27], where self-comparisons were not considered on the computation, D_2 values was found lower than the theoretical value.

Hereinafter, due to the effect of different norms on D_2 estimation, all the results presented in this thesis were computed using the ℓ_∞ -norm.

MIX(P) processes were analyzed by considering P values of 0.1, 0.4, and 0.8. The greater the P value, the higher the level of randomness of the time series is. \hat{D}_2 was found increased as P increases, thus, these estimates can be considered as measures of the degree of randomness of the time series, as shown in Fig 2.8.

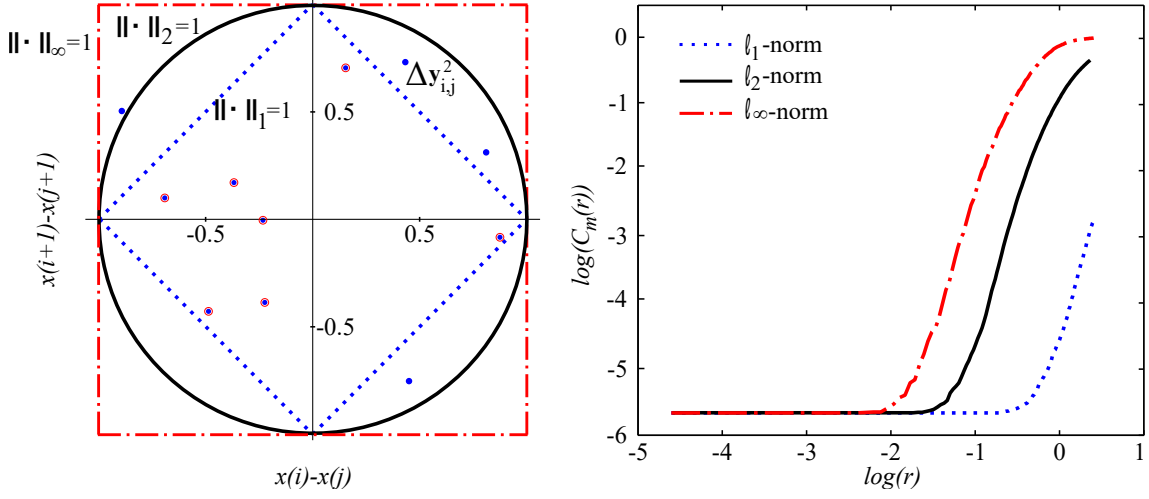


Figure 2.7 In the left panel, vector differences of any two reconstructed vectors for $m=2$, $\Delta\mathbf{y}_{i,j}^2$, are shown, where dotted circles and dashed lines represent the points whose ℓ_2 -norm and ℓ_1 -norm are equal to 1, respectively. The dots are the differences below ℓ_2 -norm unity and the dots with circles are below ℓ_1 -norm unity. In the right panel $\log\log$ curves of one HRV signal (300 samples) used in the study are shown for a $m = 10$ and ℓ_1 , ℓ_2 and ℓ_∞ norms.

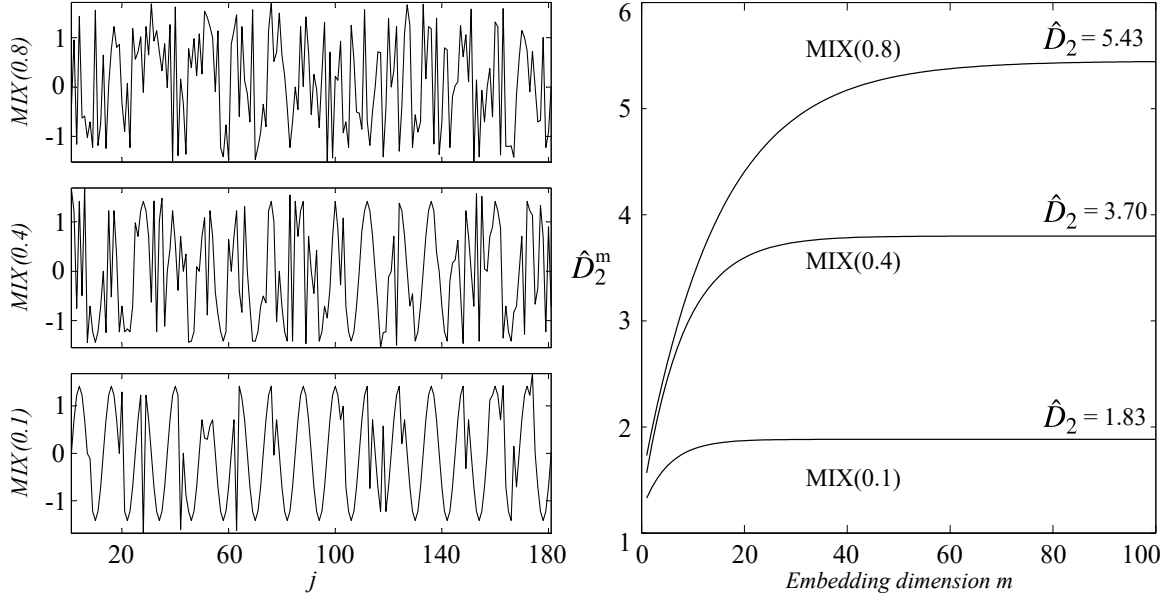


Figure 2.8 $\text{MIX}(P)$ signals with different degree of randomness and their correspondent estimation of the \hat{D}_2 .

2.4.2 HRV Time Series Results

Same database, as the one used in [27], was studied in this chapter. The results, shown in Tab. 2.2, are divided into hypotensive and non-hypotensive groups. As an example, Fig. 2.9 shows the RR time series of one woman of each group (left panel) and their $\hat{D}_{2(\perp)}$ estimate (right panel).

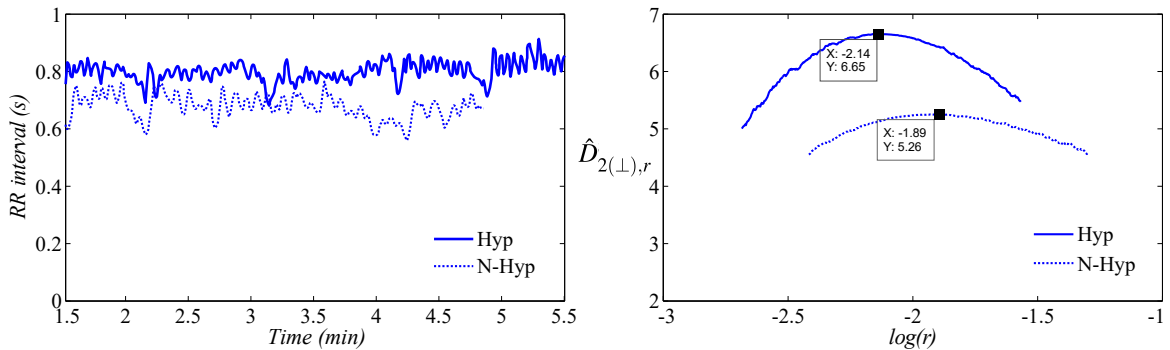


Figure 2.9 The left panel shows two RR intervals, one corresponding to a patient who developed a hypotensive event (Hyp) and the other to one who did not (N-Hyp); the right panel shows the $\hat{D}_{2(\perp)}$ estimation using the perpendicular points in the $\log\log$ curves.

Besides the approaches proposed in this paper, the sequential approach used in [27], referred to as classical, was added for the sake of comparison. The data distribution of the results was found to be not normal by the Kolmogorov-Smirnov test, and, therefore, the Mann-Whitney U test was applied. The differences between both groups for all estimates were found to be significant with a p -value lower than 0.03. In order to evaluate their discriminant power, comparing normotensive and hypotensive groups, a receiver operating characteristic (ROC) analysis was performed. The area under the ROC curve, accuracy, sensitivity, and specificity for all the indices were computed, see Tab. 2.3. Similar accuracy value with respect to the one reported in [27] was achieved by the proposed \hat{D}_2 estimate, whereas the proposals, based on the gradient descent and *SampEn* surface, were higher, reaching an accuracy of 90.9% in both cases.

2.4.3 Evaluation of the Computational Load

The computational time cost of the correlation sums depends on the length of the data to analyze, the maximum embedding dimension considered, and the number of thresholds used. The results shown in Tab. 2.4 correspond to the computational time cost, estimating correlation dimension on Lorenz attractor series by varying the data length (where $m = 1 - 16$ and $r = 0.01-3$ with 0.01 step size). The computational time required for a sequential approach is denoted by T_{Seq} , whereas the time required for the proposed technique, based on matrix operations to estimate correlation sums, is denoted by T_{MO} . The speed-up is defined as $S_p = T_{Seq}/T_{MO}$, which is the ratio between sequential and the proposed approach. As shown in Tab. 2.4, S_p was increased by one order of magnitude in the estimation of correlation sums on 5000- and 10000-sample time series with respect to 300-sample time series. It is worth noting that for a 300-sample time series, standard length for a 5-minute RR interval series, correlation sums were estimated in less than 1 s.

In table 2.4, the time cost was considered for the \hat{D}_2 estimation, but not for the other two novel proposals. Therefore, Tab. 2.5 shows the time required for the correlation dimension estimates

Table 2.2 D_2 estimated by different approaches for HRV signals (300 samples). Data expressed as median | interquartile range.

Estimates	HRV		
	Hyp	N-Hyp	p-value
D_2 [27]	5.9 0.6	4.4 1.3	0.03
\hat{D}_2	5.9 0.6	4.8 0.8	0.03
$\hat{D}_{2(\perp)}$	6.4 0.7	5.1 0.8	0.03
$\hat{D}_{2(max)}$	5.9 0.5	4.8 0.7	0.01

Table 2.3 ROC area for the nonlinear HRV analysis of all studied correlation dimension estimates for real data. Accuracy (Acc.), sensibility (Sen.), and specificity (Spe.) are expressed in percentage.

Estimates	ROC area	Acc.	Sen.	Spe.
D_2 [27]	0.90	81.8	71.4	100
\hat{D}_2	0.90	81.8	71.4	100
$\hat{D}_{2(\perp)}$	0.90	90.9	100	85.7
$\hat{D}_{2(max)}$	0.97	90.9	83.3	100

Table 2.4 Computational time of correlation sums estimated for Lorenz attractor series of different sample lengths. S_p is the speed-up achieved and defined as $S_p = T_{Seq}/T_{MO}$, where T_{Seq} is the time demand for a sequential algorithm and T_{MO} the time demand for the proposed technique, based on matrix operations.

N (samples)	T_{Seq} (s)	T_{MO} (s)	S_p
300	1086	0.9	≈ 1200
5000	$8.69 \cdot 10^5$	50	≈ 16000
10000	$3.63 \cdot 10^5$	300	≈ 12000

Table 2.5 Computational load for correlation dimension estimates by all proposed approaches analyzing Lorenz attractor series and HRV signals where ℓ_∞ -norm was selected. Data expressed as mean \pm standard deviation.

Time Estimate	Lorenz attractor (5000 samples)	HRV (300 samples)
T_{D_2} (s) [27]	$(8.86 \pm 0.35) \cdot 10^5$	3314 ± 180
$T_{\hat{D}_2}$ (s)	194 ± 29	4.66 ± 0.58
$T_{\hat{D}_{2(\perp)}}$ (s)	260 ± 38	214 ± 30
$T_{\hat{D}_{2(max)}}$ (s)	194 ± 29	4.30 ± 0.56

including the one used in [27]. To do so, 10 realizations of Lorenz attractor series were generated, whose initial conditions were randomly chosen. It is noticeable that the time cost of $\hat{D}_{2(\perp)}$ was higher compared to the others in both cases, the Lorenz series and the HRV signals (11 subjects), since sets of slope estimations per *log-log* curve to compute correlation dimension are considered. Each of the

different sets of thresholds was associated with an r value within an interval centered on the maximum slope for $m = 1$. The boundaries of this interval were defined taking into account a decrease of 50% in the amplitude of the maximum slope value by considering the SCF first derivative. The more abrupt the transition zone in the sigmoid, the lower the amount of starting points. Thus, different number of points were considered on each realization, leading to computational time variations.

2.5 Discussion

In this chapter, a methodological framework was proposed to compute the D_2 of a finite duration time series and also to reduce the computational time cost of the estimation. A new approach for estimating the slope of the linear region from the *log-log* curves was proposed, fitting *log-log* curves through sigmoid ones. Finally, D_2 was estimated, exploiting the asymptotic value of an exponential relationship between \hat{D}_2^m and m .

One important limitation for the application of D_2 on HRV analysis is the long computational time required for the correlation sums. In an attempt to solve this problem, an algorithm has been proposed based on matrix operations. In [205], another approach was described based on parallel computing, which also decreased the time demand with respect to the sequential approach. Nevertheless, the computational times, achieved in the present work, were obtained with a regular computer (Windows® 7 based PC, Intel® Core i7 3.5 GHz, 16 Gb RAM with Matlab® R2011a). As an example, for a signal of 300-sample length (a usual length in typical 5 min HRV analysis, ≈ 300 beats), the time demand was reduced with respect to the sequential approach from 18 minutes to 1 second, which allows the on-line computation of D_2 in clinical practice.

Another limitation for the D_2 estimation is the reliability. Non-stationary data can lead to an unreliable measurement of D_2 . Regarding this problematic issue, several techniques, attempting to characterize dynamical systems, have been reported [180, 190, 205]. Searching the linear region of the *log-log* curves becomes a difficult challenge, when the system is non-stationary, since more than one linear region could appear and classical D_2 estimate would be unreliable. The SCF approach is robust against those cases, since no estimate is provided when fitting is not good enough, below to 0.8 of determination coefficient.

The novel approaches, proposed in this thesis regarding estimation of D_2 , use the SCF approach. $\hat{D}_{2(\perp)}$ exploits the fact that the linear regions of the *log-log* curves tend to be parallel when embedding dimension increases. This allows the consideration of a set of points surrounding the maximum slope point, and therefore, several D_2 estimates are obtained for these starting points. $\hat{D}_{2(max)}$ is based on the differences between two consecutive *log-log* curves, defining the $SampEn_{i-j}$ surface. This surface showed maximum values for each embedding dimension, m , and a specific threshold, r , providing another estimation of the D_2 , $\hat{D}_{2(\perp)}$. This estimation was found to be the closest to the theoretical D_2 for the Lorenz attractor, resulting in a relative error of 4%, considering 5000-sample size and for a differential equation resolution of 0.01.

D_2 is known to be a surrogate of the fractal dimension of a chaotic attractor [60]. However, when applied to finite duration time series, nonzero finite D_2 values do not imply the existence of an underlying chaotic attractor. For example, when applied to MIX(P) processes, nonzero finite D_2 values were obtained, the higher the value was as much as the random content. Thus, although D_2 could not be interpreted as the fractal dimension of an underlying chaotic attractor, in this case, it still provides a measure of the complexity of the process, at least regarding its unpredictability.

D_2 estimate in HRV signals may shed light on the degree of complexity of the ANS regulation. The group of women (Hyp) suffering from hypotension during a programmed cesarean section under spinal anesthesia showed higher D_2 values than the group who did not (N-Hyp), at least when evaluated during lateral decubitus position. All the proposed correlation dimension estimates not only maintain the accuracy obtained in [27], but they increased it. Predicting hypotension is a challenge, since it occurs in the 60% of the cases and may lead to fetal stress [42]. On one hand, estimates that performed 100% of specificity, D_2 [27], \hat{D}_2 , and $\hat{D}_{2(max)}$, may provide clinicians valuable information to apply prophylaxis to any woman that might potentially suffer from a hypotensive event. On the other hand, estimates that performed 100% of sensitivity, $\hat{D}_{2(\perp)}$, may provide information about the usage of prophylaxis on the less number of patients to prevent hypotension. The effect of prophylaxis on patients who finally are not going to suffer from a hypotensive event and its relation with fetal stress deserves further studies. This clinical study will be deeply assessed in chapter 5.

2.6 Conclusion

The contribution of this chapter is the introduction of a novel methodological framework for a reliable estimation of the correlation dimension from a limited time series, such as HRV signals. Three alternatives for estimating correlation dimension were proposed. Sigmoid curve fitting was used to assess the slope of the linear region of the *log-log* curves based on considering self-comparisons. The computational speed-up achieved may allow considering correlation dimension for monitoring in clinical practice. Nevertheless, the main limitation for the application of these methodologies to HRV analysis lies in its relation to the underlying physiology, which is still unclear and needs further studies. In spite of the fact that the framework proposed in this chapter focuses on the characterization of HRV signals, its applicability could be extended to a wide range of fields.

*"I am enough of the artist to draw
freely upon my imagination.
Imagination is more important than
knowledge. Knowledge is limited.
Imagination encircles the world."*

- Albert Einstein (1879-1955) -

3

Nonlinear HRV Measurement Dependencies

Summary

The purpose of this study is to characterize the influence of mean HR on nonlinear HRV indices. The hypothesis is that HR, which is considered the intrinsic sampling rate of HRV signal, may influence nonlinear HRV indices, leading to biased ANS modulation information.

3.1 Introduction

In the previous chapter, a framework for improving D_2 estimation was presented. Using this methodology, sample and approximate entropy can be concomitantly computed, since they are also based on correlation sums (see section 1.4.3 and 2.1.3). Despite the improvements achieved in terms of estimation reliability and computational load, these nonlinear indices still require further analysis for their application to HRV analysis.

The physiological interpretation of HRV as a marker of ANS activity may be misled by how intrinsic pacemaker cells and ANS activity are expressed in HRV [194]. The nonlinear relationship between temporal and complexity HRV indices with respect to HR has been addressed, emphasizing the importance of attenuating this effect [202, 146, 123, 195]. Furthermore, different mathematical models have demonstrated a relationship between HRV amplitude and HR, and alternatives to correct it [33, 121, 8, 159, 150, 19].

Nonlinear indices, such as D_2 , *SampEn*, and *ApEn* are computed over linearly detrended and normalized series, so this effect on HRV amplitude is already compensated for [135, 143, 148, 187, 22]. Despite this normalization, HR may still influence nonlinear HRV indices, due to the fact that HR is the intrinsic sampling rate of HRV signal. This implies that the amount of information captured during the same time interval depends on HR. Alternatives to increase nonlinear index reliability (e.g. increasing data length), such as interpolating RR time series, have been used [180, 135, 64, 152, 79, 94]. However, the reported dependence of nonlinear indices on data length may compromise the comparison between different studies[67]. Our hypothesis is that the influence of HR, as sampling rate, on nonlinear HRV indices is still noticeable even when the same data length is considered.

To summarize, in this chapter the assessment of HR influence on nonlinear HRV indices is tackled. To do so, a simulation study is carried out emulating ANS conditions of healthy subjects during resting supine position. Since this HR influence might mislead the physiological interpretation of nonlinear HRV indices in terms of ANS evaluation, alternative methods are proposed to attenuate this effect. Finally, the methodology is applied to evaluate a body position changes database consisting of supine and standing position.

3.2 Materials

3.2.1 Fantasia Database

Twenty young rigorously-screened healthy subjects underwent 120 min of supine resting while continuous ECG and RP signals were recorded at 250 Hz while watching the movie Fantasia (Disney 1940), to help maintain wakefulness. Further database information is available elsewhere [77] and can be downloaded from <http://www.physionet.org/> [59].

3.2.2 BPC Database

This database was developed collaboratively at Harvard Medical School, Massachusetts Institute of Technology, and the Favaloro Foundation Medical School. The whole cohort of short-term recordings comes from two data collecting studies. Further details of this database can be found in [175].

First Study: Thirteen male subjects of age 21.6 ± 4.4 years (Mean \pm SD; range, 19-38 years) with no history of cardiopulmonary disease participated in a study carried out at Clinical Research Center at the Massachusetts Institute of Technology, USA.

Second Study: It comprises groups of subjects of different ages. The database was created to evaluate the effect of age distinguishing three ranges. In this thesis, only the young group was included (9 subjects, 26.7 ± 4.7 years; range, 20-35 years).

Thus, subjects from the first and second study were selected, being 22 subjects. Two recordings per subject were acquired containing 7-min ECG and respiration (RP) signals, sampled at 360 Hz. The protocol included postural changes. First, ECG and RP signals were recorded while subjects were in supine position. Then, subjects changed to standing position and after 5 min, to allow reaching hemodynamic equilibrium, ECG and RP signals were recorded in standing position. Subjects were asked to breathe following an irregular sequence of tones.

3.2.3 Simulation Study

A simulation study was conducted to assess the mathematical relationship between HR and nonlinear HRV indices. The simulation study was carried out based on a HRV representation through the IPFM model. This model assumes that ANS influence on the sinoatrial node can be represented by a modulating signal, $\mathfrak{M}(t)$ [115]. According to this model, when the integral of $1 + \mathfrak{M}(t)$ reaches a threshold, T , a new heartbeat is generated at time instant $t(k)$. Threshold T represents the inverse mean HR.

Fantasia database was selected to compute modulating signals, according to the following procedure. Assuming that $\mathfrak{M}(t)$ is causal, band-limited and $\mathfrak{M}(t) < 1$ then, the instantaneous HR can be described as:

$$d_{HR}(t) = \frac{1 + \mathfrak{M}(t)}{T} \quad (3.1)$$

Instantaneous heart rate $d_{HR}(t)$ is obtained from the heartbeat times, $t(k)$, based on the IPFM model [116], and sampled at 4 Hz. A time-varying mean heart rate $d_{HRM}(t)$ is computed by low pass filtering $d_{HR}(t)$ with a cut-off frequency of 0.03 Hz. The heart rate variability signal is obtained as $d_{HRV}(t) = d_{HR}(t) - d_{HRM}(t)$. Finally, the modulating signal, $\mathfrak{M}(t) \approx d_{HRV}(t)/\overline{d_{HRM}(t)}$ [8], that is the HRV signal corrected or normalized by the mean HR.

Spectral analysis was applied to 5-min modulating signals $\mathfrak{M}(t)$ by Welch periodogram. Frequency domain indices were estimated based on spectral bands (LF band from 0.04 to 0.15 Hz and HF band from 0.15 to 0.4 Hz). Respiratory frequency was checked to be within the HF band.

Among all modulating signals, only those which presented one marked peak on each band (LF and HF band) were selected for the simulation study. Spectral indices such as the powers and the frequency peaks were used to generate synthetic stochastic modulating signals using an autoregressive moving average (ARMA) technique [134]. A total of one hundred 5-min segments were selected and their spectral indices were used to feed the ARMA model. A total of $M = 50$ stochastic modulating signals $\mathfrak{M}^j(t)$ with $j = 1, \dots, M$, were simulated for each $\mathfrak{M}(t)$, where the stochastic content was modeled in the moving-average term by zero-mean unit variance white noise. Figure 3.1 shows the spectra of 50 stochastic realizations, their median spectrum and one of the segment-recording they are based on.

Then, the IPFM model was applied to each stochastic realization, varying the parameter T_n , where $n = 1, \dots, 16$, corresponding to T from 0.46 to 1.1 s in steps of 0.04 s, to simulate the heartbeat occurrence times, $t_{T_n}^j(k)$. In this way, simulated 300-sample RR series are generated, where ANS modulation is independent of changes in mean HR. Simulation scheme is illustrated in Fig. 3.2. D_2 , $SampEn$ and $ApEn_{max}$ were computed over these simulated RR time series.

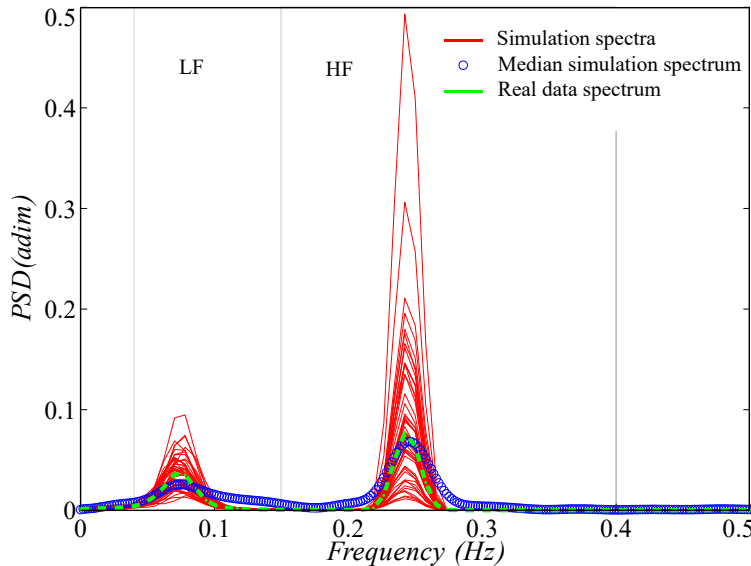


Figure 3.1 Spectra derived from 50 stochastic realizations of simulated modulating signals during supine conditions (data simulates subject conditions from Fantasia database) applying ARMA technique fixing LF and HF spectral content (red lines). Average spectrum is shown in circles (blue) and spectrum belonging to real data in dashed line (green).

Another simulation was done based on the BPC database characteristics. However, since subjects were asked to breathe following an irregular sequence of tones, the spectral analysis did not reveal dominant peaks on HF band, evaluating all subjects. The ARMA model was fed, on one hand,

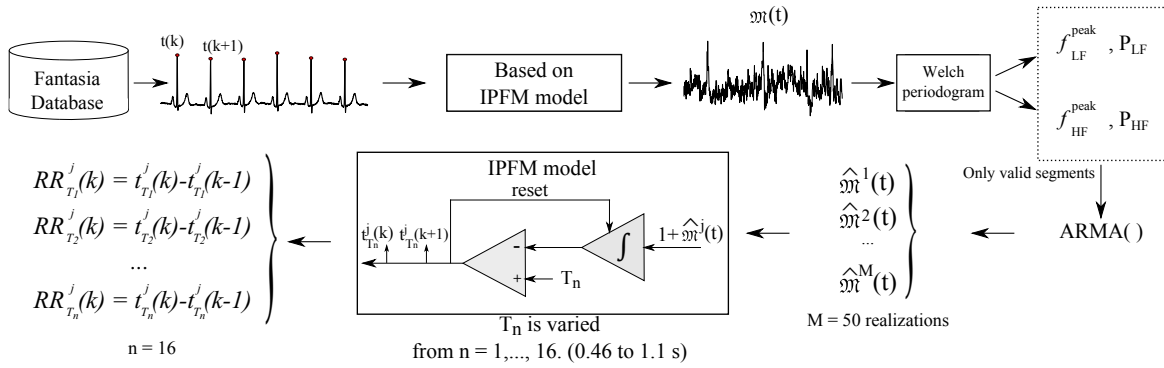


Figure 3.2 Simulation data scheme is illustrated. Heartbeat time occurrences are detected from ECG. Based on the IPFM model the ANS modulating signal $\mathfrak{M}(t)$ is estimated. Spectral analysis by Welch periodogram is computed on $\mathfrak{M}(t)$ in order to estimate the parameters needed for the simulation, frequency and power of LF and HF components, which are used to construct a new set of modulating signals, $\mathfrak{M}_j(t)$, through ARMA technique, with $M = 50$ realizations. Then, IPFM model is used to generate simulated heartbeat occurrences $t_{T_n}^j(k)$ with different values of T from 0.46 to 1.1 s. Simulated RR series are computed from the $t_{T_n}^j(k)$.

by the power spectral density from LF and HF bands and, on the other hand, by the middle band frequencies of LF and HF, 0.095 and 0.275 Hz respectively. Then, modulating signals were simulated from spectral indices derived from supine and upright positions. This extends the analysis of HRV dependence on HR under enhanced sympathetic activity.

3.3 Evaluation by Nonlinear Techniques

ECG preprocessing: Because the reliability of the HRV analysis can be compromised by low sampling frequency of ECG recordings [120], the ECGs belonging to BPC and Fantasia databases were interpolated by cubic splines to a frequency of 1080 and 1000 Hz, respectively. Then, heartbeat times, $t(k)$, where k symbolizes the k^{th} beat, were estimated using an ECG wavelet-based detector [114]. Ectopic beats were identified imposing a time-varying threshold on instantaneous heart rate variations. Then, these ectopic beats were corrected using the IPFM model, as described in [116].

3.3.1 Correlation Dimension

Correlation dimension, D_2 , measures the degree of complexity of the system that generates the time series [60]. In the previous chapter 2, techniques to improve the estimation of D_2 were introduced. On that study, *log-log* curves (logarithm of correlation sums vs. logarithm of thresholds) were fitted to sigmoid curves, thus, increasing the accuracy of maximum slope estimation. Moreover, another estimate of D_2 denoted as $D_{2(\max)}$ based on the points that maximize the difference between each pair of sigmoid curves was presented. Both D_2 and $D_{2(\max)}$ were computed by varying $m = 1\text{-}16$ and $r = 0.01\text{-}3$ in steps of 0.01.

3.3.2 Approximate and Sample Entropy

SampEn and *ApEn* are irregularity measurements of the time series [140]. Although both entropies are closely related to each other, *SampEn* was introduced to overcome the self-pairs-related limitation of *ApEn* computation. Briefly, patterns of time series values (reconstructed vectors) of a certain length (embedding dimension, m) are compared to the rest of the possible pattern candidates. Those comparisons, whose differences are below a threshold r , are summed up and used to calculate correlation sums. The final entropy value measures the changes produced when increasing the length of the patterns in one unit. The parameters m and r have to be previously defined to estimate these entropy values. In this chapter, parameter values are set to $m = 2$ and $r = 0.15$ for *SampEn*.

The computation of approximate entropy recalls the definition to estimate correlation dimension. But in this case, time series of interest is normalized by its standard deviation. In this approach, correlation sums are modified with respect to the ones used by correlation dimension as follows:

$$C_i^m(r) = \frac{1}{N_m} \sum_{j=1}^{N_m} H(r - d_{i,j}^m) \quad (3.2)$$

where $C_i^m(r)$ is the correlation sum and H is the Heaviside function 2.4; the amount of reconstructed vectors is $N_m = N - (m - 1)$ for each embedding dimension, m ; and the distance, computed by the ℓ_∞ norm, between each pair of reconstructed vectors, $\mathbf{y}_i^m, \mathbf{y}_j^m$, is denoted as $d_{i,j}^m$.

This procedure is repeated with all reconstructed vectors and the probability of a pattern of length, m , appearing along the time series is denoted by:

$$\phi^m(r) = \frac{1}{N_m} \sum_{i=1}^{N_m} \log(C_i^m(r)) \quad (3.3)$$

ApEn provides information about how regular the time series is when two consecutive length patterns are compared:

$$ApEn(m, r) = \phi^m(r) - \phi^{m+1}(r) \quad (3.4)$$

For the further *ApEn* estimations, the embedding dimension was set to $m = 2$. A graphical interpretation of *SampEn* and *ApEn* estimation, based on Eq. 2.11 and Eq. 3.4 respectively, is shown in Fig. 3.3.

Maximum Approximate Entropy, $ApEn(m, r_{max}(m))$

Figure 3.4 shows an example of the dependence of *ApEn* estimate on threshold r , when embedding dimension m is fixed, by analyzing a 2000-sample Lorenz attractor time series.

Here, threshold values used in the literature, varying commonly between 0.1 and 0.2, provides an underestimation of *ApEn* value, whereas the proposed methodology is able to provide the maximum

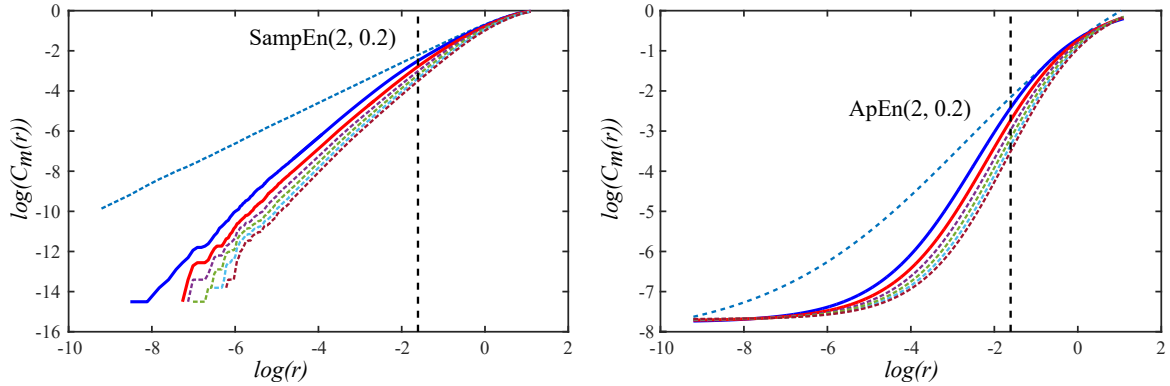


Figure 3.3 Graphical representation of *SampEn* and *ApEn* computation. The vertical dashed lines in both panels illustrates the threshold value as $r = 0.2$. To compute *SampEn*(2, 0.2) and *ApEn*(2, 0.2) the lost of probability as embedding dimension increases is evaluated, therefore, differences of solid lines, $m = 2$ and $m = 3$, are considered.

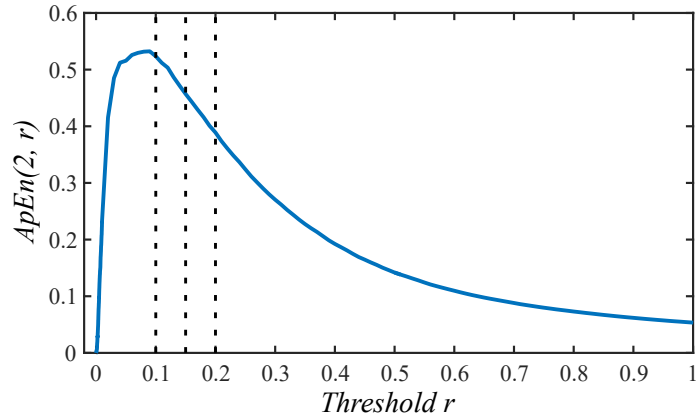


Figure 3.4 Dependence of *ApEn* on threshold r . Example of *ApEn* estimation using the proposed methodology for correlation dimension described in chapter 2. Vertical dotted lines indicate the three most common threshold values, $r = 0.1$, 0.15 , and 0.2 . Data analyzed extracted from a 2000-sample time series of Lorenz attractor system.

value which it is not found in the *SampEn* estimation as a consequence of considering self-comparisons [117].

As mentioned before, the framework for estimating correlation dimension, described in chapter 2, was used to obtain: the value of the threshold r that maximizes *ApEn* for a given value of m , denoted by $r_{max}(m)$ [196, 155]; and the maximum entropy value for a given value of m , $ApEn(m, r_{max}(m))$. In particular, $ApEn(2, r_{max}(2))$ and $SampEn(2, 0.2)$ were considered for further analysis.

3.4 Nonlinear Indices Dependence on HR as Sampling Rate

The methodology used to compute nonlinear HRV indices, considered in this study, was applied to linearly detrended and normalized RR time series. The detrending ensures that mean HR values are

removed from the series, whereas the normalization eliminates the influence of mean HR on HRV amplitude. Despite this fact, the effect of mean HR, as sampling rate, might still be present on them. In this section, this effect is investigated on the simulation study, where changes in mean HR are independent from changes in ANS modulation. First, a mathematical relationship between nonlinear HRV indices and HRM is assessed by two regression formulas; then, a HR-correction is proposed based on these formulas. Second, alternatives based on interpolation of RR series and instantaneous mean RR, provided by point-process model, are proposed for attenuating the sampling rate influence of mean HR on nonlinear HRV indices.

3.4.1 Regression Formulas

In order to explore the relationship between nonlinear HRV indices and HR, the following regression models were proposed.

$$X = \beta + \alpha RR \text{ (Linear),} \quad (3.5)$$

$$X = \beta (RR^\alpha) \text{ (Parabolic),} \quad (3.6)$$

where $X \in \{D_2, SampEn, ApEn\}$ and α and β are regression coefficients.

Based on the former models, HR-correction formulas were obtained by projecting each nonlinear index onto a standard level of $RR = 0.5$ s, hence:

$$\text{Linear : } X_{C1} = X + \xi (0.5 - RR), \quad (3.7)$$

$$\text{Parabolic : } X_{C2} = X \left(\frac{0.5}{RR} \right)^\xi, \quad (3.8)$$

where ξ is the correction factor.

Transformation of X_{C1} or X_{C2} and RR into linear relationship was used to compute Pearson's correlation coefficient ρ . Then, optimization was assessed by total least squares, providing correction factors by a golden cut search algorithm to minimize $\rho(\xi)$.

Correction factors were computed on each stochastic realization. Thus, subject-specific correction was defined, considering the correction factors of the 50 stochastic realization for each modulating signal and computing the median of the HR-corrected indices.

Furthermore, a unique correction parameter was additionally computed, considering all stochastic realization for all modulating signals. In that case, the transformation and optimization technique, described above, was applied to obtain median values for each nonlinear index, thus, defining a median correction approach to obtain X_{C1}^ξ and X_{C2}^ξ .

3.4.2 Interpolation

RR series are unevenly sampled, being the HR its sampling rate. This implies that the number of data information for the same time interval is dependent on HR. On the other hand, it is known that estimation of nonlinear indices, such as D_2 , *SampEn*, and *ApEn*, are data length dependent [67]. Therefore, interpolating RR time series at the same sampling rate may alleviate the influence of mean HR on nonlinear HRV indices, since it allows considering the same number of data for the same time interval. Interpolation at 2, 4 and 8 Hz were studied (X_{I2} , X_{I4} , and X_{I8} respectively).

3.4.3 Point-process

Point-process modeling: Another alternative to overcome the dependency of RR time series on HRM is based on the point-process paradigm, where derived time series resolution is not related to HRM. Point-process model provides a probabilistic framework to characterize the stochastic properties of the beat-to-beat RR time series [10]. It is based on the assumption that the beat generation events follow a probability distribution, in particular, the inverse Gaussian probability distribution. In this study, history dependence of previous events was considered. Thus, the distribution is named history-dependence inverse Gaussian distribution:

$$f(t|H_{t(k)}, \boldsymbol{\theta}) = \left[\frac{\theta_{p+1}}{2\pi(t-t(k))^3} \right]^{\frac{1}{2}} \exp \left(-\frac{\theta_{p+1}(t-t(k)-\mu(H_{t(k)}, \boldsymbol{\theta}))^2}{2\mu(H_{t(k)}, \boldsymbol{\theta})^2(t-t(k))} \right) \quad (3.9)$$

where $t(k)$ represents the time occurrence of the k^{th} heartbeat,

$H_{t(k)} = \{t(k), RR(k), RR(k-1), \dots, RR(k-p+1)\}$ the elements involved in the history-dependence of p order of previous beats and $RR(k) = t(k) - t(k-1)$ the RR values.

The estimation of $\boldsymbol{\theta}$ parameters is carried out by considering the local maximum-likelihood within a time interval l ($l = 60$ s for this study). This interval should be long enough to obtain an estimate of $\mu(H_{t(k)}, \boldsymbol{\theta})$ that represents the behavior of the beat-to-beat time series. Statistical Kolmogorov-Smirnov test is used to measure the goodness-of-fit, comparing heartbeat events $t(k)$ and the ones obtained after time-rescaling derived from the point-process model [203]. The parameters $\boldsymbol{\theta}$ are updated by shifting the estimation interval, Δ ms, which is considered the point-process resolution, see Fig. 3.5.

Therefore, the instantaneous mean RR can be defined as:

$$\mu(H_{t(k)}, \boldsymbol{\theta}) = \theta_0 + \sum_{j=1}^p \theta_j RR(k-j+1) \quad (3.10)$$

Ectopic-free RR time series were obtained by a point-process model based on the methodology described in [36]. Instantaneous mean RR was computed by setting a resolution of $\Delta = 50$ ms, trying to capture the effect of right censoring, described as the influence of the next event out of the analysis

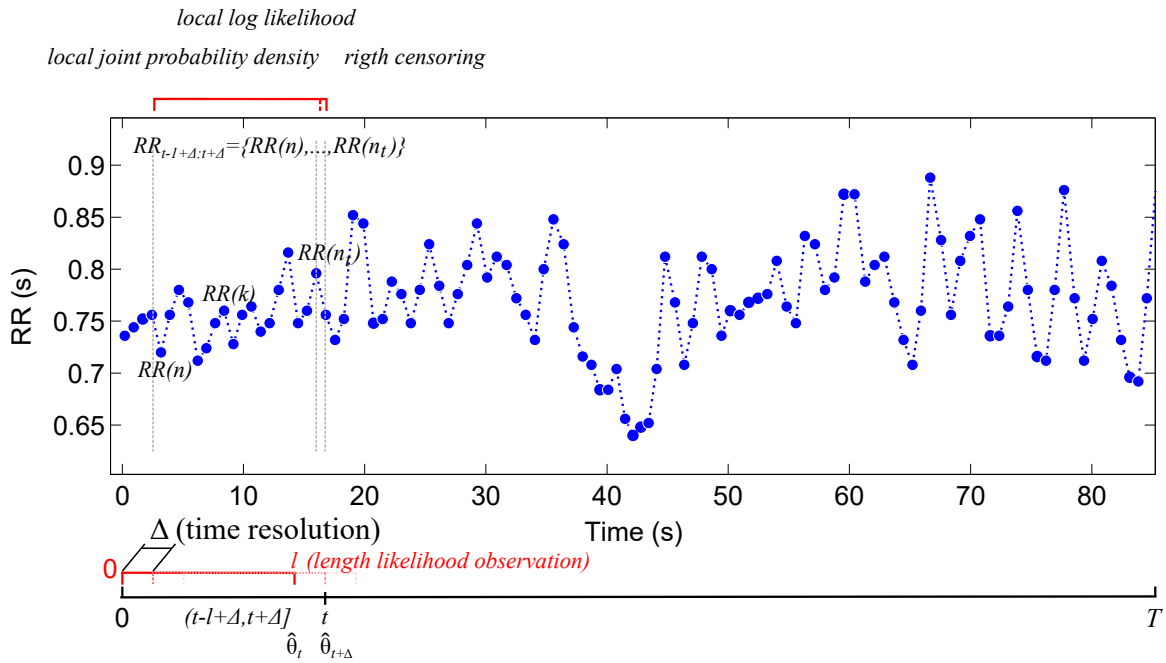


Figure 3.5 Graphical representation of the intervals for estimation of θ_t using the local log likelihood.

window, and a model order of $p = 12$, set as a trade-off to represent subject resting conditions from Fantasia database and supine and standing conditions from BPC database [5].

The nonlinear indices considered on this study are commonly computed over raw RR time series. The embedding dimension, m , needs to be reviewed for the analysis of point-process derived time series, since it is related to the number of events in the raw RR time series. In order to compare nonlinear HRV indices computed from the point-process instantaneous mean RR with those computed from the interpolated RR time series, the embedding dimension was scaled by a factor, depending on the point-process model resolution.

$$m_{adap} = m \frac{\Delta_{2Hz}}{\Delta_{XHz}} \quad (3.11)$$

where m values $\in \{1, \dots, 16\}$, Δ_{2Hz} is the resolution of RR time series interpolated at 2Hz corresponding to 500 ms, and Δ_{XHz} refers to the new resolution of the RR time series at sampling rate of X Hz corresponding to $\frac{1}{X}$ s.

For instance, embedding dimension m is set as 2 for maximum approximate entropy for interpolated RR time series at 2 Hz. Then, the computation of the same index over derived point-process time series at 50 ms resolution needs to adapt the embedding dimension value by a factor of 10 to represent the same information.

3.5 Statistical Analysis

Kolmogorov-Smirnov test was used to test the normality of data distributions and Mann-Whitney U-test or paired T-test were used, according to data normality. Furthermore, Pearson correlation was used to assess linear correlation between corrected nonlinear HRV indices and RR. $p < 0.05$ was considered as statistically significant.

Bland-Altman plots were used to analyze the agreement of subject-specific vs. median correction formulas. The intraclass correlation coefficient (ICC) was computed by SPSS for Windows, Version 15.0. Chicago, SPSS Inc.

3.6 Results

3.6.1 Nonlinear HRV Indices and Mean HR Reflect Body Position induced Changes

Nonlinear HRV indices, D_2 , *SampEn*, and $ApEn(2, r_{max}(2))$, were computed for the BPC database, considering 300-sample segments. All of them were found significantly higher in supine than in standing position (see Fig. 3.6 b)). Mean RR was also significantly higher in supine than in standing position (Fig. 3.6 a)), which might explain the statistical differences observed in the computed nonlinear HRV indices.

3.6.2 Nonlinear HRV Indices and RR Relationship by Simulation Study

The relationship between nonlinear HRV indices and RR was assessed in the simulation study, where RR was changed remaining ANS modulation. Nonlinear HRV indices computed from simulated data are illustrated in Fig. 3.7 (median values shown as blue circles). The correlation of nonlinear indices and mean RR was evaluated by Pearson correlation coefficient, finding high correlation for a wide range of median index values, being these ranges 3.5-5.02 for D_2 , 0.42-1.02 for *SampEn*, and 0.72-1.24 for $ApEn(2, r_{max}(2))$, see Table 3.1.

HR-Corrected Nonlinear Indices by Regression Formulas

Regression formulas were applied to the nonlinear HRV indices derived from each simulated modulating signal (subject-specific approach), providing corrected indices with minimal mean RR correlation. The obtained HR-corrected nonlinear indices are shown in Fig. 3.7 (median values by taking into account all segments, in triangles right and left for linear and parabolic regressions, respectively). The application of correction formulas provided nonlinear HRV indices where the effect of mean RR values was attenuated. The range covered by them was highly reduced, being in this case 3.81-3.95 for D_2 , 0.57-0.61 for *SampEn*, and 0.8-0.9 for $ApEn(2, r_{max}(2))$, see Table 3.1.

A set of correction factors (median approach) was obtained by considering the median of all nonlinear index values for each heart rate and computing global correction parameters (Table 3.1).

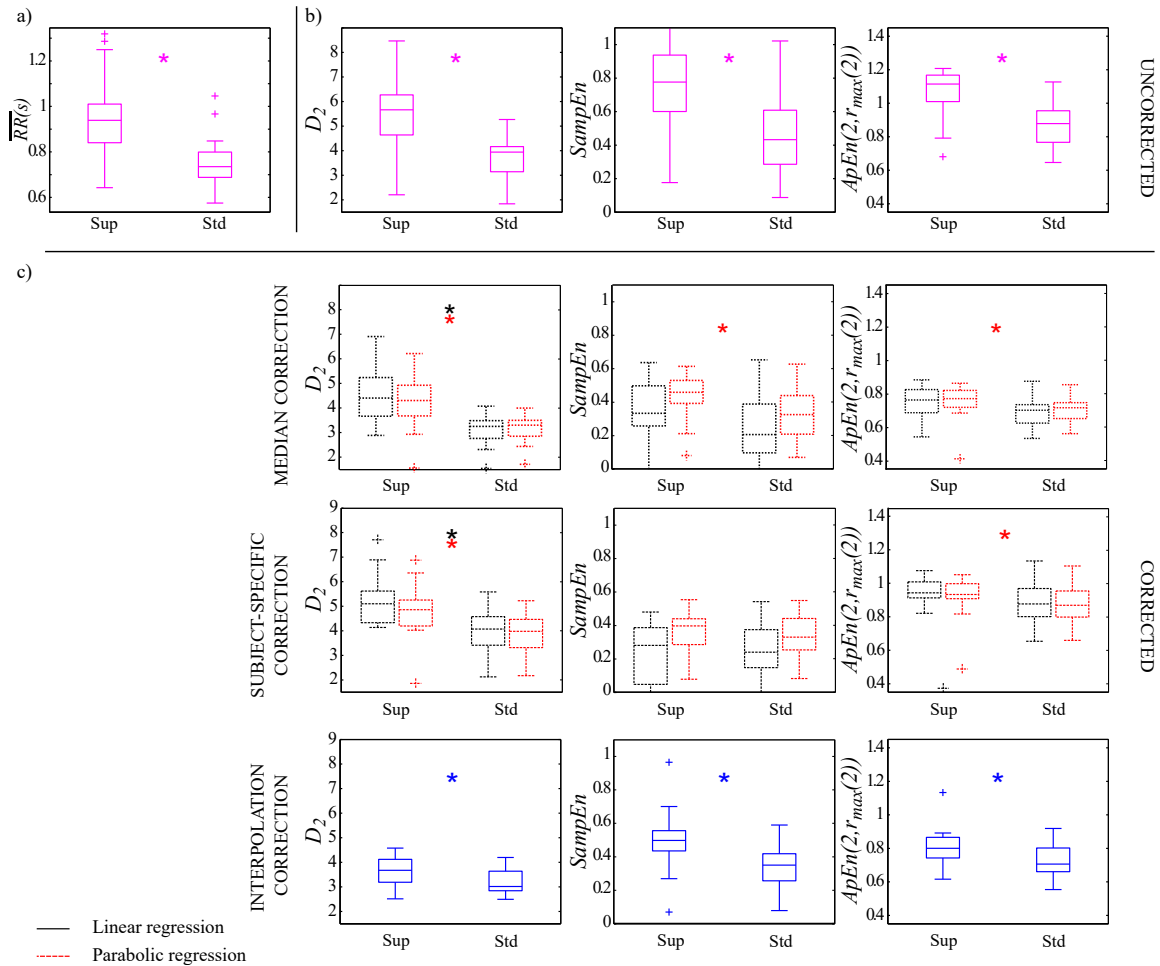


Figure 3.6 BPC database (22 subjects) was analyzed in which supine and standing positions were compared. (a, b) illustrate mean RR and uncorrected nonlinear HRV indices while c) shows HR-corrected nonlinear HRV indices. * indicates $p < 0.05$ by Mann-Whitney U-test between supine (Sup) and standing (Std) positions.

To evaluate the agreement between subject-specific vs. median correction approaches, the intraclass correlation coefficient (ICC) of data distributions was analyzed. It was found above 0.8 for all HR-corrected nonlinear indices and for both proposed regression formulas. The Bland-Altman plot in Fig. 3.8 illustrates the difference between linear and parabolic approaches for D_2 , $SampEn$, and $ApEn(2, r_{max}(2))$.

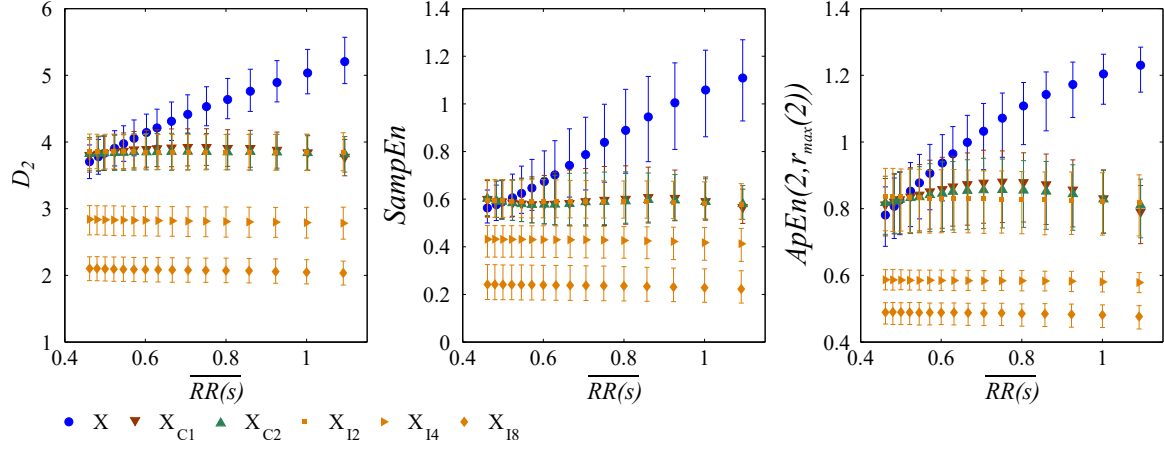


Figure 3.7 Nonlinear HRV indices computed from simulation study, $X \in \{D_2, \text{SampEn}, \text{ApEn}(2, r_{\max}(2))\}$, varying mean heart period, distribution of all uncorrected nonlinear HRV indices are shown in (blue) circles, corrected by linear regression in (brown) down triangles, corrected by parabolic regression in (green) up triangles, both former cases only subject-specific correction value of non-linear indices for each RR were shown. Finally, HR-corrected nonlinear indices by interpolating RR time series at 2, 4, and 8 Hz in (orange) diamonds. Data corresponds to all simulations derived from Fantasia database. Data distributions are represented by median and interquartile range.

Table 3.1 Pearson correlation factor ρ and p -values of nonlinear indices and RR obtained from simulation study. Linear and parabolic dependence of nonlinear indices on RR were evaluated. Coefficient of determination (R^2) as well as Pearson correlation factor and p -values (considering subject-specific and median correction) and ξ correction factor are presented for both regressions. Pearson correlation factor ρ and p -values of nonlinear indices and RR obtained, interpolating the simulated RR time series at 2 Hz. Data are shown as median \pm interquartile range.

Uncorrected		D_2		SampEn		$\text{ApEn}(2, r_{\max}(2))$	
ρ		0.959 ± 0.068		0.947 ± 0.1		0.949 ± 0.074	
p -value		0.0002 ± 0.0015		0.0004 ± 0.0044		0.0003 ± 0.0022	
$\text{Median} \pm \text{IQR}$		4.26 ± 0.7		0.72 ± 0.30		0.98 ± 0.26	
Regression Formulas							
Subject-specific		Linear		Parabolic			
Subject-specific		D_{2C1}	SampEn_{C1}	$\text{ApEn}(2, r_{\max}(2))_{C1}$	D_{2C2}	SampEn_{C2}	$\text{ApEn}(2, r_{\max}(2))_{C2}$
R^2		0.919 ± 0.129	0.896 ± 0.186	0.902 ± 0.139	0.923 ± 0.129	0.896 ± 0.179	0.910 ± 0.125
$\rho(-10^{-5})$		0.013 ± 0.20	0.016 ± 0.21	-0.0051 ± 0.20	-0.016 ± 0.20	0.0109 ± 0.20	0.01 ± 0.20
p -value		1 ± 0	1 ± 0	1 ± 0	1 ± 0	1 ± 0	1 ± 0
$\text{Median} \pm \text{IQR}$		3.88 ± 0.07	0.59 ± 0.02	0.85 ± 0.04	3.85 ± 0.02	0.59 ± 0.01	0.84 ± 0.03
Median correction		D_{2C1}^ξ	SampEn_{C1}^ξ	$\text{ApEn}(2, r_{\max}(2))_{C1}^\xi$	D_{2C2}^ξ	SampEn_{C2}^ξ	$\text{ApEn}(2, r_{\max}(2))_{C2}^\xi$
R^2		0.997	0.988	0.970	0.999	0.990	0.982
$\rho(-10^{-5})$		-0.787	-0.109	-0.051	0.661	0.232	0.061
p -value		1	1	1	1	1	1
$\text{Median} \pm \text{IQR}$		3.88 ± 0.07	0.59 ± 0.02	0.85 ± 0.05	3.85 ± 0.02	0.59 ± 0.01	0.84 ± 0.03
ξ Correction factor		2.068	0.869	0.541	0.375	0.813	0.417
2 Hz Interpolation		D_{2I2}		SampEn_{I2}		$\text{ApEn}(2, r_{\max}(2))_{I2}$	
ρ		-0.47 ± 1.41		-0.39 ± 1.09		-0.29 ± 0.77	
p -value		0.0005 ± 0.04		0.008 ± 0.19		0.07 ± 0.37	
$\text{Median} \pm \text{IQR}$		3.85 ± 0.01		0.59 ± 0.002		0.83 ± 0.006	

HR-Corrected Nonlinear Indices by Interpolation

The nonlinear indices were computed from simulated RR time series interpolated at 2, 4, and 8 Hz. As shown in Fig. 3.7, the corrected nonlinear index values obtained by regression formulas projected

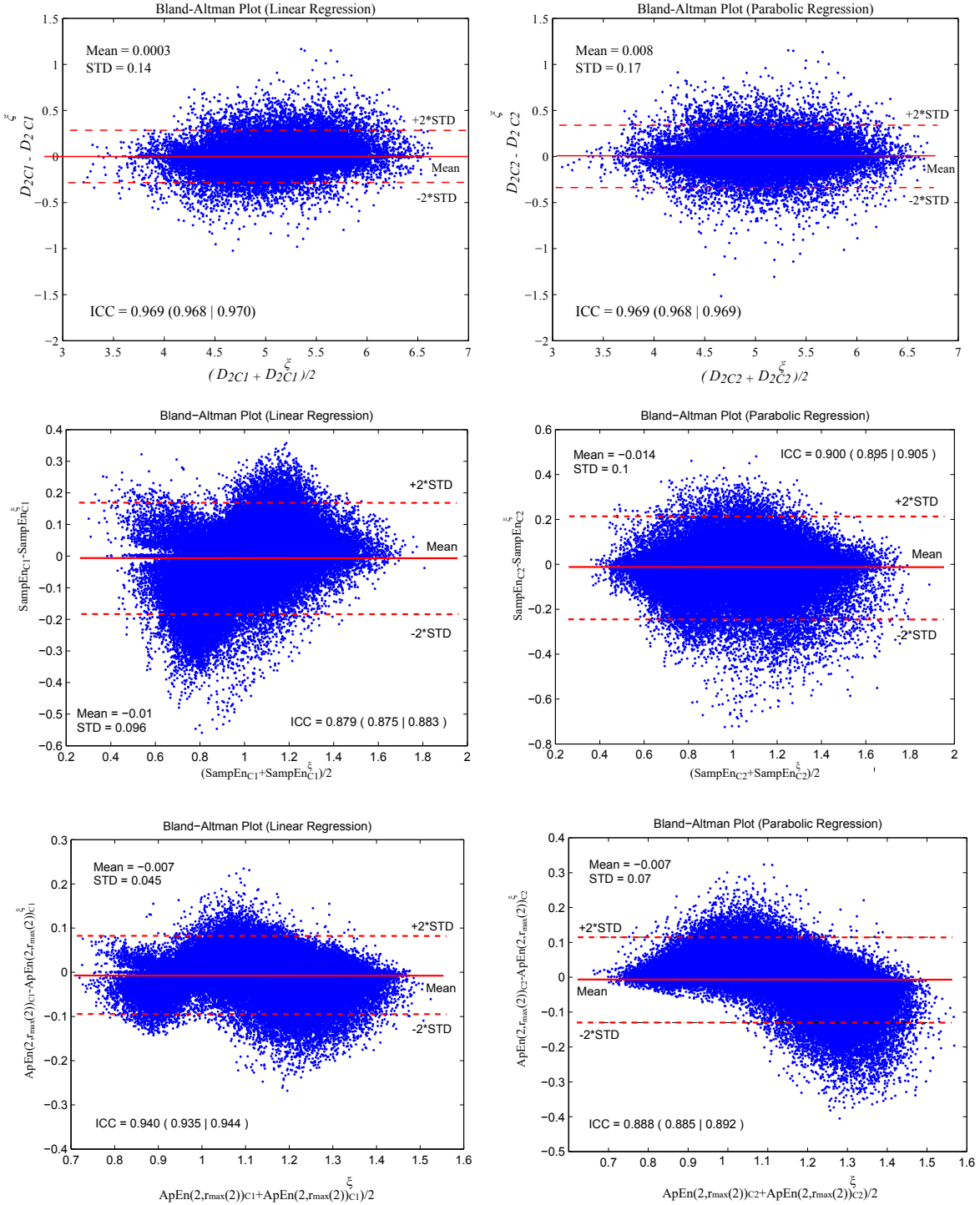


Figure 3.8 Bland-Altman plots and ICC illustrate the agreement between subject-specific and median correction approaches computed on Fantasia database to correct HR effect for both proposed regressions for corrected D_2 , $SampEn$, and $ApEn(2, r_{max}(2))$ indices: linear (left panels) and parabolic (right panels).

onto $RR = 0.5$ s and by interpolating RR time series at 2 Hz revealed similar median values. However, the interpolation of RR time series at 4 and 8 Hz resulted in decreased nonlinear values. In these cases, m values were not adapted, regarding Eq. 3.11. Despite the fact that Pearson correlation factor computed between HR-corrected nonlinear HRV indices, by interpolation, and mean HR values is still significant, their range is now much reduced, being 3.84-3.86 for D_2 , 0.588-0.592 for $SampEn$, and 0.824-0.836 for $ApEn(2, r_{max}(2))$, almost negligible compared to the range of uncorrected nonlinear ones.

Nonlinear Indices of Synthetic Point-process Time Series

The obtained heartbeat occurrence times, $t_{T_n}^j(k)$, from the simulation study were used to generate instantaneous mean RR time series by considering a point-process model resolution of 500 ms. Nonlinear indices were computed over these synthetic time series, where the mean RR was varied, see Fig. 3.9. The dependence of nonlinear indices, in particular, for $SampEn$ and $ApEn(2, r_{max}(2))$, on mean RR above 0.5 s was found attenuated compared with same index values computed over synthetic raw RR time series (Fig. 3.6, with the exception of D_2 index, whose dependence on mean RR values was still present. Instantaneous mean RR time series derived from the point-process could not capture variations of mean RR below 0.5 s, due to model resolution ($\Delta = 500$ ms) and then, this effect influenced the studied nonlinear indices (Fig. 3.9).

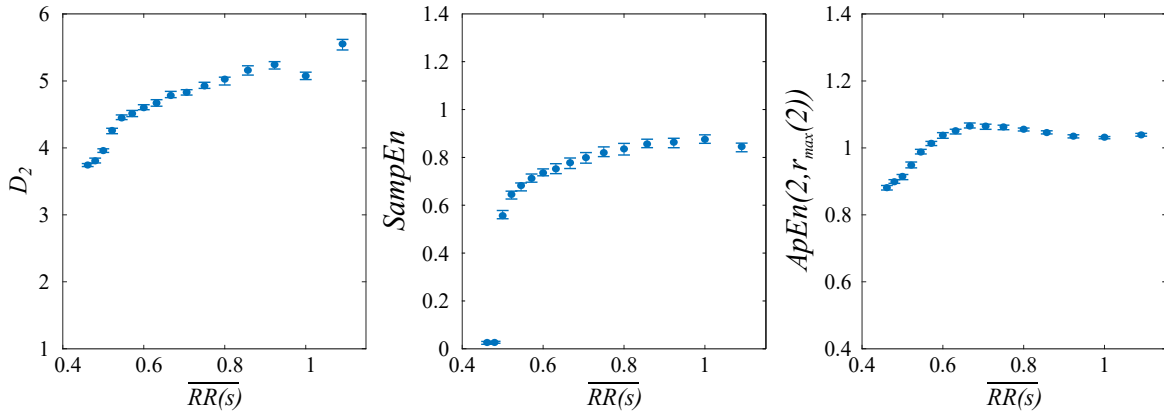


Figure 3.9 Nonlinear HRV indices, $X \in \{D_2, SampEn, ApEn(2, r_{max}(2))\}$, computed from synthetic point-process time series at 500 ms resolution and model order of 12 where mean heart period were varied. Data corresponds to all simulations derived from Fantasia database. Data distributions are represented by median and interquartile range.

3.6.3 Nonlinear Analysis of BPC Database

The proposed HR-corrections were evaluated in the BPC database. The results shown in Fig. 3.6 c) illustrate the differences found between supine and standing conditions. Median and interquartile range of uncorrected and HR-corrected nonlinear HRV indices are provided in Table 3.2.

Table 3.2 Uncorrected nonlinear HRV indices and HR corrected by proposed approaches evaluated in the BPC database. Data are shown in terms of median and interquartile range. C1 and C2 refer to HR-correction by linear and parabolic regression formulas respectively applied to all cases separately. ξ refers to HR-correction by C1 or C2 approach but regression parameters were obtained as the median values of all regression formulas according to C1 or C2. Statistical differences were tested by Mann-Whitney U-test.

Nonlinear index	Supine	Standing	p-value
D_2	5.61 (4.88 6.38)	4.41 (3.64 4.88)	0.003
D_{2C1}	5.10 (4.33 5.62)	4.07 (3.41 4.57)	0.001
D_{2C2}	4.85 (4.19 5.25)	3.97 (3.31 4.46)	0.002
$D_{2\xi}^{C1}$	4.66 (3.98 5.27)	3.88 (3.24 4.42)	0.005
$D_{2\xi}^{C2}$	4.47 (3.93 4.93)	3.82 (3.25 4.32)	0.006
D_{2I2}	3.67 (3.23 4.08)	3.02 (2.84 3.64)	0.02
<hr/>			
$SampEn$	0.73 (0.53 0.83)	0.48 (0.37 0.67)	0.008
$SampEn_{C1}$	0.28 (0.05 0.38)	0.24 (0.15 0.37)	0.7
$SampEn_{C2}$	0.40 (0.28 0.44)	0.33 (0.25 0.44)	0.4
$SampEn_{C1}^\xi$	0.33 (0.16 0.43)	0.27 (0.19 0.42)	0.4
$SampEn_{C2}^\xi$	0.44 (0.34 0.49)	0.36 (0.27 0.47)	0.06
$SampEn_{I2}$	0.50 (0.42 0.54)	0.35 (0.26 0.42)	0.001
<hr/>			
$ApEn(2, r_{max}(2))$	1.11 (1.03 1.17)	0.88 (0.77 0.95)	0.008
$ApEn(2, r_{max}(2))_{C1}$	0.94 (0.91 1.01)	0.88 (0.80 0.97)	0.06
$ApEn(2, r_{max}(2))_{C2}$	0.94 (0.91 0.99)	0.87 (0.79 0.96)	0.04
$ApEn(2, r_{max}(2))_{C1}^\xi$	0.78 (0.68 0.84)	0.77 (0.71 0.86)	0.5
$ApEn(2, r_{max}(2))_{C2}^\xi$	0.78 (0.74 0.83)	0.78 (0.71 0.84)	0.9
$ApEn(2, r_{max}(2))_{I2}$	0.80 (0.74 0.85)	0.71 (0.66 0.80)	0.01

In a first study, the value of the median correction factor ξ extracted from the simulation study was used. It is worth noting that after linear correction there was no significant difference in $SampEn$ and $ApEn(2, r_{max}(2))$ between supine and standing positions, while parabolic correction only reduced differences below significance for $SampEn$.

In a second study, regression formulas were used to correct nonlinear indices of each simulated recording's, referred as subject-specific correction. HR-corrected D_2 was found statistically significantly different for linear and parabolic regression formulas, whereas $ApEn(2, r_{max}(2))$ was only significant for parabolic.

Finally, nonlinear HRV indices were computed on RR time series interpolated at 2, 4, and 8 Hz. We can conclude that the higher the interpolation order, the lower the nonlinear HRV values. In all cases, HR-corrected nonlinear indices calculated by interpolation showed statistical differences between position, regardless of the interpolation order used, being their range notably reduced.

Assessing HRV Analysis by Point-process Paradigm

Time-varying series generated from the previously described point-process model are shown in Fig. 3.10. There, an example of a set of heartbeat occurrence times from subject number 1 of the BPC database, during supine position, is illustrated.

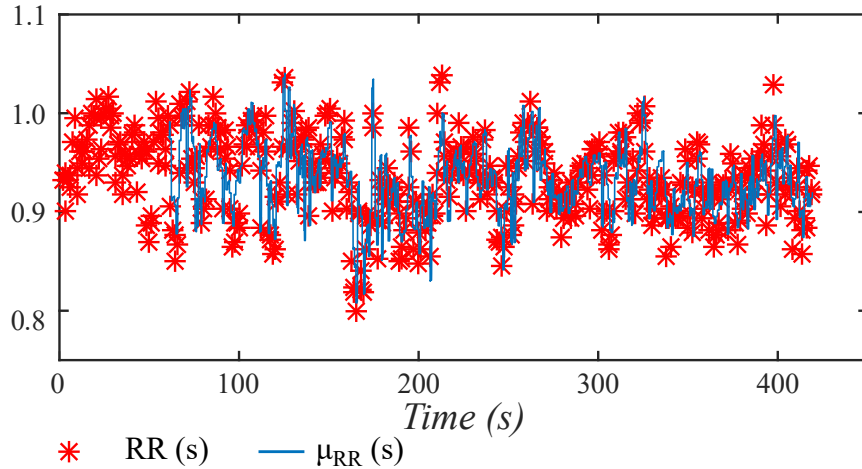


Figure 3.10 Example of instantaneous RR series derived from point-process (Data correspond to subject 1 during supine conditions from BPC database).

Interpolated RR time series at 20 Hz and instantaneous RR derived from a point-process model at 50 ms resolution were analyzed by means of nonlinear indices, see Fig. 3.11. Embedding dimension m values were adapted in both cases by a multiplying factor of 10. Nonlinear indices computed over point-process derived time series were not found statistically significant, whereas the nonlinear indices obtained by interpolation of RR time series at 20 Hz provided statistically significantly different values between supine and standing positions.

3.7 Discussion

3.7.1 Simulated Data

HRV analysis has been widely used as non-invasive technique to assess and quantify cardiac ANS modulation [179, 187, 161]. However, HRV analysis is still under investigation, due to HRV characteristics that could lead to physiological misinterpretations [135, 33]. ANS modulation is linked to ANS tone (HR mean) and, as a consequence, an increase in the sympathetic activity and a decrease in the vagal tone are related to an increment in the HR and a reduction on its variability [33, 91]. This implies that there is a physiological correlation between HRV and HR. However, we have demonstrated that it exists also a methodological influence between nonlinear HRV indices and HR, due to the fact that HR is the intrinsic sampling rate of HRV signal. A simulation was carried out to study an hypothetical case, where the relationship of ANS modulation and HR is uncorrelated.

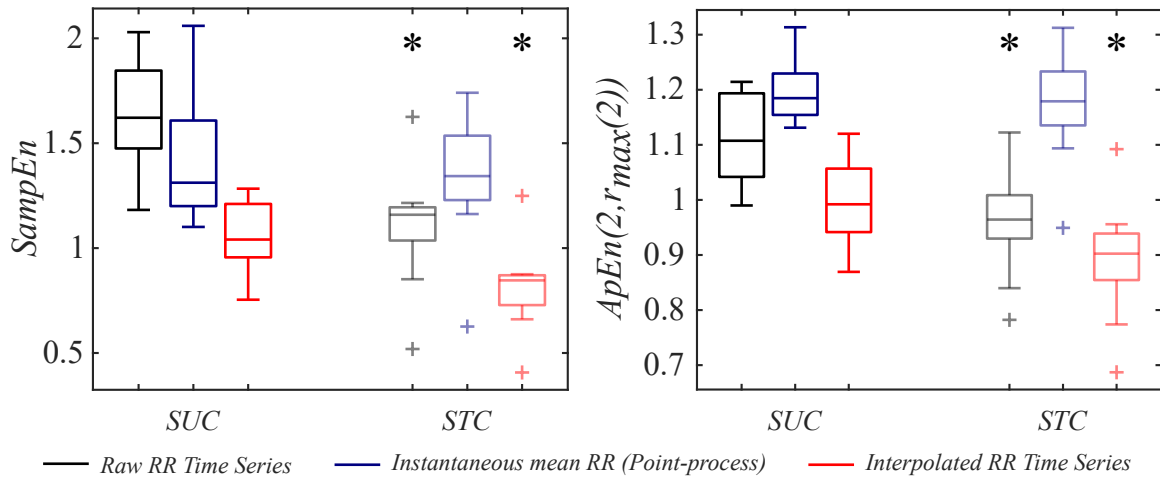


Figure 3.11 Nonlinear indices computed over i) raw RR time series and over ii) instantaneous heart rate ($\mu_{RR}(t)$) considering a memory order of 12 varying with 50 ms resolution, and iii) RR time series interpolated at 20 Hz. Embedding dimension m was adapted to point-process and interpolation resolution.

ANS modulating signals were generated as realizations of stochastic processes [134]. Then, heartbeat occurrences were calculated, using an IPFM model, which is based on action potential generation in SA node cells, and has been proven appropriate to describe the genesis of HRV [115]. This simple model allows keeping the ANS modulation constant, emulating healthy subject's conditions at resting, for different mean HR values. Two approaches have been proposed to attenuate the effect of HR in nonlinear HRV indices, as shown by the simulation study: regression formulas and interpolation.

Regression Formulas

Regression formulas are commonly used to characterize the relationship between two magnitudes such as ventricular repolarization and heart rate [151, 174, 13]. The relationship between D_2 , *SampEn*, and *ApEn*, computed over simulated 300-sample RR series, and mean HR was studied by linear and parabolic regression formulas. Although the usage of other regression models, different from linear or parabolic ones, may provide improved fittings to the relationship between nonlinear HRV indices and mean RR, coefficients of determination $R^2 \geq 0.9$ were obtained for all cases for these to regression models. Then, a correction was proposed based on regression formulas derived for each simulated case, the so-called subject-specific correction, minimizing nonlinear HRV indices correlation to mean HR. A correction based on regression formulas derived from median parameters was proposed as an extension to be applied to other databases. ICC values > 0.8 were found, when evaluating subject-specific vs. median correction approaches for all nonlinear HRV indices, suggesting the usage of either of the approaches, see Fig. 3.8.

Interpolation

Simulated RR time series were interpolated at 2, 4, and 8 Hz. The higher the interpolation rate, the lower the nonlinear index values. The addition of new data, resulting from interpolation, can be interpreted, in terms of entropy, as an increase in signal regularity, being in concordance with a previous work where electroencephalogram complexity through D_2 was evaluated by varying the sampling rate [81]. In this chapter, interpolation was used as a technique to reduce the dependence of nonlinear HRV indices on mean HR as sampling rate effect, since it allows the estimation of nonlinear indices over the same time interval and the same number of points. Sampling rate value should be greater than the maximum HR. HR-correction nonlinear HRV indices computed by interpolating at 2 Hz and by regression formulas presented similar values and range. In some studies, RR time series were interpolated to increase the number of data points for improving the accuracy of nonlinear measurements, thus, compensating mean HR effect on them. The used sampling rates varied including 2, 4, and 8 Hz, or even higher, 20 KHz [135, 64, 94]. However, since nonlinear HRV indices estimates are strongly dependent on the selected sampling rate, results should be compared with caution.

On the Comparison with Respect to Point-process

Interpolation of raw RR time series has been proposed, in this thesis, as a method to attenuate the influence of mean HR on nonlinear HRV indices. Furthermore, another alternative to overcome this limitation was explored by using a point-process model, which provides a representation of the RR time series, based on a probability description, whose resolution is not dependent on HR. In particular, the influence of HR on D_2 , *SampEn* and $ApEn(2, r_{max}(2))$, computed over the point-process derived instantaneous mean RR (see Fig. 3.6), was lower than when these indices were computed over the raw RR time series, see Fig. 3.9.

Despite the dependence of nonlinear HRV indices, computed over raw RR time series, on mean HR revealed by the simulation study, no HR-correction of nonlinear HRV indices is considered in most of the studies found in the literature, where mean HR values are even not provided in some cases [137, 146, 119, 97, 124, 188]. The application of nonlinear indices without HR correction should be restricted to HR steady-state group conditions, avoiding study cohorts that present statistically different mean HR, as for example in [188].

3.7.2 Real Data

Classical nonlinear HRV indices evaluated in the BPC database showed around 21, 34, and 21% of reduction in median values from standing with respect to supine position for D_2 , *SampEn*, and $ApEn(2, r_{max}(2))$ respectively, while mean HR increased by around 28%. Changes in these indices may reflect changes in mean HR as well as additional changes in ANS modulation, as suggested in previous studies [146, 195].

In the BPC database, HR-corrected nonlinear indices were computed under supine and standing conditions and D_2 was found to be significantly different for all regression approaches, while $ApEn(2, r_{max}(2))$ only showed statistical differences for subject-specific by parabolic regression. Linear and parabolic regression formulas were selected to be suitable for the three indices under simulation conditions, although coefficients of determination were slightly lower for $ApEn(2, r_{max}(2))$ and $SampEn$ than for D_2 .

On the other hand, all nonlinear HRV indices were still found significantly different, when corrected by interpolation. It was found a statistically significant reduction in standing with respect to supine of 18, 30, and 12% for HR-corrected D_2 , $SampEn$, and $ApEn(2, r_{max}(2))$ respectively, mostly reflecting ANS modulation changes, while mean HR effect was attenuated. HR-corrected nonlinear index ranges, calculated as the difference of median values for supine and standing positions, were found reduced, when compared to uncorrected nonlinear HRV index ranges.

The embedding dimension, m , refers to the length of reconstructed vectors whose elements correspond to values of the raw RR time series. The same set of values for embedding dimension were assumed either for interpolated RR time series, interpolated at 2Hz, and for raw RR time series. Based on this, the necessity to adapt this parameter setting to the resolution of the derived point-process time series was suggested, since nonlinear index values computed over interpolated RR time series at 4 and 8 Hz were found reduced, but unrelated to a loss of complexity/irregularity, see Fig. 3.6.

The adaptation of the embedding dimensions, m , was taken into account for nonlinear HRV analysis in the BPC database, where analysis results (Fig. 3.11) were obtained from: RR time series derived from the point-process model at 50 ms resolution; and interpolated RR time series at 20 Hz. Results regarding nonlinear HRV analysis over raw RR time series were also displayed for the sake of comparison. $SampEn$ and $ApEn(2, r_{max}(2))$ computed over raw and interpolated RR time series were statistically significantly decreased, comparing supine with respect to standing position, whereas no statistical differences were found for both indices, when point-process derived time series were analyzed. The point-process model was used by setting the same parameters for all considered subjects in supine and in standing position. The results could be influenced by not adjusting the model parameters in a subject-specific way, but this was not addressed in the thesis. The analysis of derived point-process time series at 50 ms resolution in a 5-min window was found more time-consuming than the analysis of interpolated RR time series at 2 Hz, due to the increase of data length as it was described in section 2.4.1 Table 2.4. This fact may suppose a limitation in the application of point-process model in the clinical practice, being, in such a case, suitable for an off-line approach.

Note that, although HR-correction attenuates the effect of mean HR as sampling rate, HR-corrected nonlinear HRV indices may be still correlated with mean HR, since both parameters could vary in the same direction. After HR-correction, nonlinear HRV indices were able to capture information about ANS modulation in response to body position changes, regardless HRM values. Correction

approaches may lead to better understanding the complexity and irregularity ANS changes unbiased by mean HR, as natural sampling rate of RR time series.

HR-corrected nonlinear HRV indices addressed in this thesis, pointed out to a reduction in the complexity of the underlying system and an increase in the HRV series regularity caused by an increase of the sympathetic activity, when changing from supine to standing position, being in agreement with previous works with similar conditions, considering tilt table test or even exercise [135, 83, 152, 79, 148, 23]. Nevertheless, these results and their physiological interpretation are limited by the low number of subjects of study and further studies are needed.

3.8 Conclusion

In this chapter, changes in nonlinear HRV indices were studied under different sympathetic conditions, where mean HR also was changed. D_2 , $SampEn$, and $ApEn(2, r_{max}(2))$ dependence on mean HR, as sampling rate, was explored. A simulation study was carried out, emulating ANS modulation unrelated to mean HR. Simulation results showed that heart rate affects nonlinear indices as it is the intrinsic sampling rate of HRV signal, even when considering the same data length. Two HR-correction methodologies, regression formulas and interpolation, were proposed. Another alternative, based on a point-process model, was explored. The evaluation on a BPC database revealed a reduction of all studied HR-corrected nonlinear HRV indices in standing with respect to supine position. After HR-correction, nonlinear HRV indices were able to capture changes in the sympathetic modulation by body position-induced changes. HR-correction by interpolation was found suitable to attenuate the mean HR effect. Although the application of a point-process model was also found as an alternative to obtain HRV representation unrelated to its resolution, its computation was more time-consuming than for interpolation approach. HR-correction could represent an improvement for nonlinear HRV analysis, extending its application in such cases of non-steady mean HR.

*“A right-hand glove could be put on
the left hand, if it could be turned
round in four-dimensional space.”*

- Ludwig Wittgenstein (1889-1951) -

4

Multidimensional Approximate Entropy: *A priori*-free Approximate Entropy-based Index

Summary

Nonlinear HRV indices, such as $ApEn$, requires the selection of *a priori* parameters to be computed. In this chapter, an approximate entropy-based index called multidimensional approximate entropy, $MApEn_{max}$, is proposed. This index is independent of the *a priori* parameters, taking into account information from long-term correlations (large embedding dimensions). The validation of the proposed index was carried out by analyzing synthetic time series by varying their degree of stochasticity. $MApEn_{max}$ was applied to characterize aging and congestive heart failure to capture ANS regulation changes.

4.1 Introduction

ApEn was introduced by Pincus and co-workers [144] in 1991 as an entropic measurement to quantify the regularity of medical data. Ten years later, Richmann and Moorman [125] introduced *SampEn*, a variation of *ApEn*, reducing the bias of considering self-comparisons and being less dependent on data length. Both approaches have been widely used to characterize and distinguish between healthy and pathological conditions [53, 100, 141, 164, 197, 15, 158].

However, caveats in the computation of these nonlinear indices have been pointed out, such as the dependence on mean HR and on certain parameters needed for their estimates. The dependence of nonlinear HRV indices has already been addressed in chapter 3, while in this chapter, the analysis is focused on the relevance of *a priori* parameters, that have to be selected for their computation, evaluating their effect on *SampEn* and *ApEn* results' interpretation. In particular, the embedding dimension, m , (i.e. the length of reconstructed vectors); and the tolerance threshold, r , used to evaluate reconstructed vectors which are similar to each other, are the two parameters considered for further analysis. These parameters have been assigned diverse values in published HRV studies (e.g. $m = 1$ or 2 ; and $r = 0.1$ to 0.25 times the standard deviation of the time series) [158, 145, 176, 201, 1, 52, 40, 140, 168, 11, 3]. Thus, one main drawback lies in the comparison between studies, since the *a priori* selection of m and r values can lead to different physiological interpretations.

Different approaches have been proposed to identify the values for the embedding dimension m or the threshold r used by nonlinear dynamics characterizing chaotic time series [92, 28, 110, 34, 171, 106]. With regards to the embedding dimension, the false nearest neighbor method has been used to search for the lowest embedding dimension, m , that allows the phase-space reconstruction, with very different values of m in accordance with the diverse underlying dynamics of the analyzed time series [92]. Minimum values of m were reported, being 2, 3 and 6 for Hénon, Lorenz, and Mackey-Glass time series, respectively [28]. With regards to the tolerance threshold, some studies have been focused on searching for the value of the threshold r , denoted by $r_{max}(m)$, maximizing *ApEn* estimate. This *ApEn*-based index has served to show that white noise series is more irregular than the cross-chirp signal [34]. Furthermore, this index has been reported to better enhanced HRV and blood pressure variability differences between supine and upright position with respect to the usage of fixed r values, such as 0.1-0.25 times the standard deviation [171]. It should be noted that, although, in those cases, r is generally referred as fixed, to be precise, the parameter that is fixed is the factor multiplying the standard deviation, rather than the threshold r itself. In the literature, identification of the values of r and m used to characterize different types of time series is still unclear, as highlighted by the high diverse published values [171, 106].

Multiscale entropy (MSE) and refined MSE methods have been introduced to account for complexity properties at different scales [40, 41, 183]. These methods provide information from *SampEn* across a range of time scales. By applying the coarse-graining technique, each time scale is represented as a new time series derived from the original one [40]. Short time scales (1 to 4) have been

proposed to be more related to parasympathetic and respiratory control, whereas long time scales (5 to 20) have been postulated to be more related to sympathetic control [170]. However, one caveat of the MSE methods lies in the usage of coarse-graining technique, since the data length is reduced as the scale increases. This limits the applicability of MSE for short-term HRV analysis and the reliability of *SampEn* estimation becomes compromised for short data length [183].

In this study, a novel *ApEn*-based index, exploiting maximum *ApEn* and multidimensional, properties is presented for short-term HRV analysis. This proposed index, $M\text{ApEn}_{max}$, avoids the usage of the coarse-graining technique and, thus, the variations in data length for the different time scales. Furthermore, its computation provides an entropic estimation without the need of selecting input parameter values *ad hoc*. The ability of the proposed index $M\text{ApEn}_{max}$ to represent different degrees of randomness in time series was firstly tested on synthetic signals and subsequently, the index was used to characterize HRV changes induced by aging and by CHF.

4.2 Approximate Entropy-based Indices

The mathematical definition of *ApEn* was previously described in section 3.3.2. The use of fixed threshold values and the one, denoted by $r_{max}(m)$, that maximizes the *ApEn*, referred as $ApEn(m, r_{max}(m))$, were introduced. In this chapter, $ApEn(2, 0.2)$ and $ApEn(2, r_{max}(2))$ were considered for the sake of comparison.

4.2.1 Multidimensional Approximate Entropy

$ApEn(m, r)$ and $ApEn(m, r_{max}(m))$ provide information about the regularity of the time series when two consecutive length patterns (embedding dimensions m and $m + 1$) are compared. Increasing the length pattern, m , the probability of finding similar patterns decreases. Although this probability tends to zero as m approaches infinity, the information contained could still be of great interest. Therefore, one of the novelties in the multidimensional approach proposed in this thesis lies in considering a range of embedding dimensions to compute a single entropy value, making it independent of the embedding dimension m . The multidimensional entropy index, $M\text{ApEn}(r)$, is defined as:

$$M\text{ApEn}(r) = \sum_{m=1}^M ApEn(m, r), \quad (4.1)$$

where $M = 15$ was set based on correlation dimension estimation described in [22]. The other novelty lies in considering $r_{max}(m)$ for each given value of m . In this way, the definition of $M\text{ApEn}(r)$ can be used to define $M\text{ApEn}_{max}$.

$$M\text{ApEn}_{max} = \sum_{m=1}^M ApEn(m, r_{max}(m)), \quad (4.2)$$

Note that the proposed index $MApEn_{max}$ does not require any *a priori* selection of embedding dimension or tolerance threshold values for its definition, regardless of M .

Correlation dimension and sample entropy were also computed, using the methodology described in chapter 2. All nonlinear HRV indices were computed over RR time series interpolated by cubic splines at 2 Hz to attenuate the HR effect as sampling rate, as described in chapter 3.

4.2.2 Time- and Frequency-domain HRV Indices

Time- and frequency-domain indices were obtained from the raw RR time series and from the modulating signal of the IPFM model, respectively, using the same analysis windows.

Mean heart rate HRM and the square root of the mean squared differences of successive normal heartbeat intervals RMSSD were calculated.

Spectral analysis was performed on a modulating signal, $\mathfrak{M}(t)$ estimated by applying the IPFM model, where the influence of HRM was compensated[8]. Power spectral density content regarding low frequency (P_{LF} , 0.04-0.15 Hz) and high frequency (P_{HF} , 0.15-0.4 Hz) bands, as well as normalized low frequency power ($P_{LFn} = P_{LF}/(P_{LF} + P_{HF})$) were estimated [179, 161].

4.3 Materials

4.3.1 Synthetic Signals

MIX Processes: a family of processes combining deterministic and stochastic behavior were studied. The degree of stochasticity was controlled by parameter P . $MIX(P)$ generated a sine for $P = 0$ (pure deterministic) and became more random as P increased up to 1 ($P = 1$, pure stochastic) [144], see section 2.2.2 for its definition.

For each P value in $\{0, 0.25, 0.5, 0.75, 1\}$, 30 processes were generated, each containing 300 samples.

Noise Time Series: white and pink noise ($1/f$) time series with zero mean and unit variance were studied. A total of 30 white and pink noise processes, respectively, were generated, each containing 300 samples.

4.3.2 HRV Signals

Fantasia Database: ECG signals sampled at 250 Hz were acquired from twenty young (21-34 years old, 25.9 ± 4.3) and 20 elderly (68-85 years old, 74.5 ± 4.5) rigorously-screened healthy subjects undergoing 120 minutes of supine resting while watching the movie Fantasia (Disney, 1940) to help maintain wakefulness. Further database information is available in [77]. Recordings can be downloaded from www.physionet.org [59].

Congestive Heart Failure Database: ECG recordings from the Congestive Heart Failure RR Interval Database (including patients in NYHA classes I, II, and III) and the BIDMC Congestive Heart Failure Database (including patients in NYHA classes III and IV) were selected. These recordings, sampled at 128 and 250 Hz respectively, can be downloaded from www.physionet.org [59]. The mixed databases consist of a total of 44 CHF patients aged 55.5 ± 11.4 y.o. Heartbeat locations were obtained from automatic ECG annotations and subsequently manually reviewed and corrected by experts, are available in the same repository. ECG recordings from 72 healthy subjects, aged 54.6 ± 16 y.o., were obtained from the Normal Sinus Rhythm Database available from www.physionet.org. Long-term ECG recordings sampled at 128 Hz and their corresponding heart beat annotations are included.

Heartbeat locations provided by the repository were corrected for ectopic beats based on instantaneous heart rate variation [116]. The time interval between consecutive heartbeats was used to define the RR interval time series.

4.3.3 Statistical Analysis

For the Fantasia database, the whole 2-hour recordings were analyzed. For the CHF and Normal Sinus Rhythm databases, a 3-hour night period was selected centered on the minimum HRM to establish a fair comparison under similar stationary conditions, with minimal influence of potentially different daily activities. 5-minute windows with 50% overlapping were used for analysis in all cases.

The proposed index, $MApEn_{max}$, as well as all other nonlinear HRV indices were evaluated on synthetic and real data. The normality of data distributions was tested by Kolmogorov-Smirnov test. Nonlinear as well as time- and frequency-domain HRV indices were used for the comparison between young and elderly subjects, and between CHF patients and healthy subjects by ANOVA test or Mann-Whitney U test depending on whether data distributions satisfied the normality criterion or not respectively.

4.4 Results

4.4.1 Synthetic Data

Figure 4.1 and Fig. 4.2 show the values of the nonlinear HRV indices computed over $MIX(P)$ processes and pink and white time series. In the comparison of $MIX(P)$ processes with the degree of randomness below $P = 0.75$ (0 vs. 0.25; 0.25 vs. 0.5; and 0.5 vs. 0.75) all nonlinear indices led to statistically significant differences. In the comparison between $MIX(P)$ processes with P above 0.75 (0.75 vs. 1) no statistically significant differences were found for any of the nonlinear indices. On the other hand, all the analyzed indices were able to separate pink and white noise time series. In addition, the multidimensional index $MApEn(r)$ was able to separate pink and white noise time series for all tested values of the tolerance threshold r (results only shown for $r = 0.2$, Fig. 4.2).

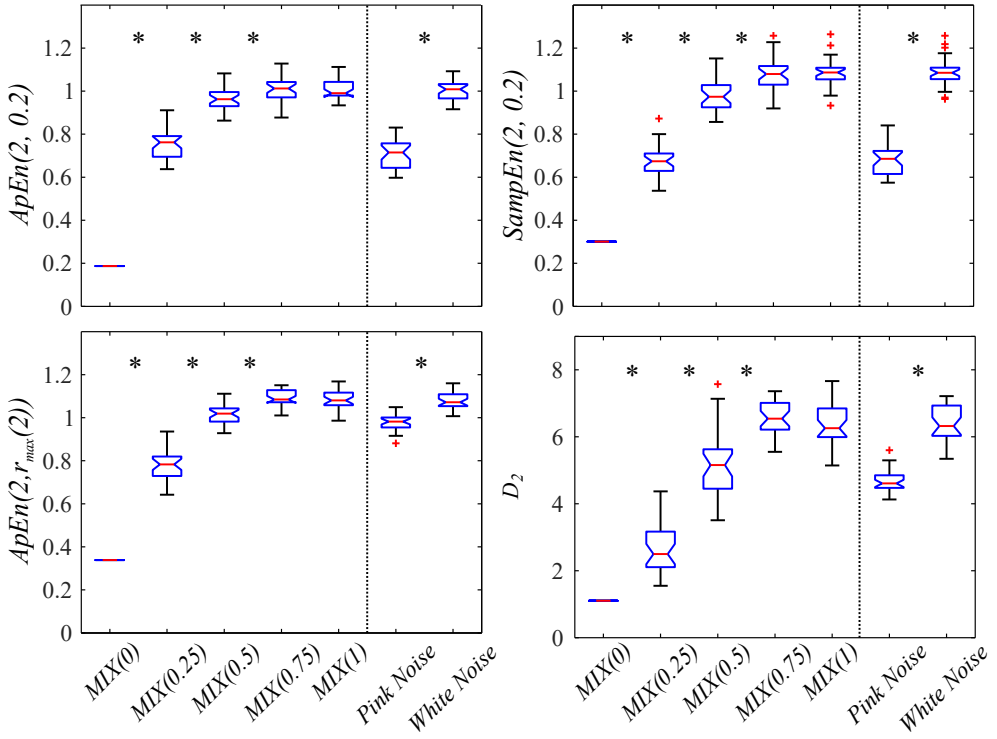


Figure 4.1 Nonlinear indices evaluated over $MIX(P)$ processes with varying stochastic levels and pink and white noise time series. Data are shown as median and interquartile range over 30 realizations.

While statistically significant differences were found for both $MApEn(0.2)$ and $MApEn_{max}$ when comparing different stochastic processes, the former presented decreased values as randomness increased, while the latter showed opposite results. To analyze these differences, the results of evaluating $ApEn$ for two embedding dimensions, namely $m = 2$ and $m = 6$, are illustrated in Fig. 4.3. The use of a fixed threshold did not always allow $ApEn$ to characterize the randomness level of the $MIX(P)$ processes. As an example, for $m = 6$, the use of the fixed threshold $r = 0.2$ led to $MIX(0.25)$ having much larger complexity than $MIX(0.5)$, $MIX(0.75)$, and $MIX(1)$. For $m = 2$, however, $MIX(0.25)$ presented the lowest complexity. When combining results from different scales, $MApEn(0.2)$ showed lower values as the randomness level increased, thus, not being able to reflect the degree of stochasticity in the time series (Fig. 4.2 left panel). However, $MApEn_{max}$ served to characterize $MIX(P)$ processes according to their stochasticity level for any value of m , which then rendered $MApEn_{max}$ suitable to characterize stochasticity levels (Fig. 4.2 right panel).

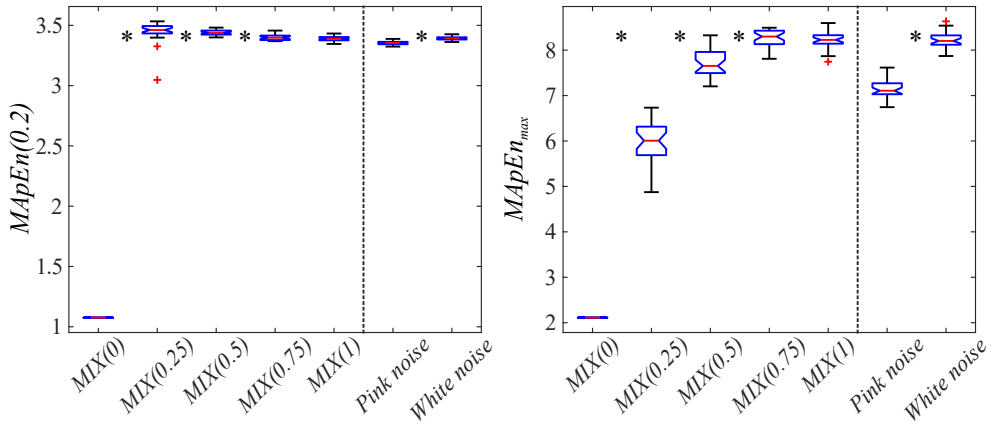


Figure 4.2 $MApEn(0.2)$ and $MApEn_{max}$ evaluated on $MIX(P)$ processes with varying stochastic levels as well as white, and pink noises. Data are shown as median and interquartile range by considering 30 realizations.

In Fig. 4.4 a) $ApEn(m, 0.2)$ and $ApEn(m, r_{max}(m))$ are shown for pink and white noises when the embedding dimension m was varied from 1 to 15. $ApEn(m, 0.2)$ values were higher for white noise than for pink noise for low embedding dimension values, while presented the opposite behavior for large embedding dimensions. The multidimensional index $MApEn(0.2)$ resulted in higher values for white than for pink noise, reflecting the behavior found for the lowest embedding dimensions (Fig. 4.4 b) left). On the other hand, $ApEn(m, r_{max}(m))$ was consistently larger for white than pink noise throughout all embedding dimensions and, consequently, differences between these noise time series were amplified when computing $MApEn_{max}$ (Fig. 4.4 b) right) with respect to $MApEn(0.2)$.

4.4.2 HRV Data

Nonlinear HRV Analysis

One subject from the young cohort and another one from the elderly cohort were discarded for analysis, as their RR time series were not suitable for ectopic beats correction. Their variability values reached the maximum allowed HR variation, thus precluding distinction between normal and ectopic beats [116].

$ApEn(2, 0.2)$, $ApEn(2, r_{max}(2))$, $MApEn(0.2)$, $MApEn_{max}$, $SampEn(2, 0.2)$, and D_2 values showed a trend for higher values in young than in elderly subjects, but only $MApEn_{max}$ showed statistically significantly higher values in young subjects (see Fig. 4.5 and 4.6). On the other hand, all analyzed nonlinear HRV indices, with the exception of $MApEn(0.2)$, were statistically significantly larger in CHF patients than in healthy subjects (4.5 and 4.6).

Figure 4.7 illustrates the contribution of $ApEn(m, 0.2)$ and $ApEn(m, r_{max}(m))$ throughout the embedding dimensions for $MApEn(0.2)$ and $MApEn_{max}$ respectively, for each of the analyzed cohorts. The index $ApEn(m, 0.2)$ was found to have higher values in young subjects than in elderly subjects for

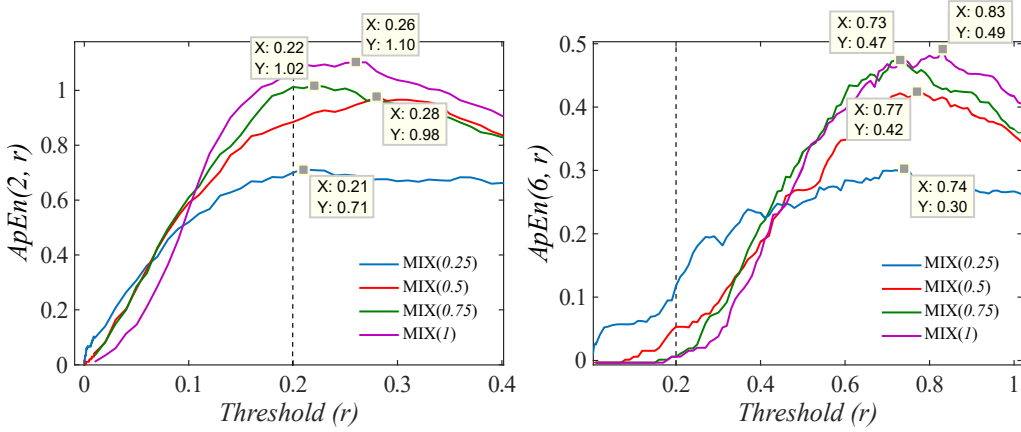


Figure 4.3 Approximate entropy values computed over $MIX(P)$ processes considering a set of thresholds and evaluated by setting $m = 2$ (left panel) and $m = 6$ (right panel) for a particular stochastic realization. Dashed line indicates $r = 0.2$ in both panels. $ApEn(2, r_{max}(2))$, $ApEn(6, r_{max}(6))$, $r_{max}(2)$ and $r_{max}(6)$ values are displayed for each case.

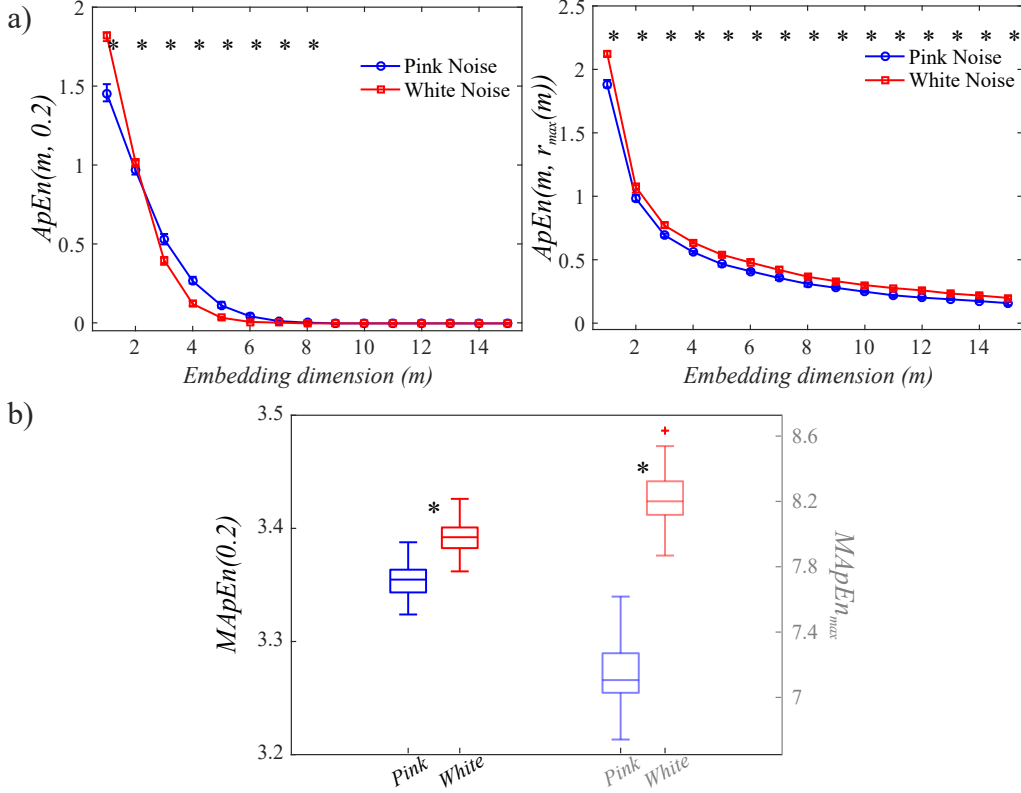


Figure 4.4 a) $ApEn$ computed throughout embedding dimensions for pink noise (blue) and white noise (red) using different thresholds. b) $MApEn(r)$ computed using different thresholds. * indicates statistically significant differences (p -values < 0.05). Data are shown as median and interquartile range by considering 30 realizations.

low embedding dimensions ($m \leq 3$), even if not achieving statistical significance in all cases (Fig. 4.7, left upper panel). Similarly, CHF patients showed higher $ApEn(m, 0.2)$ values than healthy subjects for low values of the embedding dimension m (Fig. 4.7 left lower panel). For large embedding

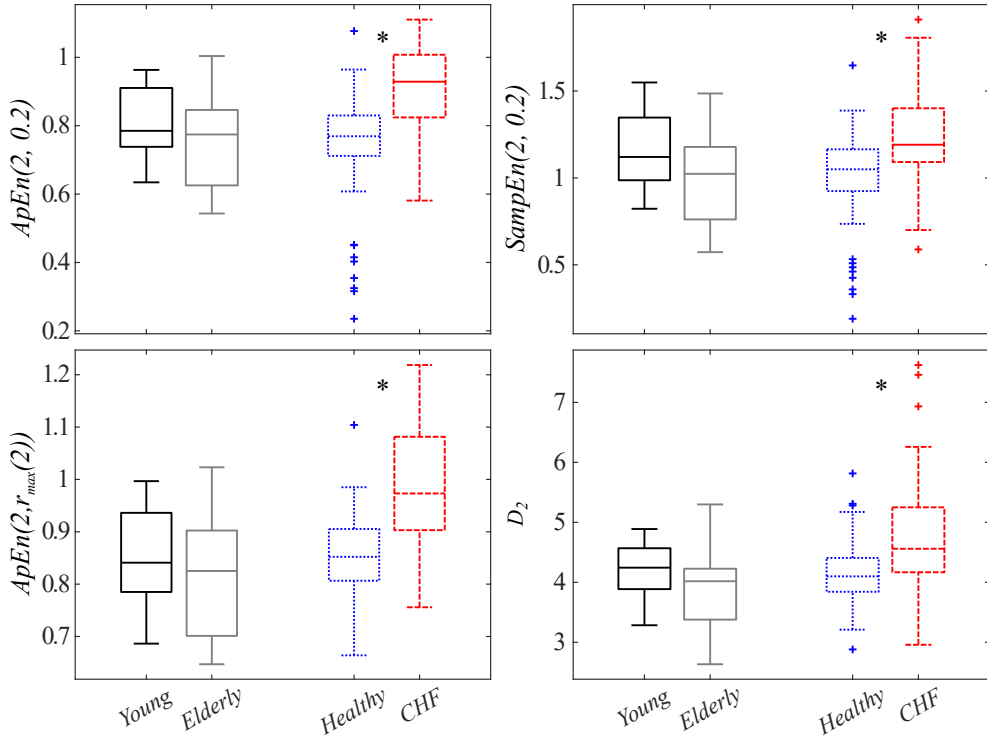


Figure 4.5 Regularity and complexity indices comparing young vs. elderly, and healthy subjects vs. CHF patients. * indicates statistically significant differences (p -values < 0.05). Data are shown as median and interquartile range.

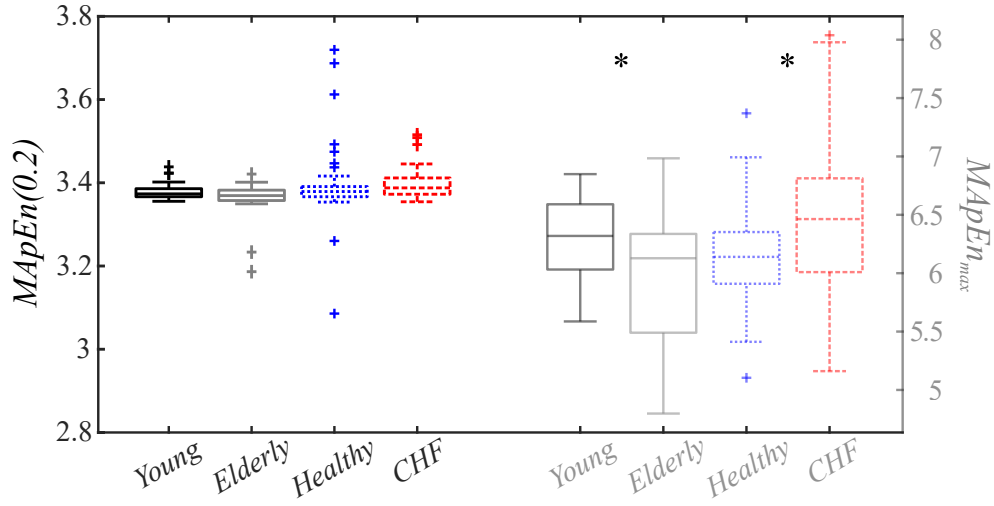


Figure 4.6 $MAPEn(0.2)$ and $MAPEn_{max}$ values computed for young (solid black) vs. elderly (solid gray), and healthy subjects (dotted blue) vs. CHF patients (dashed red). * indicates statistically significant differences (p -values < 0.05). Data are shown as median and interquartile range.

dimensions, opposite results were found in the two comparisons. Regarding $ApEn(m, r_{max}(m))$, statistically significantly higher values were found in young vs. elderly and in CHF patients vs.

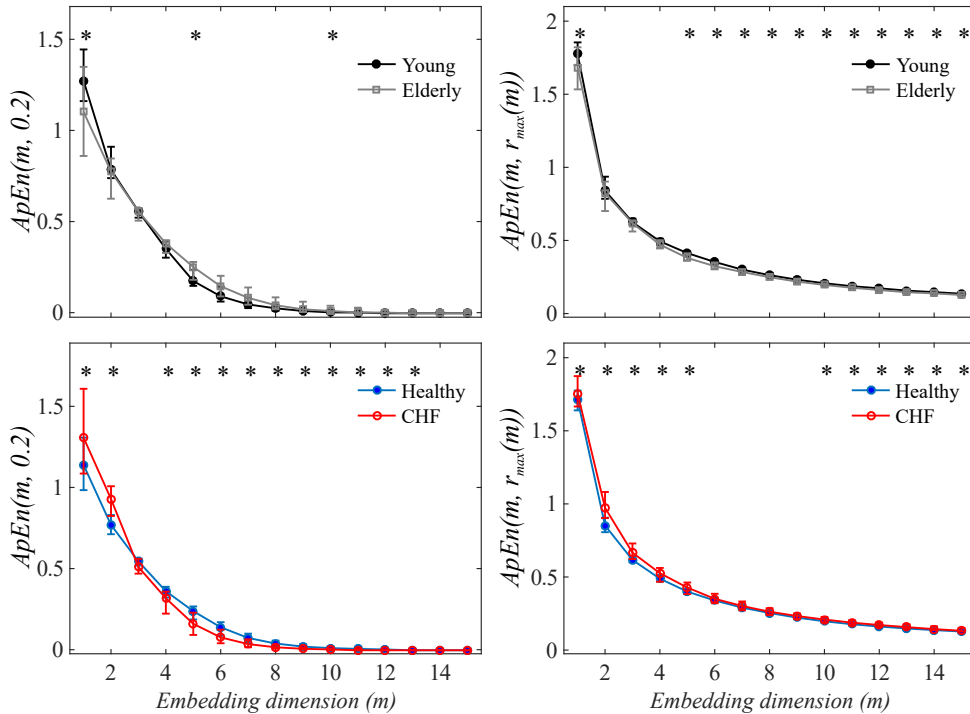


Figure 4.7 $ApEn$ values computed for thresholds set at 0.2, and $r_{max}(m)$ through embedding dimensions in young (black) and elderly (gray) groups shown in the upper panels, and in healthy subjects (blue) and CHF patients (red) during the night period in the lower panels. * indicates statistically significant differences. Data are shown as median and interquartile range.

healthy subjects for most values of the embedding dimension m , while for the remaining values of m the compared values could not be statistically distinguished.

Figure 4.8 shows results for the comparison of healthy subjects and CHF patients obtained when: i) restricting the age range (from 50 to 75 years old); and ii) considering only those CHF patients classified III-IV regardless their age. Nonlinear index values were found statistically higher for CHF patients than for healthy subjects in both comparisons.

In addition, $MAPEn_{max}$ values were computed for young, elderly, CHF, and healthy subjects in 4000-sample time series and results are displayed in Fig. 4.9. Statistical differences between studied groups are maintained when data length was increased with respect to the case of considering 5-minute analysis window.

Time- and Frequency-domain HRV Analysis

HRM and RMSSD are displayed in Fig. 4.10 for the studied groups. No statistically significant differences were found for HRM when comparing young and elderly subjects, although a tendency to lower HRM values for the elderly group was observed with respect to the young group. HRM was statistically significantly higher in CHF patients as compared to healthy subjects. On the other

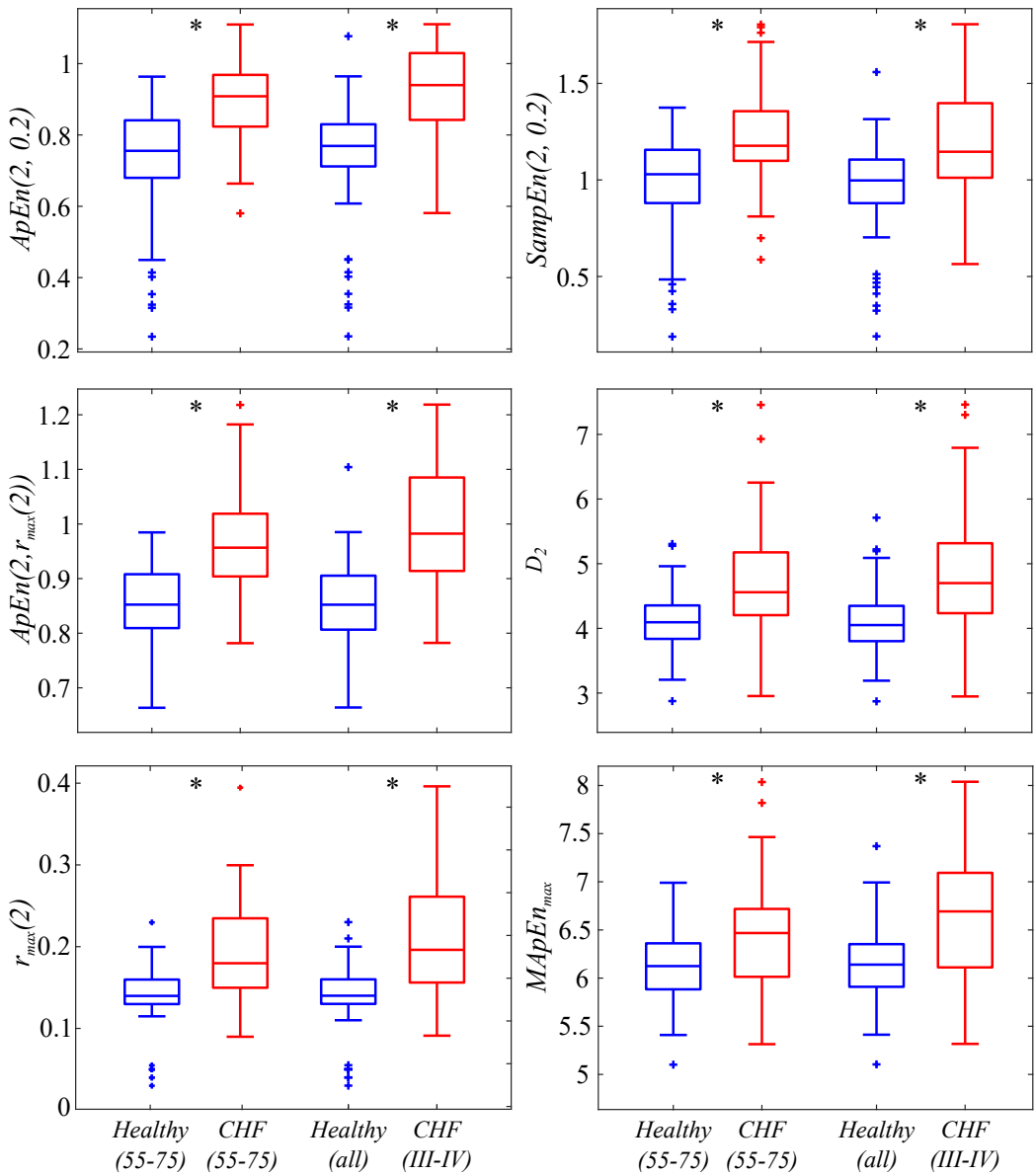


Figure 4.8 Regularity and complexity indices comparing healthy subjects vs. CHF patients restricted to an age range of 50 to 75 years old and all healthy subjects with respect to CHF patients classified III-IV. (*) indicates statistically significant differences (p -values < 0.05). Data are shown as median and interquartile range.

hand, the RMSSD index showed statistically significant differences between both pairs of groups, with elderly subjects and CHF patients presenting reduced RMSSD values.

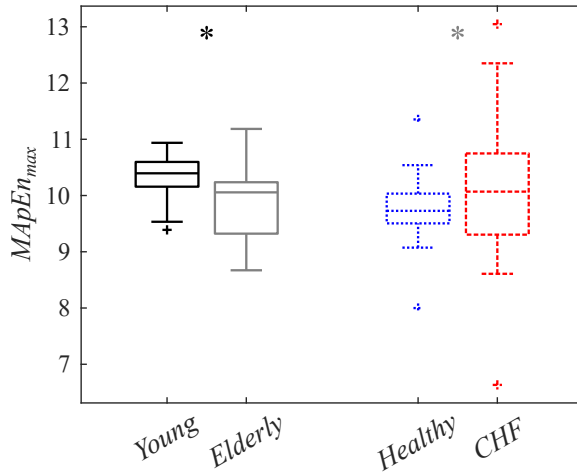


Figure 4.9 $MAppEn_{max}$ values computed for young (solid black) vs. elderly (solid gray), and healthy subjects (dotted blue) vs. CHF patients (dashed red) in time series of 4000 samples. (*) indicates statistically significant differences (p -values < 0.05 (dark), p -values < 0.07 (gray)). Data are shown as median and interquartile range.

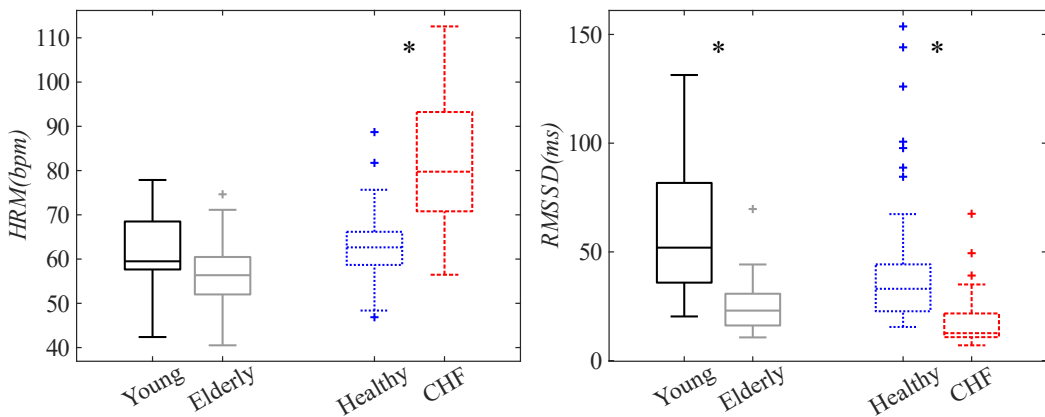


Figure 4.10 HRM and RMSSD values in young vs. elderly and CHF patients vs. healthy subjects during the night period. (*) indicates statistically significant differences.

Values of frequency-domain HRV indices P_{LF} , P_{HF} , and P_{LFn} are shown in Fig. 4.11 for the four studied groups. Significant differences were found for P_{LF} and P_{HF} in the two comparisons. P_{LFn} only showed statistically significant differences for the comparison between CHF patients and healthy subjects.

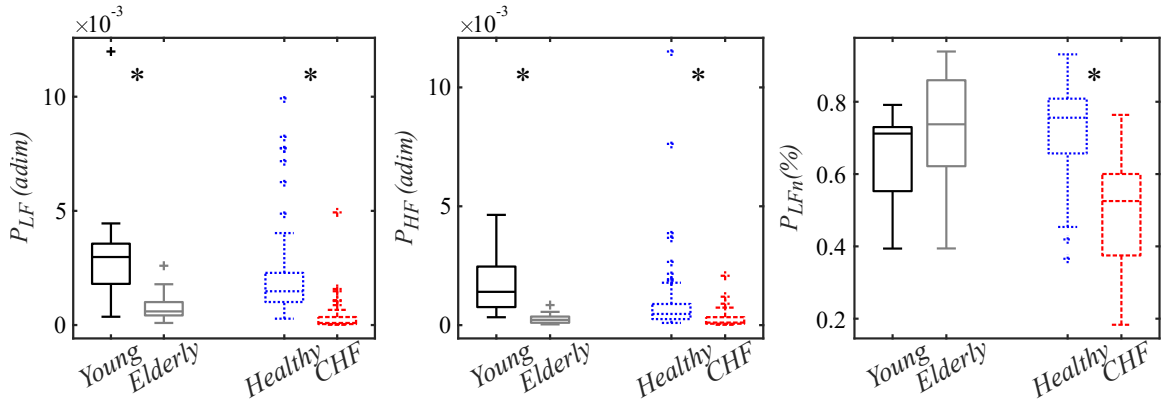


Figure 4.11 Frequency domain indices computed comparing young vs. elderly, and CHF patients vs. healthy subjects during the night period. (*) indicates significant p -values < 0.05 .

4.5 Discussion

Searching for Standardizing Approximate Entropy

Nonlinear HRV analysis has extended the description of ANS regulation of cardiac electrical activity. The use of nonlinear HRV indices has provided new physiological insights into ventricular dysfunction, ventricular tachycardia, obstetrical complications under anesthesia, mental disorders and aging, among others [53, 100, 141, 164, 198, 15, 158]. Nevertheless, the physiological interpretation of some common nonlinear HRV indices could be biased by the *a priori* selection of parameter values intrinsic to their definitions. Automatic search for those parameter values based on methodological and/or time series characteristics has already been addressed [110, 106]. Nevertheless, indices like maximum approximate entropy are still linked to the embedding dimension m by definition. The values of m vary from one study to another even though there is a general tendency to set $m = 2$ to estimate $ApEn(2, r_{max}(2))$, commonly denoted as $ApEn_{max}$. In this study, the index $MApEn_{max}$ has been proposed, which is based on the summation of maximum approximate entropies for a set of embedding dimensions, and thus, the necessity of selecting a particular value for the dimension parameter is avoided. Additionally, the proposed index does not rely on the definition of a tolerance threshold, since the threshold used is the one leading to the maximal entropy value in each embedding dimension.

Analysis of Synthetic Data

The proposed index $MApEn_{max}$ has been tested for characterizing synthetic time series. $MApEn_{max}$ values were found statistically significantly larger for white than for pink noise. This behavior was also reproduced by all other tested nonlinear HRV indices including $MApEn(0.2)$, although such differences were found to be attenuated when using a fixed tolerance threshold as compared to using the one leading to maximum entropy.

The evaluation of the proposed marker on synthetic data, generated by MIX(P) processes, revealed that the greater the stochastic level, the higher the $MApEn_{max}$ value, which is in agreement with the results shown by other nonlinear HRV indices, like correlation dimension or approximate and sample entropy, describing complexity of time series. On the contrary, the usage of a fixed threshold r , e.g. with value 0.2, in the computation of $MApEn(r)$ was not able to reflect the degree of randomness according to the MIX(P) time series.

Aging and CHF Assessment by Nonlinear HRV Analysis

The effect of aging was evaluated on healthy subjects during supine resting conditions, with subjects being awake. Lower values were found for all analyzed nonlinear indices in the elderly cohort with respect to the young one, with differences being statistically significant for our proposed $MApEn_{max}$ index. Our results are in agreement with previous studies where aging was reported as a cause for decreased complexity and irregularity of beat-to-beat RR series [41, 77, 89, 15]. This reduction has been associated with an impairment to adapt against external or internal perturbations [77, 154]. HRM, RMSSD, and P_{HF} values were also decreased, while P_{LFn} values were increased in the elderly cohort, pointing to a potential enhancement in the sympathetic modulation of SA node activity.

Congestive heart failure was assessed by comparing failing patients and healthy controls during the night period while they were sleeping. According to the results obtained for all the studied nonlinear HRV indices, including the proposed $MApEn_{max}$ index, statistically significantly higher complexity and irregularity were found in CHF patients with respect to healthy subjects. Similar results were found when restricting the age of the individuals to the range covering from 55 to 75 years old, pointing out that age has no relevant effect on the comparison between CHF patients and healthy subjects for the compared cohorts. Similarly, NYHA class had no impact on the distinction between CHF patients and healthy subjects, as demonstrated by restricting the analysis to CHF patients in NYHA classes III-IV, which led to similar results to those found for the whole CHF population (Fig. 4.8).

Spectral HRV analysis showed a significant decrease in P_{LFn} for CHF patients with respect to healthy subjects. In previous studies CHF has been reported to be associated with an increase of the sympathetic tone and a decreased peripheral response to adrenergic input [93, 62]. In other studies, a reduction in HRV low frequency content has been associated with the progression of heart failure in CHF patients with advanced disease [62].

CHF has been characterized by $ApEn$ in the literature, but results were found dependent on methodological factors [204]. Multiscale entropy, which extends the classical $SampEn$ definition to a time-scale representation, has been applied to describe heart rate dynamics in CHF [40]. Costa et al. reported that healthy subjects presented greater MSE values than CHF patients, but in particular, the elderly healthy cohort showed lower MSE values than CHF group in the first scale. In our study CHF patients and healthy subjects showed diverse $ApEn$ values, being greater in one or in the other

group depending on the tolerance r and the embedding dimension m . Therefore, the different results obtained in the present study and those in [183] could be due to the method itself ($ApEn$ here and $SampEn$ in [183]) and/or to the values used for the tolerance threshold ($r_{max}(m)$ in this study and fixed thresholds in [183]).

$ApEn(m, r_{max}(m))$ values were found greater for CHF patients than healthy subjects for all considered embedding dimensions, contrary to the lower MSE values in CHF reported for all scales in [183]. Additionally, to discard the effect of data length in underlying differences between the results presented here and results described in [183], our proposed multidimensional index $MApEn_{max}$ was also tested on increased HRV signal lengths (4000 samples), confirming its discriminant capacity between healthy and CHF patient's groups, with higher values for CHF patients (Fig. 4.9).

Although a relationship between derived-MSE indices and sympathetic/parasympathetic modulation has been reported [170], the methodological differences comparing derived-MSE and $MApEn_{max}$ do not allow the translation of the physiological interpretation to the present study.

The CHF patients included in the present study were enrolled in a long-term study to evaluate the efficacy of drugs, in particular, milrinone and digoxin, and these drugs may have had an effect into the ANS response mechanisms. In addition, no information was available in relation to other concomitant disorders that CHF patients might suffer, such as obstructive sleep apneas, which could interfere, misleading the nocturnal nonlinear analysis [129].

4.6 Conclusion

A multidimensional approximate entropy index, $MApEn_{max}$, was introduced as *a priori*-free parameter entropy measurement. The evaluation on synthetic time series, such as MIX(P), pink and white noise, revealed that $MApEn_{max}$ characterized the degree of randomness in the series consistently. In the analysis of aging, $MApEn_{max}$ was higher in the elderly than the young population, thus, capturing the heart rate complexity changes due to aging that may reflect loss of ANS adaptability. In addition, $MApEn_{max}$ was increased in CHF patients as compared to healthy subjects during the night period suggesting greater complexity in CHF than healthy subjects. The addition of $MApEn_{max}$ in nonlinear HRV analysis could provide robust information according to the HR dynamics complexity, since maximum approximate entropy computed throughout embedding dimensions contribute to its value.

*“Prediction is very difficult,
especially if it's about the future.”*

- Niels Bohr (1885-1962) -

5

Improvement in the Prevention of Hypotensive Episodes after Spinal Anesthesia in Cesarean Delivery by Nonlinear Analysis

Summary

Prophylactic treatment has been proved to reduce hypotension incidence after spinal anesthesia during cesarean labor. However, the use of pharmacological prophylaxis could lead to undesirable side effects on mother and fetus. Thus, the prediction of hypotension becomes an important challenge to reduce the number of women that needed to be treated. One of the hypotheses underlying these kind of hypotension events may be due to the malfunctioning of ANS on blood pressure regulation. In this chapter, ANS response of pregnant women to body position changes was explored for hypotension prediction.

5.1 Motivation

The amount of cesarean deliveries worldwide has been increased by a global average of 12.4% from 1990 to 2014 [17]. Although the use of spinal anesthesia has been beneficial reducing mortality and morbidity during labor [68], side effects such as hypotension and bradycardia in the mother [99] and hypoxia and acidosis in the fetus [157] might be triggered after its administration. In particular, the incidence of hypotension events has been reported between 30 and 100% of cases [111, 131]. This wide range of incidence could be associated with discrepancies in the hypotension definition and measurement techniques [76].

The use of prophylaxis has led to a notable reduction in the number of hypotension events [37]. However, prophylaxis through sympathomimetic drugs administration can lead to a non-desired reactive hypertension with dose-dependent incidence up to 82% of the patients [4]. Prediction of hypotension events during cesarean section would help to: 1) decrease the latency time between hypotension event and its treatment; 2) increase efficiency in the anesthetic administration to better control for the hemodynamic consequences of spinal block; 3) decrease the number needed to treat (NNT), thus avoiding unneeded pharmacological exposition and therefore, reducing the derived side effects. Prediction of hypotension after spinal anesthesia during elective cesarean delivery has been reported in the literature [71, 31, 66, 25, 55, 76, 22, 199, 160]. However, results have been found to be highly dependent on the number of studied subjects, the definition of hypotension episode, and the features considered for the analysis.

The malfunctioning or disability of ANS to compensate a drop in blood pressure induced by anesthesia is one of the hypotheses underlying hypotension episodes. Besides, the physiological and psychological stress response is altered by the last period of pregnancy. ANS regulation on the heart can be assessed by HRV analysis, which was found to be correlated with hypotension episodes the day of surgery [21, 31, 66, 199]. ANS responsiveness through an elicitation protocol, consisted of postural changes, and the occurrence of hypotension events have been related during the day before surgery [160].

The analysis of pulse rate variability (PRV), extracted from pulse photoplethysmographic signal (PPG) recording, has been proved suitable for the assessment of ANS regulation of the heart, taking into account information about the peripheral vascular regulation [58]. These recordings present the advantage of reducing number of sensors, being convenient in clinical practice. pulse transit time (PTT) and its surrogate pulse arrival time (PAT) derived from the ECG and PPG signals, were introduced as non-invasive approaches for capturing blood pressure changes [189, 61]. They have been also related to the arterial stiffness, ANS, respiration, and blood pressure [35, 101, 127, 139]. An increase of PTT values has been associated with a drop in arterial blood pressure (hypotensive episode) [166]. Based on this, although several studies attempted to shed light into the role of HRV and pulse oximeter derived index analysis for predicting hypotension after spinal anesthesia for cesarean section delivery, hypotension prediction is still a challenge [71, 31, 66, 25, 55, 76, 22, 199, 160].

In this chapter, ANS responsiveness through body position change protocol is analyzed by HRV, PRV, and PAT indices to avoid side effects caused by prophylaxis used for preventing hypotensive events induced by spinal anesthesia during cesarean delivery. A classifier focused on the minority class, normotensive cases, is developed to provide clinicians valuable information for making better preventive treatment decisions.

5.2 Materials and Methods

5.2.1 Programmed Cesareas Database

The database consisted of a total of 105 pregnant women programmed for an elective cesarean section at the University Hospital Miguel Servet of Zaragoza, Spain. A subset of this database was already used in an exploratory research addressed in chapter 2. After obtaining approval from the Clinical Research Ethics Committee, the parturients were recruited, informed, and asked to sign the written consent. Indications for programmed cesarean delivery were: iterative cesarean labor; breech presentation; shoulder presentation; placenta previa; previous uterotomy and other causes. Exclusion criteria were urgent surgery, uterine contractions and maternal or fetal pathology.

The subjects were randomly selected to belong to a control group (no prophylactics were administered, 51 subjects) and to prophylactic group (54 subjects). A prospective study of this work is based on the factors related to hypotension within the control group. Thus, subjects were grouped according to hypotensive outcome. A hypotensive episode was defined as a drop in systolic arterial pressure greater than 20% from baseline value, estimated as mean of three consecutive measurements taken in lateral decubitus). 33 subjects of the control group suffered from hypotension after spinal injection until delivery, reaching a 64.7% incidence.

Demographic data were obtained at admission. Biomedical signals were recorded in the surgical area the day of surgery. Two-lead ECG and PPG were recorded both at 1 kHz during a protocol designed to enhance ANS alterations by hemodynamic changes. Protocol stages were: 7 minutes of lateral decubitus (LD) assuming baseline pregnancy conditions, 7 minutes of supine decubitus (SD) increasing hemodynamic stress due to aorto-cava compression, 7 minutes of sitting position (SP). LD and SD were recorded for all subjects of the database, whereas sitting position was recorded for 40 subjects. Thus, two subgroups are referred as LD-SD and LD-SD-sitting position (SP).

After recording ECG and PPG signals, all patients received an infusion of Hartmann's solution at 15 ml/kg/h. Thereafter, standardized spinal anesthesia was performed: puncture site was lumbar interspace L2/3 or L3/4 with the patient in a sitting position. Next, 9 to 11 mg of hyperbaric bupivacaine anesthetic 0.5% according to patient height (<150 cm, 9 mg; 150-165 cm, 10 mg; > 165 cm, 11 mg) and 10 µg fentanyl was injected via 27-G Whitacre needle. Immediately after injection, patients were positioned supine with a left lateral tilt of about 10°, facilitating left uterine displacement. Blood pressure was measured at 2-min intervals beginning 1 min after spinal injection.

The database of study contains demographic data recorded from the beginning of the pregnancy period until the day of admission to the hospital. These baseline characteristics grouped according to their hypotensive outcome are shown in Tab. 5.1.

Table 5.1 Parturient characteristic data. (n) refers to the number of subjects on each group. * indicates number of subjects different from 18 caused by unavailable data.

Demographic data	Hypotensive			Normotensive		
	n	Mean	SD	n	Mean	SD
Age (yr)	33	35.3	4.7	18	33.7	4.6
Height (cm)	33	161.8	5.9	17 *	161.4	5.8
Weight (kg)	33	73.8	10.5	17 *	72.3	10.5
Pre-gest. weight (kg)	33	61.9	9.9	15 *	62.5	8.9
Gained weight (kg)	33	11.5	4.4	14 *	11.3	3.1
Pre-gest. BMI (kg/m^2)	33	23.7	3.7	14 *	24.0	3.1
BMI (kg/m^2)	33	28.2	4.1	17 *	28.5	3.9
Gest. age (days)	33	263.2	6.7	18	267.6	6.3

5.2.2 Methods

Series to Study

Heartbeat time occurrences were detected from the ECG lead with the highest signal quality (signal-to-noise ratio) by a wavelet-based ECG detector [114]. Ectopic beats were detected and corrected [116]. Then consecutive heartbeat occurrence times were used to generate the beat-to-beat RR time series.

Temporal location of each PPG pulse wave was detected as the medium-amplitude point where amplitude reaches 50% of its maximum value [103]. Ectopic and undetected pulses were identified and their corresponding pulse wave times corrected [116]. Then, consecutive pulse wave times were used to generate the pulse-to-pulse (PP) time series.

In this chapter, PAT, is referred to the spend time used by pulse waves to travel from the aortic valve to an arterial point placed at the periphery. The time interval between an R peak in the ECG signal and its corresponding PPG pulse wave location time defines PAT estimation. It is worth noting that this estimate, PAT, although considered as a surrogate of PTT, includes the pre-ejection period (PEP) and the pulse transit time (PTT), the systolic and the propagation time interval respectively, since the detection of the time instant when the aortic valve opens was replaced by R peak in the ECG signal.

Respiratory rate was extracted from ECG signals by applying a QRS morphology-based technique that exploits respiration-induced variations in QRS slopes and R-wave angle [102].

Temporal Analysis

RR, PP and PAT time series were used to calculate the temporal indices such as mean value (μ^X), standard deviation (σ^X), square root of the mean squared differences of successive values ($RMSSD^X$), standard deviation of differences of successive values ($SDSD^X$), where $X \in \{RR, PP, PAT\}$. Median value (\bar{f}^R) and interquartile range ($IQR[\bar{f}^R]$) were computed from the respiratory rate.

Spectral Analysis

The IPFM model was applied to estimate the modulating signals from heartbeat locations. As described in chapter 3, these modulating signals are assumed to carry information about ANS activity once compensated for the mean HR effect [8]. In the following, these modulating signals are referred to as HRV signals. Similarly as for heartbeat locations, pulse wave occurrence times were used to compute modulating signals through the IPFM model labeled as PRV signals. HRV and PRV signals were interpolated at 4 Hz. The IPFM model was not applied to the PAT signal and, this series was only interpolated at 4 Hz as the other two signals, being suitable for further spectral analysis.

Welch-periodogram was used to estimate spectral properties of the HRV, PRV and PAT signals. Fixed spectral band of LF (0.04-0.15 Hz) and a variable HF band centered in f^R with a fix bandwidth of 0.25 Hz were used to compute the power content on each band (P_{LF}^Y and P_{HF}^Y), their normalized values (P_{LFn}^Y and P_{HFn}^Y) as well as the sympathovagal balance (LF/HF^Y), where $Y \in \{HRV, PRV, PAT\}$. The variable HF band aims to better capture parasympathetic activity, since respiratory rate in pregnant women can be higher and often near the classical HF upper bound of 0.4 Hz [7]. However, in those cases where HF band overlapped with LF band, the lower limit of HF band was set as the upper LF band limit. No estimation based on spectral analysis was given in those cases when f^R was found below 0.15 Hz due to the uncertainty in the physiological interpretation of these measurements.

Nonlinear Analysis

D_2 , $SampEn(2, 0.2)$, $ApEn(2, r_{max}(2))$, and $MApEn_{max}$ were selected as nonlinear indices whose interpretation has been related to complexity and irregularity in previous chapters. In order to simplify the notation, hereinafter D_2 , $SampEn$, $ApEn_{max}$, and $MApEn_{max}$ are used to refer to these studied indices. RR, PP and PAT time series were interpolated at 2 Hz to be suitable to attenuate the effect of HR on the estimated nonlinear indices as described in chapter 3.

Statistical Analysis

ANS activity was assessed by analyzing the variations of HR, PR and PAT from ECG and PPG signals recorded few minutes before surgery on each protocol stage, consisted of lateral decubitus, supine decubitus, and sitting position. Differences between body position stages were also evaluated. As an example of notation, $P_{HF}^{HRV(SD-LD)}$ will be the difference of high frequency power from HRV analysis between supine and lateral decubitus position.

The normality of statistical distributions was analyzed by Kolmogorov-Smirnov test. Sensitivity analysis of features, comparing hypotensive and normotensive groups was tested by T-Student test on normal distributions and by Mann-Whitney U test on non-normal ones. A univariate statistical significance was considered for p -values < 0.05 .

Due to the large amount of computed features (more than 200), only those showing statistical sensitivity on hypotension were used as candidates for classification purposes. In this case, *a post hoc* correction, such as Bonferroni's, was not applied, since our purpose is to obtain a combination of features, no single ones, to better distinguish both groups of study. A set of classifiers were tested such as Logistic Regression, Naive Bayes, Nearest Neighbor, Linear and Quadratic Discriminant Analysis, and Supported Vector Machine to search for the best classification results. On the one hand, some of these classifiers provide their outcome in discrete values of 1 or 0, depending on whether the subject belongs or not to the non-hypotensive (or normotensive) group. On the other hand, classifiers such as the one based on a logistic regression provide their outcome as a probability of belonging to the hypotensive group, see Eq. 5.1.

$$p = \frac{1}{1 + \exp^{-(\beta_0 + \beta_1 X_1 + \beta_2 X_2 + \dots + \beta_N X_N)}}, \quad (5.1)$$

where β_0, \dots, β_N are the coefficients and X_1, \dots, X_N represent the selected N-features. Then, a probability threshold, p_{th} , determines the risk of suffering from hypotension.

Feature selection was done by a Greedy forward algorithm by maximizing F1 score as inclusion criteria [39]. F1 score is defined as a measurement equilibrating the positive predictive value and sensitivity, thus improving the classification of the minority class, which, in our case, is the normotensive group. Overtraining was avoided by using the leave-one-out technique combined with bootstrapping [51] (see Fig. 5.1) and by restricting the maximum number of selected features for classification to be less than the square root of the number of subjects in the smallest group as a rule of thumb.

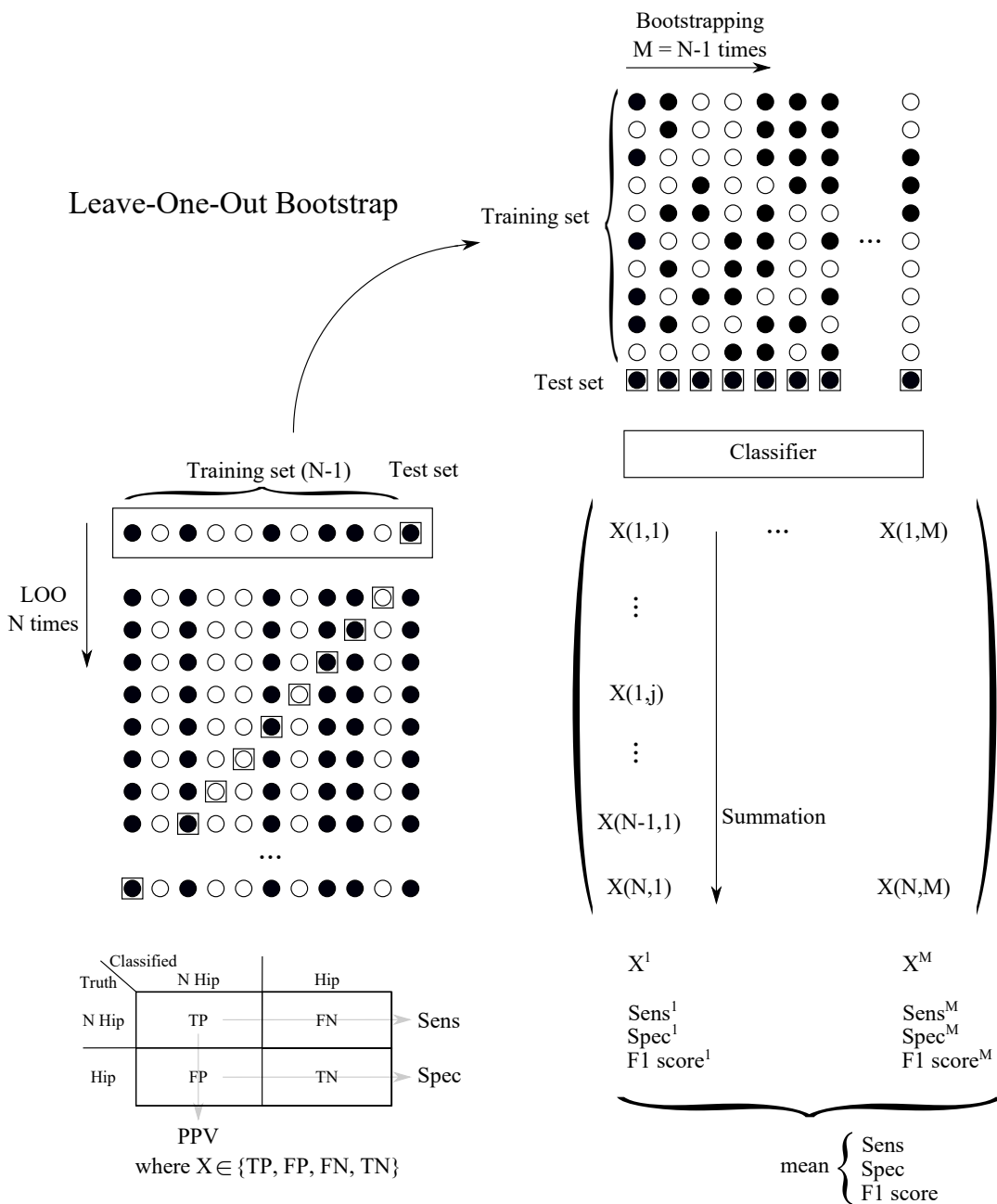


Figure 5.1 Cross-validation scheme combining leave-one-out (LOO) technique with bootstrapping reducing the variance of classification results. Circles represent each subject of the database, whereas the color white or black illustrate their truly hypotension outcome as normotensive or hypotensive respectively. First, leave-one-out is applied to define a training and a test set (dashed rectangle). Next, bootstrapping is $N-1$ times applied to this training set. Then, these bootstrapped training sets are evaluated in the classifier. Leave-one-out procedure is N times repeated generating the resulting X matrix.

5.3 Results

In Fig. 5.2 RR, PR and PAT signals are shown for two subjects belonging to hypotensive (Hyp) and normotensive (N-Hyp) groups during supine position.

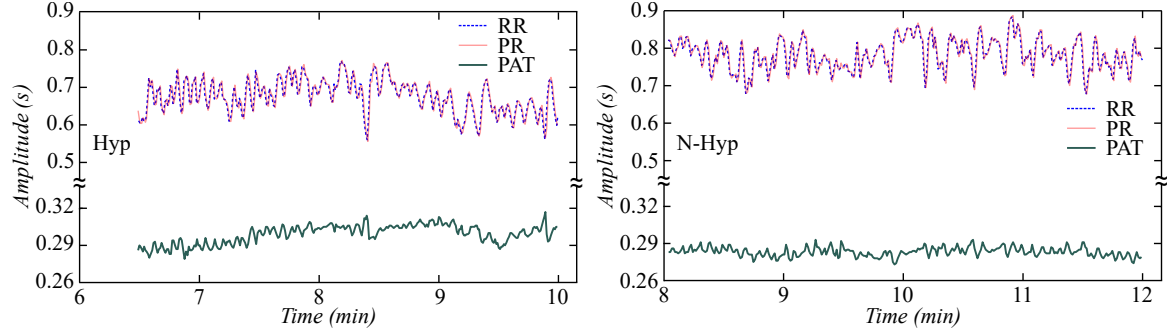


Figure 5.2 RR, PR and PAT signals for two subjects belonging to hypotensive group (left panel) and normotensive group (right panel) during supine position.

Tab. 5.2 shows those indices that were found statistically significantly different between the two groups in LD-SD and LD-SD-SP cohorts. Correlation between derived nonlinear indices computed over RR and PR that present statistically significant p -values in LD-SD cohort is illustrated in Fig. 5.3.

The evolution of $ApEn_{max}^{PR(SD-LD)}$ with respect to m and the contribution of each position are displayed in Fig. 5.4. Only $ApEn_{max}^{PR(SD-LD)}$ at $m = 2$ and 3 were found to be statistically significant comparing hypotensive and normotensive groups. $MApEn_{max}^{PR(SD-LD)}$ index computed as the contribution of all embedding dimensions appeared statistically significant comparing both groups of study but less than $ApEn_{max}^{PR(SD-LD)}$ as illustrated in Tab. 5.2.

Tab. 5.3 shows the classification results for the different tested classifiers. For all classifiers $ApEn_{max}^{PR(SD-LD)}$ and $\sigma^{PAT(SD)}$ were selected as the combination of features that achieved the best classification results in the LD-SD cohort. The classifier showing the highest F1 score was the one based on logistic regression.

Table 5.2 Relation of features extracted from ECG derived respiration, RR, HRV, PR, PRV, and PAT analysis for the LD-SD and LD-SD-SP cohorts. Only those that were found statistically significant are shown. (n) refers to the number of subjects on each group. * indicates number of subjects different from 18 for LD-SD and 28 for LD-SD-SP respectively, corresponding to cases where respiratory rate overlapped to LF band. p -values < 0.05 were statistically significant by Mann-Whitney U test.

Features	Hypotensive				Normotensive			
	Cohorts	n	Mean	SD	n	Mean	SD	p -value
LD-SD								
$SampEn^{RR(SD)}$ (a.u.)	33	0.45	0.17	18	0.56	0.18	0.03	
$SampEn^{RR(SD-LD)}$ (a.u.)	33	-0.03	0.16	18	0.05	0.11	0.03	
$MAPEn_{max}^{RR(SD-LD)}$ (a.u.)	33	-0.35	0.65	18	0.06	0.6	0.03	
$SampEn^{PR(SD)}$ (a.u.)	33	0.48	0.16	18	0.59	0.17	0.03	
$SampEn^{PR(SD-LD)}$ (a.u.)	33	-0.04	0.16	18	0.06	0.11	0.02	
$ApEn_{max}^{PR(SD-LD)}$ (a.u.)	33	-0.04	0.09	18	0.03	0.07	0.01	
$MAPEn_{max}^{PR(SD-LD)}$ (a.u.)	33	-0.35	0.63	18	0.12	0.6	0.02	
$\sigma^{PAT(SD)}$ (ms)	33	6.20	4.45	18	4.31	1.13	0.03	
$P_{LF}^{PAT(SD)} (\text{ms}^{-2}) (10^{-4})$	33	0.15	0.39	17*	0.04	0.03	0.02	
$P_{LFn}^{PAT(SD)} (\%)$	33	63.22	0.39	17*	51.56	16.3	0.03	
$P_{LF}^{PAT(SD-LD)} (\text{ms}^{-2}) (10^{-4})$	33	0.08	0.24	17*	0.02	0.02	0.02	
$LF/HF^{PAT(SD)}$ (adim.)	33	2.90	3.38	17*	1.31	0.84	0.03	
$SampEn^{PAT(SD-LD)}$ (a.u.)	33	-0.04	0.21	18	0.12	0.21	0.01	
$IQR[f^R]^{(SD)}$ (Hz)	33	0.05	0.04	18	0.03	0.03	0.03	
LD-SD-SP								
$ApEn_{max}^{RR(SP-SD)}$ (a.u.)	28	0.04	0.12	12	-0.05	0.11	0.04	
$SampEn^{RR(SD-LD)}$ (a.u.)	28	-0.03	0.12	12	0.07	0.11	0.02	
$ApEn_{max}^{PR(SD-LD)}$ (a.u.)	28	-0.02	0.07	12	0.05	0.06	0.008	
$SampEn^{PR(SP-SD)}$ (a.u.)	28	0.07	0.15	12	-0.04	0.18	0.04	
$ApEn_{max}^{PR(SP-SD)}$ (a.u.)	28	0.012	0.11	12	-0.07	0.13	0.05	
$\sigma^{PAT(SD)}$ (ms)	28	6.36	4.76	12	4.16	0.84	0.002	
$\sigma^{PAT(SP-SD)}$ (ms)	28	-0.75	3.6	12	0.94	1.22	0.02	
$P_{LF}^{PAT(SD)} (\text{ms}^{-2}) (10^{-4})$	28	0.17	0.43	12	0.03	0.02	0.01	
$P_{LFn}^{PAT(SD)} (\%)$	28	62.4	16.9	12	45.9	15	0.009	
$LF/HF^{PAT(SD)}$ (adim.)	28	2.81	3.41	12	0.99	0.59	0.009	
$LF/HF^{PAT(SP-SD)}$ (adim.)	27 *	-1.56	2.48	12	-0.14	0.78	0.02	
$\bar{f}^{R(SD)}$ (Hz)	28	0.29	0.06	12	0.26	0.04	0.04	

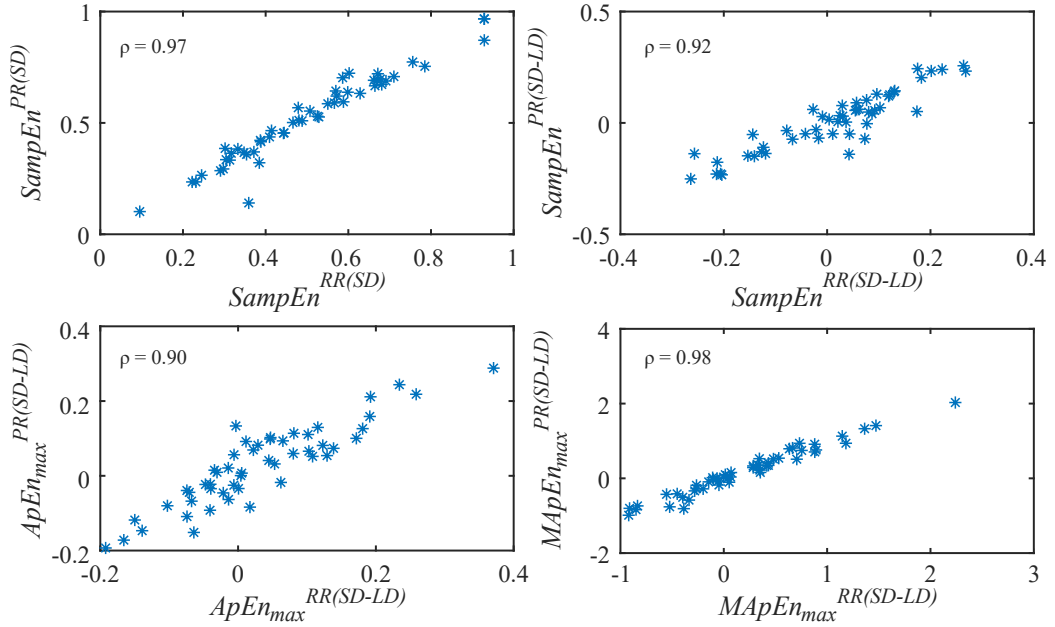


Figure 5.3 Correlation of nonlinear indices computed over RR and PR time series. Statistically significant nonlinear features are shown for LD-SD cohort.

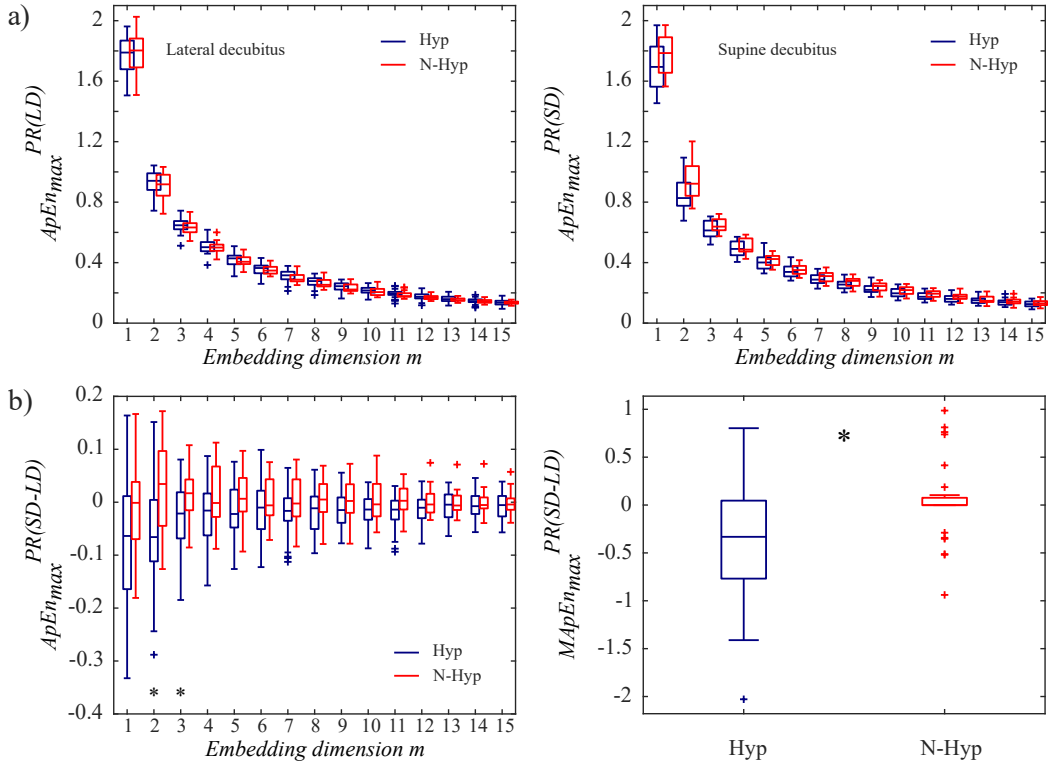


Figure 5.4 a) $ApEn(m, r_{max}(m))$ vs. m computed on PR time series during lateral decubitus (left panel) and during supine decubitus (right panel). b) $ApEn(m, r_{max}(m))$ vs. m computed over PR time series evaluating differences between supine and lateral decubitus (left panel). Data distribution of $MapEn_{max}^{PR(SD-LD)}$ for hypotensive and normotensive groups are shown (right panel). p -values ≤ 0.05 were statistically significant by Mann-Whitney U test.

Table 5.3 Classification results for the LD-SD cohort for the different considered classifiers. In all cases $ApEn_{max}^{PR(SD-LD)}$ and $\sigma^{PAT(SD)}$ were selected by Greedy algorithm as best feature combination. (#) number of features, (Sens.) sensitivity, (Spec.) specificity, (PPV) positive predictive value, (Acc.) accuracy, and F1 score.

Classifiers	#	Sens.(%)	Spec.(%)	PPV (%)	Acc. (%)	F1
Logistic Regression	2	76.55	69.81	57.84	72.20	0.66
Naive Bayes	2	73.78	58.91	49.75	64.16	0.59
Nearest Neighbor Method	2	44.78	73.33	47.96	63.25	0.46
LDA	2	41.56	79.64	49.45	66.20	0.46
QDA	2	68.00	59.70	48.27	62.63	0.56
SVM (linear kernel)	2	81.56	61.03	53.94	68.27	0.65
SVM (quadratic kernel)	2	71.33	58.30	48.70	62.90	0.57
SVM (polynomial order 3 kernel)	2	64.56	57.03	45.59	59.79	0.53
SVM (Radial Basis kernel)	2	75.67	60.48	51.52	65.84	0.61
SVM (Multilayer perceptron kernel)	2	77.67	59.76	50.92	66.08	0.62

Subsets of features from the two studied cohorts (LD-SD and LD-SD-SP) and a third one (LD-SD¹) that matches the same subjects from LD-SD-SP group discarding the SP position were evaluated for classification using the logistic regression approach. The classification results are shown in Tab. 5.4 and the parameters of the logistic models for the different studied cohorts can be found in Tab. 5.5.

It is worth noting that the features $ApEn_{max}^{PR(SD-LD)}$ and $\sigma^{PAT(SD)}$ were selected by the classifier in the three cohorts, and $\bar{f}^{R(SP)}$ was added in the set for the LD-SD-SP cohort. In Fig. 5.5 box-plots of the selected features for LD-SD and LD-SD-SP cohorts are illustrated.

Table 5.4 Classification results considering ECG derived respiration, RR, HRV, PR, PRV, and PAT analysis features for the three subgroups of the database depending on protocol segments. (#) number of features, (Sens.) sensitivity, (Spec.) specificity, (PPV) positive predictive value, (Acc.) accuracy, and, F1 score.

Features Cohorts	#	Sens.(%)	Spec.(%)	PPV (%)	Acc. (%)	F1
LD-SD (33 vs. 18)						
$ApEn_{max}^{PR(SD-LD)}$ (a.u.)	2	76.55	69.81	57.84	72.20	0.66
$\sigma^{PAT(SD)}$ (ms)						
LD-SD ¹ (28 vs. 12)						
$ApEn_{max}^{PR(SD-LD)}$ (a.u.)	2	78.42	68.13	51.17	71.22	0.62
$\sigma^{PAT(SD)}$ (ms)						
LD-SD-SP (28 vs. 12)						
$ApEn_{max}^{PR(SD-LD)}$ (a.u.)						
$\sigma^{PAT(SD)}$ (ms)	3	75.44	74.85	56.66	75.03	0.65
$\bar{f}^{R(SP)}$ (Hz)						

Table 5.5 Logistic regression parameters for the different cohorts.

Logistic reg. parameters	LD-SD (33 vs. 18)	LD-SD ¹ (28 vs. 12)	LD-SD-SP (28 vs. 12)
$\hat{\beta}_0$	0.306	0.446	3.13
$\hat{\beta}_1$ [$\sigma^{PAT(SD)}$]	-0.38	-0.479	-0.555
$\hat{\beta}_2$ [$ApEn_{max}^{PR(SD-LD)}$]	8.36	10.48	-3.753
$\hat{\beta}_3$ [$\bar{f}^{R(SP)}$]	-	-	-10.55
p_{th}	0.342	0.268	0.344

where $\hat{\beta}$'s are the coefficients and in [] is represented the corresponding feature following eq. 5.1. p_{th} is the probability threshold of risk of suffering from hypotension.

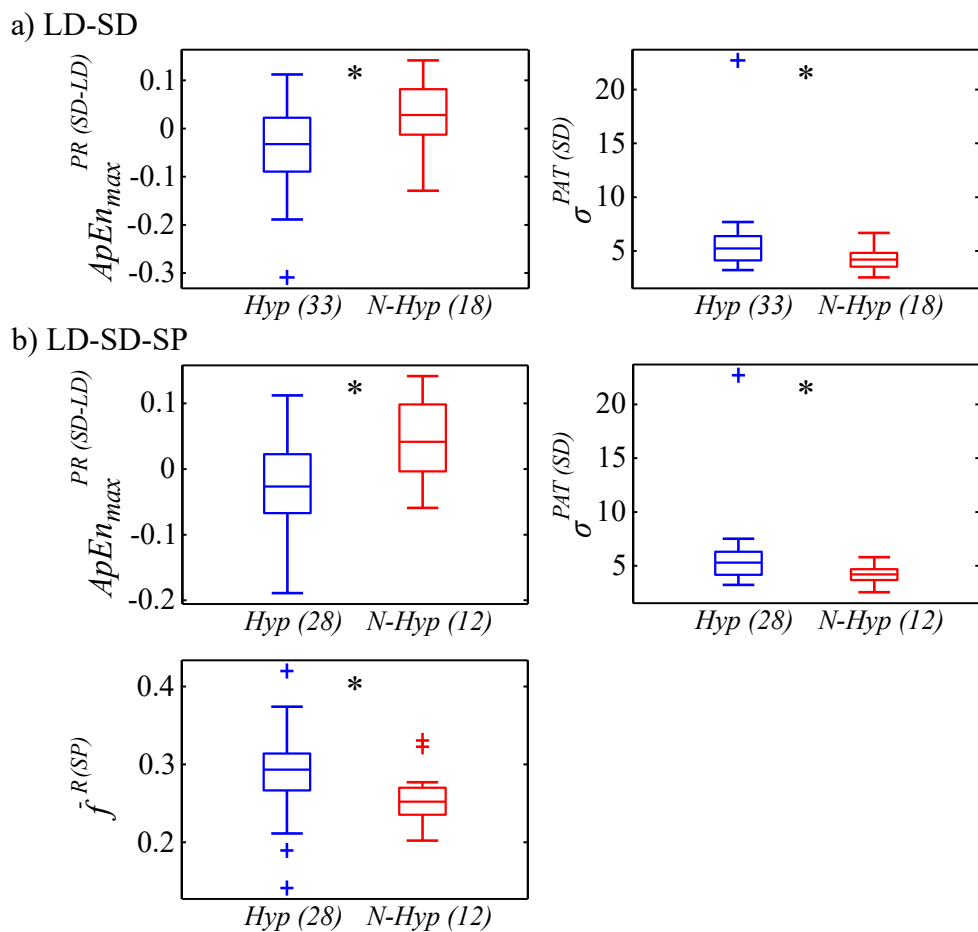


Figure 5.5 Box-plots of the features that were finally selected by classification procedure for a) LD-SD and b) LD-SD-SP cohorts.

5.4 Discussion

Hypotensive episodes after spinal anesthesia during cesarean delivery were hypothesized to be more frequent in patients with high level of stress. The risk of suffering from hypotensive events could be related to alterations in the ANS response associated with the stress caused by the proximity of surgery and the last period of pregnancy [46, 133]. To evaluate this hypothesis, the database used in this study was recorded following a specific protocol enhancing the ANS response due to hemodynamic changes. Aside from using an ANS elicitation protocol (body position changes), which has been proved to be helpful to identify women at risk of severe hypotensive events [95], one of the novelties of this study lies in the inclusion of the PAT signal analysis as an alternative to blood pressure measurement that can be more easily obtained in clinical practice [127]. Furthermore, PAT signal provides beat-to-beat information related to arterial stiffness and respiration whereas this information is missed in blood pressure (BP) measurements by cuff recordings. Improving the accuracy in predicting hypotensive events to avoid the side effects that pharmacological prophylaxis may produce in the mother and fetus in the low risk patient is the goal of our study. However, the performance obtained by predicting hypotension could be affected by the clinical criterion for considering an event as hypotensive, since BP was measured every 2 minutes after spinal injection. To minimize this effect, clinical hypotension was also considered when women showed symptoms of dizziness, nausea or discomfort.

In this work, the influence of respiration on the ANS modulation of the heart was also taken into account. This effect, known as respiratory sinus arrhythmia (RSA), is reflected in the HRV, PRV and PAT through the HF band, corresponding to the parasympathetic activity [71]. Variability analysis, in particular HRV analysis, could lead to misinterpreted results depending on respiratory rate [7]. As mentioned above, stress induced by surgery proximity may produce an increase of respiratory rate (towards upper boundary of HF band) and also compression of diaphragm. In such case, parasympathetic activity could be reflected in HRV at higher frequencies and thus classical HF band would not be able of capturing the information of interest properly. Therefore, variability analysis was proposed to be guided by respiration, defining an HF band centered in the respiratory rate.

The analyses of HRV and PRV were found to be highly correlated to each other, being in agreement with the results of Gil et al.[57], see Fig. 5.3. The evaluation on lateral decubitus, considered as a basal condition, revealed no differences between both groups of study when analyzing RR, HRV or PR, and PRV. However, a decreased tendency on the standard deviation of PAT was found as well as on its complexity, in terms of D_2 , $SampEn$, $ApEn_{max}$, and $MApEn_{max}$ values for the normotensive group with respect to the hypotensive one.

The hemodynamic stress was generated by supine decubitus position via aorto-cava compression. The analyses of RR, HRV and PR, PRV showed similar temporal and spectral values for both groups without statistical significance. Nevertheless, the normalized low frequency power of PAT increased and therefore, greater sympathetic activity [56] was recorded in the hypotensive group with respect

to the normotensive group. In addition, greater and significant changes were observed for *SampEn* pointing out to a decrease in the time series irregularity of RR and PR for hypotensive group. This tendency was found for *MAPEn_{max}* index as well but not statistically significant. PAT analysis revealed an increase in the amplitude variation values in the hypotensive group, see Fig. 5.2. On the one hand, PAT measure is affected by pulse wave velocity, which is related to BP [61]. On the other hand, in the present study, PAT values include the PEP which was reported to experiment changes under enhanced sympathetic conditions [74, 113]. PEP was also highlighted to represent from 12% to 35% of the PAT [139] and its variations could have a strong influence on the variations of the PAT measure [126]. Variations on PEP could help in the prediction of hypotensive episodes, since those variations might be enhanced in the same way as the ones in pulse wave velocity increasing the PAT discrimination power. Although one limitation of this study is the impossibility of separating those effects, the studied PAT measure can be easily obtained in the clinical routine and has discriminant power between hypotensive and normotensive groups.

The responsiveness of subjects through body position changes was explored by differences between supine and lateral decubitus analysis values. The statistical differences between hypotensive and normotensive group were more notable, in terms of irregularity for RR, PR and also for PAT evaluating the position change. Thus, this position change modifies the venous return and affects the ANS activity as well as arterial pressure and stiffness. The differences of approximate entropy values between supine and lateral decubitus computed on PR, achieved the lowest *p*-value when comparing both groups of study. On the contrary, same index computed on RR signal did not reveal statistical differences, so, hemodynamic changes affect peripheral regulation (blood pressure) more than heart regulation (heart rate). The analysis of *MAPEn_{max}* index, derived from RR and PR, showed statistically lower mean values for the hypotensive than the normotensive group by evaluating differences between supine and lateral decubitus positions. In regards to the conclusions obtained by synthetic data in chapter 4, variations of *MAPEn_{max}* index indicates a decrease in the complexity of the ANS response in the hypotensive group. The difference of standard deviation of PAT values observed between groups may be measuring the capacity of ANS to react in case of a drop in blood pressure. The normotensive group presented higher reaction range (lower $\sigma^{PAT(SD)}$ values), whereas the hypotensive group shows a narrow margin (higher $\sigma^{PAT(SD)}$ values) to reach the hypothetical physiological maximum value at which a hypotensive event is triggered.

The studied features that presented statistical differences comparing normotensive and hypotensive groups were selected as candidates for classification. Due to the high incidence ratio of hypotensive events (64.7% of cases), the prediction of the normotensive cases is mandatory; otherwise looking for hypotensive cases higher accuracy values can be achieved, but neglecting the other class. Thus, classification performance was carried out by evaluating the positive predictive value and sensitivity related to the normotensive group. Several classifiers were tested and the one providing the best classification results was selected, see Tab. 5.2. In all cases, the Greedy algorithm selected $ApEn_{max}^{PR(SD-LD)}$ and $\sigma^{PAT(SD)}$ as the best combination of features. Regarding the F1 score measurement, the logistic

regression classifier provided the best classification result for the LD-SD cohort: 76.55% of sensitivity, 69.81% of specificity, 57.84% of positive predictive value, and 72.2% of accuracy. Then, hereinafter classification results are referred to the logistic regression classifier.

Sitting position was also included in the protocol to enhance the ANS activity, once the database recording was in progress. The first 20 subjects (11 of the control group) were not asked to be in the sitting position while signals were recorded. All the analysis procedure was duplicated by considering this position on a subset of the whole database (LD-SD-SP), see Tab. 5.2. In this cohort, $\bar{f}^{R(SP)}$ was selected increasing the classification performance with respect to the one obtained for LD-SD¹ cohort. On the other hand, the comparison between sitting position and lateral decubitus did not reveal any index capable of distinguishing both groups of study. The variation in the sympathetic activity caused by sitting position with respect to the other two body positions was apparently not enough to generate notable changes on the studied indices.

In the study of Brenck et al. risk factors for developing hypotension based on population characteristics were studied over 500 pregnant women, achieving accuracy around 60% [25]. A test combining the demographic data with the features derived from the ECG and PPG signals was carried out with the data presented in this chapter, and the classification results using logistic regression were superior to only considering ECG and PPG-derived indices. In particular, the Greedy algorithm selected body mass index (BMI) and the standard deviation of PAT values during supine position, altogether leading to classification performance characterized by 82.5% sensitivity, 67.9% specificity, and 72.9% of accuracy. Based on this, it is reasonable to suggest that the combination of demographic data and features derived from ECG and PPG signals can lead to better classification results. However, this statement should be validated over an extended database.

Several studies attempted to shed light into the role of HRV and pulse oximeter derived index analysis for predicting hypotension after spinal anesthesia for cesarean section delivery [31, 66, 160, 199]. Despite of Yokose et al. found heart rate as the only predictor obtaining an area under the ROC curve (area under curve (AUC)) of 0.68, this feature did not show predictive power in the database analyzed in our study. In a study carried out by Sakata and co-workers, the importance of including postural changes into the recording protocol to enhance hemodynamic changes and ANS response was highlighted achieving an area under the ROC curve of 0.76. There, LF/HF was reported to be increased in those parturient who developed hypotension. In our case, similar trend was found for the LF/HF through the PAT signal (Hyp: 2.9 ± 3.38 versus No-Hyp: 1.31 ± 0.84 in LD-SD cohort and Hyp: 2.81 ± 3.41 versus No-Hyp: 0.99 ± 0.59 in LD-SD-SP cohort), see Tab. 5.2. Ghabach et al. reported a relationship between approximate entropy and antenatal weight gain [55]. Assuming that this position was lateral decubitus, which represents the basal position without any extra hemodynamic stress, the results found in this chapter are in disagreement with the ones reported by Ghabach. In our study no statistical differences were found in the weight gain (results shown in Tab. 5.1) nor in approximate entropy during lateral position (Hyp: 0.87 ± 0.08 ; N-Hyp: 0.85 ± 0.1 and p -value: 0.95, values corresponding to LD-SD cohort). Although in the work of Yokose et al. neither HRV nor PRV

were useful to prospectively relate the analysis results to hypotensive events [199], our study provides contrary insights. Lack of standardization on hypotension definition and the low number of subjects become a limitation leading to controversial results. Thus, future studies on a larger database should be explored.

Regarding the classification results obtained in this study, first, we would like to focus our attention into sensitivity values. Normotensive cases were defined as positive cases for classification, since this is the minority group and their associated subjects the ones who may suffer from anesthetic side effects in case of a failed detection. Among normotensive cases (18 women), the 76.55% of them (≈ 14) were correctly classified, thus only the 25% (≈ 4) could present anesthetic side effects. On the contrary, among hypotensive cases (33 women), the 69.8% (≈ 23) were correctly classified, whereas the 31.2% (≈ 10) were classified as normotensive and they will suffer from hypotension caused by anesthesia, but they will be treated when hypotension will be detected. The benefits of our classification results were highlighted being only 4 out of 55 women the population that could present undesirable, but avoidable by proper prediction, side effect in mother and fetus. The classifier presented in this chapter could help to better assist clinicians to take decisions. Although the accuracy obtained is close to the clinical target of the 80%, it is still margin to continue investigating to identify those factors that triggers the hypotensive events and increase the accuracy of their prediction.

5.5 Conclusion

PR and PAT analysis could help to predict hypotension events after spinal anesthesia during cesarean section extending the description of ANS regulation and its response to postural changes. Nonlinear indices characterizing PR and PAT time series used as features to classify normotensive and hypotensive women outcome could help to better assist clinicians to take decisions. These analyses may indicate the role of peripheral regulation and blood pressure changes in order to avoid the undesirable side effects of prophylactic administration in the low-risk population.

*“How often have I said to you that
when you have eliminated the
impossible, whatever remains,
however improbable, must be the
truth?”*

Sherlock Holmes

Sign of the Four, Ch. 6, p. 111

- Arthur Conan Doyle (1859-1930) -

6

Conclusions and Future Lines

Summary

Nonlinear indices for short-term HRV analysis have been reported as promising in the description of ANS regulation of the heart, providing complementary information to the classical time- and frequency-domain methods. However, their physiological interpretation remains unclear, since quantification of nonlinear indices is highly dependent on methodological factors, such as the intrinsic sampling rate of the HRV time series or the selection of parameter values involved in the definitions. In this thesis, a methodological framework aimed at increasing estimation reliability of nonlinear HRV indices is introduced. This framework could aid in the physiological interpretation of cardiac ANS regulation and reduce the computational cost for short-term HRV analysis, thus rendering nonlinear HRV analysis more suitable for application in clinical practice. Major concluding remarks of this thesis are presented in the following.

Nonlinear HRV Analysis: Reliability and Computational Load

In chapter 2, a novel framework for estimation of correlation dimension was introduced. The inclusion of self-comparisons in computing the probability of finding similar patterns among reconstructed vectors allowed us to fit the *log-log* curves to a sigmoidal function (upper asymptote corresponding to the case of all reconstructed vectors being considered as similar to each other, and lower asymptote referring to the case of only self-comparisons being considered in the computation of correlation sums). The proposed approach improves the identification of the linear region and the slope is estimated as the maximum of the derivative of the sigmoidal function.

One of the bottlenecks in the application of nonlinear HRV analysis in clinical practice is its high computational load. An algorithm was proposed based on matrix operations that led to a notable reduction in computational load as compared to the sequential approach. With the proposed algorithm D_2 was estimated in 1 second for a 300-sample time series, while the sequential approach took 18 minutes.

Within the methodological framework proposed in this thesis, two alternatives for estimating correlation dimension were considered. The first one, with correlation dimension estimate denoted by $D_{2(\perp)}$, considered a range of slope values near the maximum slope in the *log-log* curve of $m = 1$ and a gradient descent technique was used to estimate the slopes of the remaining *log-log* curves. The second one, providing a correlation dimension estimate denoted by $D_{2(max)}$, considered maximum values of the *SampEn* surface. The proposed methodologies for D_2 computation were tested by estimating the fractal dimension of the Lorenz attractor, obtaining a relative error with respect to the theoretical value of 4% for $D_{2(max)}$ and 1% for $D_{2(\perp)}$, while the relative error for the sequential approach was of 4%.

Caveats in the Interpretation of Nonlinear HRV Indices

Effect of HRM on Nonlinear HRV Indices

In chapter 3, the influence of HR on nonlinear HRV indices was addressed. A simulation study using the IPFM model was carried out to investigate conditions where HRV and HR were uncorrelated. Stochastic realizations of IPFM modulating signals were generated based on estimates from a healthy subject at rest. The model allowed the variation of HRM values without altering the remaining model components, thus generating RR time series with similar ANS modulation but different HRM. The studied nonlinear HRV indices (correlation dimension as well as approximate and sample entropy) showed positive correlation with mean RR changes (negative with respect to HRM), being these results in agreement with the dependencies reported in previous studies [202, 146, 123, 195]. Methodologies

to attenuate this HRM effect on nonlinear HRV indices were proposed based on: interpolation of RR time series; computation of RR time series as derived from a point-process model; and regression (linear and parabolic) formulas relating HRV indices and RR.

A database consisting of ECG recordings of healthy subjects undergoing body position changes, as described in section 3.2.2, was analyzed and nonlinear HRV indices were calculated. An increase in HRM of 28% (in terms of median values) was measured when changing from supine to upright position. The corresponding nonlinear HRV indices were statistically significantly reduced by 21, 34, and 21 % for $D_{2(max)}$, $SampEn$ and $ApEn_{max}$ respectively. When introducing interpolation prior to computation of nonlinear HRV, the corrected indices were found to be significantly reduced in upright with respect to supine position, in this case by 18, 30, and 12 % for $D_{2(max)}$, $SampEn$ and $ApEn_{max}$ respectively, thus confirming attenuation of the HRM effect. Application of HRM correction of nonlinear HRV indices based on linear or parabolic regression formulas led to results similar to those obtained by interpolation, with the disadvantage of being more time-consuming. Correction using a point-process model also attenuated the dependence of nonlinear HRV indices on HRM. However, the high resolution of point-process-derived time series needed to capture the right censoring effect imply a very notable increase in data length, which possibly precludes the use of this technique in clinical applications. Globally, the approaches proposed in this thesis lead to HR-corrected nonlinear HRV indices able to capture the variation in cardiac ANS modulation induced by body position-induced changes regardless of variations in HRM values.

Application of the proposed methodologies to correct for the effects of HR could represent an improvement in the applicability of nonlinear HRV analysis, extending it to cases where HRM cannot be considered as constant. Evaluation of nonlinear HRV beyond HR is of relevance. In this regard, previous studies have demonstrated differences in nonlinear HRV indices despite controlling for HR values, as in the study by Weippert et al., who reported differences in nonlinear HRV analysis under dynamic and static exercise even if keeping similar HRs [188].

Effects of a priori Parameter Value Selection on Nonlinear HRV Indices

On top of the effect of HRM on nonlinear HRV indices, physiological interpretation of these indices can also be influenced by the value of parameters that need to be *a priori* defined when defining the indices. Approximate entropy is an example where the values of the embedding dimension, m , and the threshold, r , need to be selected prior to its computation. The effect of varying the values of these parameters was assessed in chapter 4. Rather than considering a fixed threshold value r , selecting the one that maximizes the approximate entropy (denoted by maximum approximate entropy) has been reported to be a better indicator of the degree of randomness of the time series. However, this maximum approximate entropy still remains dependent on the embedding dimension m , which hampers its interpretation. To cope with this, a nonlinear approximate entropy-based index

independent of *a priori* parameters was proposed in this thesis. This index is called multidimensional approximate entropy, $MApEn_{max}$.

Time series generated from $MIX(P)$ processes, with varying level of randomness, as well as from white and $1/f$ noises were used as a basis for evaluation of the proposed $MApEn_{max}$ index. The obtained results showed that the proposed index was able to capture the degree of randomness with increasingly higher $MApEn_{max}$ values for more random time series. The results for $MApEn_{max}$ were compared with those of $ApEn(m, r_{max}(m))$, for particular values of the embedding dimension m . The proposed index, by accounting for multidimensional information, showed more pronounced differences as a function of the level of randomness as compared to $ApEn(m, r_{max}(m))$ for any individual value of m .

By incorporating the proposed multidimensional index to nonlinear HRV analysis, the effects of aging and CHF disease were assessed. Aging on was evaluated by investigating ECG recordings of healthy awake subjects at rest. Lower $MApEn_{max}$ values were found in the elderly group as compared to the young group. Such a reduction in HRV may be indicative of a decrease in ANS regulation complexity with age. In a separate investigation, ECG recordings of CHF patients and healthy subjects were analyzed during the night period. CHF patients showed greater $MApEn_{max}$ values than healthy subjects. Although these results would reflect increased nonlinearities in ANS regulation in association with CHF, the influence of other concomitant disorders, such as sleep apnea, on HRV cannot be discarded, which would interfere in the interpretation of CHF effects.

In conclusion, the proposal of $MApEn_{max}$ as a novel index for nonlinear HRV analysis provides more robust information on the randomness level of time series and could represent a better indicator of HR dynamics complexity, with the additional important advantage of being independent of pre-selected parameter values.

Clinical Application: Improving Efficacy of Prophylaxis in Preventing Hypotensive Events during Cesarean Section

The aforementioned methodological proposals were applied to investigate a stress-related clinical problem, namely prediction of hypotensive episodes during cesarean section after spinal anesthesia. The study was carried out in collaboration with the Anesthesia Department of Hospital Miguel Servet (Zaragoza, Spain). The stress caused by the last period of pregnancy and the proximity of surgery could be factors altering ANS regulation on the heart and predisposing to hypotension. Linear and nonlinear analyses applied onto cardiovascular variability signals, such as HRV, pulse arrival time variability and pulse rate (from pulse photoplethysmographic signal) variability, were analyzed following a protocol that included variations in body position (lateral decubitus, supine decubitus and sitting) to elicit autonomic changes.

Analyzed features presenting statistically significant differences between normotensive and hypotensive groups were incorporated into a logistic regression-based classifier. The best classification results were achieved for the combination of $ApEn_{max}^{PR(SD-LD)}$ and $\sigma^{PAT(SD)}$, measured at lateral and supine decubitus, reaching 76.55% sensitivity, 69.81% specificity, 57.84% positive predictive value and 72.2% accuracy. These figures on classification performance evaluate the positive predictive value and sensitivity referred to the normotensive group, as the main objective of the study is to improve prophylaxis efficacy to avoid undesirable side effects in this low-risk normotensive group.

According to the obtained results, PR and PAT analysis could help predict hypotensive events after spinal anesthesia during cesarean section, thus extending the description of ANS regulation to other variability signals on top of HRV. Peripheral regulation and blood pressure information, incorporated into a classifier like the one proposed in this thesis, could aid clinicians in their decision making.

Importantly, the benefit of including nonlinear indices in the description of variability signals was highlighted in the evaluated stress-related clinical problem, where the combination of a nonlinear index (measuring maximum approximate entropy) and a temporal index (measuring the standard deviation) was selected as providing the best classification results. In addition, nonlinear HRV indices corrected for HR effect as well as the novel multidimensional parameter-free index proposed in this thesis, $MApEn_{max}$, demonstrated the ability to capture altered ANS modulation in the evaluated problem.

Future Lines

Based on the results achieved in this PhD thesis, the following extensions or future lines are proposed:

Nonlinear HRV Analysis under ANS Blockade Conditions

Physiological interpretation on the role of sympathetic and parasympathetic ANS branches in modulating nonlinear HRV characteristics deserves further investigation. Analysis of the nonlinear HRV indices proposed in this study under interventions inhibiting or stimulating the activity of each of the two autonomic branches would be of major interest. This proposed analysis should ideally first be performed over a healthy population to provide meaningful physiological interpretations that could be the basis for subsequent studies aimed at elucidating how specific cardiac disorders alter cardiac ANS modulation quantified via nonlinear HRV analysis.

Another investigation that should be accomplished in future studies regards the study of changes in nonlinear HRV in the presence of multiple concomitant disorders. In this thesis, nonlinear HRV was analyzed in patients with congestive heart failure. However, a relevant number of those patients presented with sleep apnea, which may notably limit interpretation of the obtained results in terms of CHF effects [129]. While patients presenting multiple disorders could have been discarded from further analysis, the low number of them fulfilling such criterion represents a major limitation. Access

to a database comprising a relevant number of patients free from any other disorder apart from CHF could be the basis of a new research line.

On the Relation of ANS and Cardio-respiratory System

Another effect interfering in HRV interpretation is respiratory sinus arrhythmia, which is associated with the high frequency content in spectral HRV analysis. Contradictory results have been reported from the analysis of the influence of controlled breathing on nonlinear HRV indices [86, 152]. The point-process methodology, introduced in chapter 3, has been used to assess the interaction of cardio-respiratory and ANS systems [184, 32]. Valenza et al. described the concept of complexity variability as variations in instantaneous dominant Lyapunov exponent estimates [185]. Based on this concept, the coupling between HRV and respiration was analyzed, quantifying the effect of respiratory sinus arrhythmia on HRV. Based on the results of this thesis, the usage of $MApEn_{max}$ may render valuable information analyzing the effect of RSA on HRV in terms of irregularity, since pattern length related to RSA could match with the embedding dimension used by $ApEn$ misleading the underlying nonlinear dynamic.

Spectral HRV Complexity

Spectral HRV analysis is commonly accepted as a method to assess sympathetic and parasympathetic contributions to ANS modulation of heart rate. Most methods based on the study of spectral components assume stationarity of heart rate signals and characterize low and high frequency powers of HRV by a single value. Spectral time-varying approaches extend the applicability of spectral analysis to conditions where ANS modulation is changing, as e.g. during exercise. The assessment of the results obtained by time-frequency approaches is limited to characterize central tendency and amplitude variations of spectral components. However, the framework developed in this thesis for nonlinear HRV analysis could be extended to this study, providing further and information of interest about nonlinear ANS modulation dynamics.

Publications

The conference as well as journal contributions are listed, on each subsection, first the ones directly related to the PhD thesis experiments, and second (separated by a dash-dotted line) to collaborative studies providing the knowledge acquired during the PhD thesis period.

Conference Proceedings

- J. Bolea, R. Bailón, E. Rovira, J.M. Remartínez, P. Laguna, A. Navarro. Heart rate variability in pregnant women before programmed cesarean intervention. *In Proc. XIII Mediterranean Conf. on Medical and Biological Engineering and Computing*, pp. 710-713, 2013
- J. Bolea, E. Pueyo, P. Laguna, R. Bailón. Non-linear HRV indices under autonomic nervous system blockade. *In Proc. of the Ann. Int. Conf. IEEE Engineering in Medicine and Biology Society*, vol 2014, pp 3252-3255
-
- L. Canga, A. Navarro, J. Bolea, J.M. Remartínez, P. Laguna, R. Bailón. Non-linear analysis of heart rate variability and its application to predict hypotension during spinal anesthesia. *In Proc. Computing in Cardiology*, vol. 39, pp. 413-416, 2012
- J.M. Remartínez, R. Bailón, E. Rovira, J. Bolea, P. Laguna, A. Navarro. Heart rate variability analysis for the prediction of hypotension during spinal anesthesia in programmed cesarean surgery and its relation with fetal cord acid-base equilibrium. *In Proc. Computing in Cardiology*, vol. 40, pp. 1231-1234, 2013
- M.T. Valderas, J. Bolea, P. Laguna, M. Vallverdú, R. Bailón. Human emotion recognition using heart rate variability analysis with spectral bands based on respiration. *In Proc. of the Ann. Int. Conf. IEEE Engineering in Medicine and Biology Society*, vol 2015, pp 6134-6137
- J. Milagro, E. Gil, J. Bolea, V-P. Seppä, L.P. Malmberg, A.S. Pelkonen, A. Kotaniemi-Syrjänen, M.J. Mäkelä, J. Viik, R. Bailón. Nonlinear dynamics of heart rate variability in children with asthmatic symptoms. *In Proc. of the European Medical and Biological Engineering Conference (EMBEC) and the Nordic-Baltic Conference on Biomedical Engineering and Medical Physics (NBC)*, vol 65, pp 815-818, 2017
- M. Nardelli, A. Greco, J. Bolea, G. Valenza, E.P. Scilingo, R. Bailón. Investigation of Lagged Poincaré Plot reliability in ultra-short synthetic and experimental Heart Rate Variability series. *In Proc. of the Ann. Int. Conf. IEEE Engineering in Medicine and Biology Society*, vol 2017, pp 2329-2332

Journals

- J. Bolea, P. Laguna, J.M. Remartínez, E. Rovira, A. Navarro, R. Bailón. Methodological framework for estimating the correlation dimension in HRV signals. *Computational and Mathematical Methods in Medicine*. Volume 2014, Article ID 129248, pp.1-11, 2014, doi: 10.1155/2014/129248.
- J. Bolea, E. Pueyo, M. Orini, R. Bailón. Influence of heart rate in non-linear HRV indices as sampling rate effect evaluated on supine and standing. *Frontiers in Physiology*, Volume 7, Article 501. doi:10.3389/fphys.2016.00501.
- J. Bolea, J. Lázaro, E. Gil, E. Rovira, J.M. Remartínez, P. Laguna, E. Pueyo, A. Navarro, R. Bailón. Pulse Rate and Transit Time Analysis to Predict Hypotension Events After Spinal Anesthesia During Programmed Cesarean Labor. *Annals of Biomedical Engineering*, Volume 45, Issue 9, pp. 2253–2263, 2017, doi: 10.1007/s10439-017-1864-y.
- J. Bolea, E. Pueyo, R. Bailón. Multidimensional approximate entropy to characterize aging and congestive heart failure by short-term HRV analysis. *To be published*.

— · — · — · —

- M. Nardelli, A. Greco, J. Bolea, G. Valenza, E.P. Scilingo, R. Bailón. Reliability of Lagged Poincaré Plot parameters in ultra-short Heart Rate Variability series: Application on Affective Sounds. *IEEE Journal of Biomedical and Health Informatics*, 2017, doi: 10.1109/JBHI.2017.2694999

Bibliography

- [1] Abásolo, D., Hornero, R., Espino, P., Poza, J., Sánchez, C. I., and de la Rosa, R. (2005). Analysis of regularity in the EEG background activity of Alzheimer's disease patients with Approximate Entropy. *Clinical Neurophysiology*, 116(8):1826–1834.
- [2] Akselrod, S., Gordon, D., Ubel, F. A., Shannon, D. C., Berger, A. C., and Cohen, R. J. (1981). Power spectrum analysis of heart rate fluctuation: a quantitative probe of beat-to-beat cardiovascular control. *Science (New York, N.Y.)*, 213(4504):220–2.
- [3] Aletti, F., Ferrario, M., Almas de Jesus, T. B., Stirbulov, R., Borghi Silva, A., Cerutti, S., and Malosa Sampaio, L. (2012). Heart rate variability in children with cyanotic and acyanotic congenital heart disease: analysis by spectral and non-linear indices. In *Proc. of the Ann. Int. Conf. IEEE Engineering Medical Biology Society*, Annual International Conference of the IEEE, pages 4189–4192.
- [4] Allen, T. K., George, R. B., White, W. D., Muir, H. A., and Habib, A. S. (2010). A double-blind, placebo-controlled trial of four fixed rate infusion regimens of phenylephrine for hemodynamic support during spinal anesthesia for cesarean delivery. *Anesthesia and analgesia*, 111(5):1221–9.
- [5] Almeida, R., Gouveia, S., Rocha, A. P., Pueyo, E., Martinez, J. P., and Laguna, P. (2006). QT variability and HRV interactions in ECG: quantification and reliability. *IEEE Trans. Biomed. Eng.*, 53(7):1317–1329.
- [6] Alvarez-Ramirez, J., Rodriguez, E., and Echeverría, J. C. (2009). Delays in the human heartbeat dynamics. *Chaos: An Interdisciplinary Journal of Nonlinear Science*, 19(2):028502.
- [7] Bailon, R., Laguna, P., Mainardi, L., and Sornmo, L. (2007). Analysis of heart rate variability using time-varying frequency bands based on respiratory frequency. *Proc. of the Ann. Int. Conf. IEEE Engineering Medical Biology Society*, 2007:6675–8.
- [8] Bailón, R., Laouini, G., Grao, C., Orini, M., Laguna, P., and Meste, O. (2011). The integral pulse frequency modulation model with time-varying threshold: application to heart rate variability analysis during exercise stress testing. *IEEE Trans Biomed Eng*, 58(3):642–652.
- [9] Bailón, R., Mainardi, L., Orini, M., Sörnmo, L., and Laguna, P. (2010). Analysis of heart rate variability during exercise stress testing using respiratory information. *Biomedical Signal Processing and Control*, 5(4):299–310.
- [10] Barbieri, R., Matten, E. C., Alabi, A. A., and Brown, E. N. (2004). A point-process model of human heartbeat intervals: new definitions of heart rate and heart rate variability. *AJP: Heart and Circulatory Physiology*, 288(1):H424–H435.
- [11] Bari, V., Valencia, J. F., Vallverdú, M., Girardengo, G., Bassani, T., Marchi, A., Calvillo, L., Caminal, P., Cerutti, S., Brink, P. A., Crotti, L., Schwartz, P. J., and Porta, A. (2013). Refined multiscale entropy analysis of heart period and QT interval variabilities in long QT syndrome type-1 patients. In *Proc. of the Ann. Int. Conf. IEEE Engineering Medical Biology Society*, Annual International Conference of the IEEE, pages 5554–5557.

- [12] Bari, V., Valencia, J. F., Vallverdú, M., Girardengo, G., Marchi, A., Bassani, T., Caminal, P., Cerutti, S., George, A. L., Brink, P. A., Crotti, L., Schwartz, P. J., and Porta, A. (2014). Multiscale complexity analysis of the cardiac control identifies asymptomatic and symptomatic patients in long QT syndrome type 1. *PloS one*, 9(4):e93808.
- [13] Baumert, M., Seeck, A., Faber, R., Nalivaiko, E., and Voss, A. (2010). Longitudinal changes in QT interval variability and rate adaptation in pregnancies with normal and abnormal uterine perfusion. *Hypertension Research*, 33(6):555–560.
- [14] Beckers, F., Verheyden, B., and Aubert, A. E. (2006a). Aging and nonlinear heart rate control in a healthy population. *American journal of physiology. Heart and circulatory physiology*, 290(6):H2560–70.
- [15] Beckers, F., Verheyden, B., Ramaekers, D., Swyndghedauw, B., and Aubert, A. E. (2006b). Effects of autonomic blockade of non-linear cardiovascular variability indices in rats. *Clin Exp Pharmacol Physiol*, 33(5-6):431–439.
- [16] Berger, S., Kliem, A., Yeragani, V., and Bär, K.-J. (2012). Cardio-respiratory coupling in untreated patients with major depression. *Journal of affective disorders*, 139(2):166–71.
- [17] Betrán, A. P., Ye, J., Moller, A.-B., Zhang, J., Gülmезoglu, A. M., and Torloni, M. R. (2016). The Increasing Trend in Caesarean Section Rates: Global, Regional and National Estimates: 1990-2014. *PloS one*, 11(2):e0148343.
- [18] Billman, G. E. (2011). Heart rate variability - a historical perspective. *Frontiers in physiology*, 2:86.
- [19] Billman, G. E., Huikuri, H. V., Sacha, J., and Trimmel, K. (2015). An introduction to heart rate variability: methodological considerations and clinical applications. *Front. Physiol.*, 6(55):1–3.
- [20] Boettger, S., Puta, C., Yeragani, V. K., Donath, L., Müller, H.-J., Gabriel, H. H. W., and Bär, K.-J. (2010). Heart rate variability, QT variability, and electrodermal activity during exercise. *Medicine and science in sports and exercise*, 42(3):443–8.
- [21] Bolea, J., Bailón, R., Rovira, E., Remartínez, J. M., Laguna, P., and Navarro, A. (2014a). Heart rate variability in pregnant women before programmed Cesarean intervention. *IFMBE Proceedings*, 41:710–713.
- [22] Bolea, J., Laguna, P., Remartínez, J. M., Rovira, E., Navarro, A., and Bailón, R. (2014b). Methodological framework for estimating the correlation dimension in HRV signals. *Computational and Mathematical Methods in Medicine*, 2014.
- [23] Bolea, J., Pueyo, E., Laguna, P., and Bailón, R. (2014c). Non-linear HRV indices under autonomic nervous system blockade. *Proceedings of the Annual International Conference of the IEEE Engineering in Medicine and Biology Society, EMBS*, 2014:3252–3255.
- [24] Bonnemeier, H., Richardt, G., Potratz, J., Wiegand, U. K. H., Brandes, A., Kluge, N., and Katus, H. A. (2003). Circadian profile of cardiac autonomic nervous modulation in healthy subjects: differing effects of aging and gender on heart rate variability. *Journal of cardiovascular electrophysiology*, 14(8):791–9.
- [25] Brenck, F., Hartmann, B., Katzer, C., Obaid, R., Brüggemann, D., Benson, M., Röhrlig, R., and Junger, A. (2009). Hypotension after spinal anesthesia for cesarean section: identification of risk factors using an anesthesia information management system. *Journal of clinical monitoring and computing*, 23(2):85–92.

- [26] Cabiddu, R., Trimer, R., Borghi-Silva, A., Migliorini, M., Mendes, R. G., Oliveira, A. D., Costa, F. S. M., and Bianchi, A. M. (2015). Are Complexity Metrics Reliable in Assessing HRV Control in Obese Patients During Sleep? *PloS one*, 10(4):e0124458.
- [27] Canga, L., Navarro, A., Bolea, J., Remartínez, J. M., Laguna, P., and Bailón, R. (2012). Non-linear analysis of heart rate variability and its application to predict hypotension during spinal anesthesia for cesarean delivery. In *Computing in Cardiology (CinC)*, 2012, pages 413–416.
- [28] Cao, L. (1997). Practical method for determining the minimum embedding dimension of a scalar time series. *Physica D: Nonlinear Phenomena*, 110(1):43–50.
- [29] Carvajal, R., Zebrowski, J. J., Vallverd, M., Baranowski, R., Chojnowska, L., Poplawska, W., and Caminal, P. (2002). Dimensional analysis of HRV in hypertrophic cardiomyopathy patients. *IEEE Engineering in Medicine and Biology*, 21(4):71–78.
- [30] Cerutti, S., Carrault, G., Cluitmans, P. J. M., Kinie, A., Lipping, T., Nikolaidis, N., Pitas, I., and Signorini, M. G. (1996). Non-linear algorithms for processing biological signals. *Computer Methods and Programs in Biomedicine*, 51(1-2):51–73.
- [31] Chamchad, D., Arkoosh, V. A., Horrow, J. C., Buxbaum, J. L., Izrailityan, I., Nakhamchik, L., Hoyer, D., and Kresh, J. Y. (2004). Using Heart Rate Variability to Stratify Risk of Obstetric Patients Undergoing Spinal Anesthesia. *Anesthesia and Analgesia*, 99(6):1818–1821.
- [32] Chen, Z., Brown, E. N., and Barbieri, R. (2009). Assessment of autonomic control and respiratory sinus arrhythmia using point process models of human heart beat dynamics. *IEEE transactions on bio-medical engineering*, 56(7):1791–802.
- [33] Chiu, H., Wang, T., Huang, L., Tso, H., and Kao, T. (2003). The influence of mean heart rate on measures of heart rate variability as markers of autonomic function: A model study. *Med. Eng. Phys.*, 25(6):475–481.
- [34] Chon, K., Scully, C. G., and Lu, S. (2009). Approximate entropy for all signals. *IEEE engineering in medicine and biology magazine : the quarterly magazine of the Engineering in Medicine & Biology Society*, 28(6):18–23.
- [35] Chua, C. P. and Heneghan, C. (2005). Pulse transit time-derived respiratory parameters and their variability across sleep stages. *Proc. In Annual International Conference of the IEEE Engineering in Medicine and Biology Society. IEEE Engineering in Medicine and Biology Society*, 6:6153–6.
- [36] Citi, L., Brown, E. N., and Barbieri, R. (2012). A real-time automated point-process method for the detection and correction of erroneous and ectopic heartbeats. *IEEE transactions on bio-medical engineering*, 59(10):2828–37.
- [37] Cleary-Goldman, J., Negron, M., Scott, J., Downing, R. A., Camann, W., Simpson, L., and Flood, P. (2005). Prophylactic ephedrine and combined spinal epidural: maternal blood pressure and fetal heart rate patterns. *Obstetrics and gynecology*, 106(3):466–72.
- [38] Cohn, J. N. (1984). Unloading the heart in congestive heart failure. *The American journal of medicine*, 77(2A):67–70.
- [39] Cormen, T., Leiserson, C., Rivest, R., and Stein, C. (2009). *Introduction to algorithms*. MIT Press, Cambridge, 3rd editio edition.
- [40] Costa, M., Goldberger, A. L., and Peng, C.-K. (2002). Multiscale Entropy Analysis of Complex Physiologic Time Series. *Physical Review Letters*, 89(6):068102.

- [41] Costa, M., Goldberger, A. L., and Peng, C. K. (2005). Multiscale entropy analysis of biological signals. *Physical Review E - Statistical, Nonlinear, and Soft Matter Physics*, 71(2).
- [42] Cyna, A. M., Andrew, M., Emmett, R. S., Middleton, P., and Simmons, S. W. (2006). Techniques for preventing hypotension during spinal anaesthesia for caesarean section. *Cochrane Database Syst Rev*, 18(4):CD002251.
- [43] Cysarz, D., Lange, S., Matthiessen, P. F., and van Leeuwen, P. (2007). Regular heartbeat dynamics are associated with cardiac health. *American journal of physiology. Regulatory, integrative and comparative physiology*, 292(1):R368–72.
- [44] De Meersman, R. E. and Stein, P. K. (2007). Vagal modulation and aging. *Biological Psychology*, 74(2):165–173.
- [45] Dimitriev, D. and Saperova, E. (2012). Nonlinear parameters of heart rate variability during mental stress. *The FASEB Journal*, 26(1 Supplement):lb618–lb618.
- [46] Dishman, R. K., Nakamura, Y., Garcia, M. E., Thompson, R. W., Dunn, A. L., and Blair, S. N. (2000). Heart rate variability, trait anxiety, and perceived stress among physically fit men and women. *International journal of psychophysiology : official journal of the International Organization of Psychophysiology*, 37(2):121–33.
- [47] Dollinger, J. W., R., M., and Nonnenmacher, T. F. (1998). Bi-asymptotic fractals: Fractals between lower and upper bounds. *J. Phys. A: Math. Gen.*, 31(16):3839–3847.
- [48] Dreifus, L. S., Agarwal, J. B., Botvinick, E. H., Ferdinand, K. C., Fisch, C., Fisher, J. D., Kennedy, J., Kerber, R. E., Lambert, C. R., Okike, O. N., Prystowsky, E. N., Saksena, S. V., Schroeder, J. S., and Williams, D. O. (1993). Heart rate variability for risk stratification of life-threatening arrhythmias. *Journal of the American College of Cardiology*, 22(3).
- [49] Du, X.-J. and Dart, A. M. (1999). Role of sympathoadrenergic mechanisms in arrhythmogenesis. *Cardiovascular Research*, 43:832–834.
- [50] Ebrahimzadeh, E., Pooyan, M., and Bijar, A. (2014). A novel approach to predict sudden cardiac death (SCD) using nonlinear and time-frequency analyses from HRV signals. *PloS one*, 9(2):e81896.
- [51] Efron, B. and Tibshirani, R. J. (1994). *An introduction to the bootstrap*. CRC press.
- [52] Ferrario, M., Signorini, M. G., Magenes, G., and Cerutti, S. (2006). Comparison of entropy-based regularity estimators: application to the fetal heart rate signal for the identification of fetal distress. *IEEE transactions on bio-medical engineering*, 53(1):119–25.
- [53] Fleisher, L. A., Pincus, S. M., and Rosenbaum, S. H. (1993). Approximate entropy of heart rate as a correlate of postoperative ventricular dysfunction. *Anesthesiology*, 78(4):683–92.
- [54] Fukusaki, C., Kawakubo, K., and Yamamoto, Y. (2000). Assessment of the primary effect of aging on heart rate variability in humans. *Clinical autonomic research : official journal of the Clinical Autonomic Research Society*, 10(3):123–30.
- [55] Ghabach, M. B., El-Khatib, M. F., Zreik, T. G., Matta, M. S., Mouawad, J. J., Karam, C. J., and Ayoub, C. M. (2011). Effect of weight gain during pregnancy on heart rate variability and hypotension during caesarean section under spinal anaesthesia. *Anaesthesia*, 66(12):1106–11.
- [56] Gil, E., Bailón, R., Vergara, J. M., and Laguna, P. (2010a). PTT variability for discrimination of sleep apnea related decreases in the amplitude fluctuations of PPG signal in children. *IEEE transactions on bio-medical engineering*, 57(5):1079–88.

- [57] Gil, E., Orini, M., Bailón, R., Vergara, J. M., and Laguna, P. (2010b). Comparative analysis between PPG variability and HRV during non-stationary tilt table test. In *European Study Group on Cardiovascular Oscillations (ESCGO)*, 6th Conference of the European Study Group on Cardiovascular Oscillations, pages 1–4.
- [58] Gil, E., Orini, M., Bailón, R., Vergara, J. M., Mainardi, L., and Laguna, P. (2010c). Photoplethysmography pulse rate variability as a surrogate measurement of heart rate variability during non-stationary conditions. *Physiological Measurement*, 31(9):1271–1290.
- [59] Goldberger, A. L., Amaral, L. A. N., Glass, L., Hausdorff, J. M., Ivanov, P., Mark, R. G., Mietus, J. E., Moody, G. B., Peng, C.-K., and Stanley, H. E. (2000). PhysioBank, PhysioToolkit, and PhysioNet: Components of a New Research Resource for Complex Physiologic Signals. *Circulation*, 101(23):e215–e220.
- [60] Grassberger, P. and Procaccia, I. (1983). Characterization of Strange Attractors. *Physical Review Letters*, 50(5):346–349.
- [61] Gribbin, B., Steptoe, A., and Sleight, P. (1976). Pulse Wave Velocity as a Measure of Blood Pressure Change. *Psychophysiology*, 13(1):86–90.
- [62] Guzzetti, S., Cogliati, C., Turiel, M., Crema, C., Lombardi, F., and Malliani, A. (1995). Sympathetic predominance followed by functional denervation in the progression of chronic heart failure. *European heart journal*, 16(8):1100–7.
- [63] Guzzetti, S., Magatelli, R., Borroni, E., and Mezzetti, S. (2001). Heart rate variability in chronic heart failure. *Autonomic Neuroscience*, 90(1-2):102–105.
- [64] Hagerman, I., Berglund, M., Lorin, M., Nowak, J., and Sylvén, C. (1996). Chaos-related deterministic regulation of heart rate variability in time- and frequency domains: effects of autonomic blockade and exercise. *Cardiovascular research*, 31(3):410–418.
- [65] Hainsworth, R. (2004). Physiological background of heart rate variability. In Malik, M. and Camm, A. J., editors, *Dynamic Electrocardiography*, pages 3–12. New York, futura pub edition.
- [66] Hanss, R., Bein, B., Ledowski, T., Lehmkuhl, M., Ohnesorge, H., Scherkl, W., Steinfath, M., Scholz, J., and Tonner, P. H. (2005). Heart rate variability predicts severe hypotension after spinal anesthesia for elective cesarean delivery. *Anesthesiology*, 102(6):1086–93.
- [67] Havstad, J. and Ehlers, C. (1989). Attractor dimension of nonstationary dynamical systems from small data sets. *Physical Review A*, 39(2):845–853.
- [68] Hawkins, J. L., Chang, J., Palmer, S. K., Gibbs, C. P., and Callaghan, W. M. (2011). Anesthesia-related maternal mortality in the United States: 1979-2002. *Obstetrics and gynecology*, 117(1):69–74.
- [69] Heffernan, K. S., Fahs, C. A., Shinsako, K. K., Jae, S. Y., and Fernhall, B. (2007). Heart rate recovery and heart rate complexity following resistance exercise training and detraining in young men. *American journal of physiology. Heart and circulatory physiology*, 293(5):H3180–6.
- [70] Hernando, A., Lazaro, J., Gil, E., Arza, A., Garzon, J. M., Lopez-Anton, R., de la Camara, C., Laguna, P., Aguiló, J., and Bailón, R. (2016). Inclusion of Respiratory Frequency Information in Heart Rate Variability Analysis for Stress Assessment. *IEEE Journal of Biomedical and Health Informatics*, 20(4):1016–1025.
- [71] Hirsch, J. A. and Bishop, B. (1981). Respiratory sinus arrhythmia in humans: how breathing pattern modulates heart rate. *The American journal of physiology*, 241(4):H620–9.

- [72] Hjortskov, N., Rissén, D., Blangsted, A. K., Fallentin, N., Lundberg, U., and Søgaard, K. (2004). The effect of mental stress on heart rate variability and blood pressure during computer work. *European journal of applied physiology*, 92(1-2):84–9.
- [73] Ho, K. K., Moody, G. B., Peng, C. K., Mietus, J. E., Larson, M. G., Levy, D., and Goldberger, A. L. (1997). Predicting survival in heart failure case and control subjects by use of fully automated methods for deriving nonlinear and conventional indices of heart rate dynamics. *Circulation*, 96(3):842–8.
- [74] Houtveen, J. H., Groot, P. F., and Geus, E. J. (2005). Effects of variation in posture and respiration on RSA and pre-ejection period. *Psychophysiology*, 42(6):713–719.
- [75] Huikuri, H. V., Perkiomäki, J. S., Maestri, R., and Pinna, G. D. (2009). Clinical impact of evaluation of cardiovascular control by novel methods of heart rate dynamics. *Philosophical transactions. Series A, Mathematical, physical, and engineering sciences*, 367(1892):1223–38.
- [76] Ilies, C., Kiskalt, H., Siedenhans, D., Meybohm, P., Steinfath, M., Bein, B., and Hanss, R. (2012). Detection of hypotension during Caesarean section with continuous non-invasive arterial pressure device or intermittent oscillometric arterial pressure measurement. *British Journal of Anaesthesia*, 109(3):413–419.
- [77] Iyengar, N., Peng, C. K., Morin, R., Goldberger, a. L., and Lipsitz, L. a. (1996). Age-related alterations in the fractal scaling of cardiac interbeat interval dynamics. *The American journal of physiology*, 271(4 Pt 2):R1078–R1084.
- [78] J., T. (1986). Spurious dimension from correlation algorithms applied to limited time-series data. *Physical Review A*, 34(3):2427–2432.
- [79] Javorka, M., Zila, I., Balhárek, T., and Javorka, K. (2002). Heart rate recovery after exercise: relations to heart rate variability and complexity. *Braz. J. Med. Biol. Res.*, 35(8):991–1000.
- [80] Jd, S. and Pelzer, A. G. (1999). Effect of respiration rate on short-term heart rate variability. *Journal of Clinical and Basic Cardiology J Clin Basic Cardiol*, 2(2):92–95.
- [81] Jing, H. and Takigawa, M. (2000). Low sampling rate induces high correlation dimension on electroencephalograms from healthy subjects. *Psychiatry and Clinical Neurosciences*, 54(4):407–412.
- [82] Kagiyama, S., Tsukashima, A., Abe, I., Fujishima, S., Ohmori, S., Onaka, U., Ohya, Y., Fujii, K., Tsuchihashi, T., and Fujishima, M. (1999). Chaos and spectral analyses of heart rate variability during head-up tilting in essential hypertension. *Journal of the Autonomic Nervous System*, 76(2):153–158.
- [83] Kamen, P. W., Krum, H., and Tonkin, A. M. (1997). The correlation dimension of heart rate variability reflects cardiac autonomic activity. *Ann Noninvasive Electrocardiol*, 2(3):206–214.
- [84] Kantelhardt, J. W., Zschiegner, S. A., KoscielnyBunde, A., Havlin, S., Bunde, A., and Stanley, H. E. (2002). Multifractal detrended fluctuation analysis of nonstationary time series. *Physica A: Statistical Mechanics and its Applications*, 316(1-4):87–114.
- [85] Kanters, J. K., Højgaard, M. V., Agner, E., and Holstein-Rathlou, N. H. (1996). Short- and long-term variations in non-linear dynamics of heart rate variability. *Cardiovascular research*, 31(3):400–9.

- [86] Kanters, J. K., Højgaard, M. V., Agner, E., and Holstein-Rathlou, N. H. (1997). Influence of forced respiration on nonlinear dynamics in heart rate variability. *American Journal of Physiology*, 272(4 Pt 2):R1149–R1154.
- [87] Kanters, J. K., Holstein-Rathlou, N. H., and Agner, E. (1994). Lack of evidence for low-dimensional chaos in heart rate variability. *Journal of cardiovascular electrophysiology*, 5(7):591–601.
- [88] Kantz, H. and Schreiber, T. (2004). *Nonlinear time series analysis*. Cambridge University Press.
- [89] Kaplan, D., Furman, M., Pincus, S., Ryan, S., Lipsitz, L., and Goldberger, A. (1991). Aging and the complexity of cardiovascular dynamics. *Biophysical Journal*, 59(4):945–949.
- [90] Karason, K., Mølgaard, H., Wikstrand, J., and Sjöström, L. (1999). Heart rate variability in obesity and the effect of weight loss. *The American journal of cardiology*, 83(8):1242–7.
- [91] Kazmi, S. Z. H., Zhang, H., Aziz, W., Monfredi, O., Abbas, S. A., Shah, S. A., Kazmi, S. S. H., and Butt, W. H. (2016). Inverse Correlation between Heart Rate Variability and Heart Rate Demonstrated by Linear and Nonlinear Analysis. *PLOS ONE*, 11(6):e0157557.
- [92] Kennel, M. B., Brown, R., and Abarbanel, H. D. I. (1992). Determining embedding dimension for phase-space reconstruction using a geometrical construction. *Physical Review A*, 45(6):3403–3411.
- [93] Kienzle, M. G., Ferguson, D. W., Birkett, C. L., Myers, G. A., Berg, W. J., and Mariano, D. J. (1992). Clinical, hemodynamic and sympathetic neural correlates of heart rate variability in congestive heart failure. *The American journal of cardiology*, 69(8):761–7.
- [94] Kim, W. S., Yoon, Y. Z., Bae, J. H., and Soh, K. S. (2005). Nonlinear characteristics of heart rate time series: influence of three recumbent positions in patients with mild or severe coronary artery disease. *Physiol. Meas.*, 26(4):517–529.
- [95] Kinsella, S. and Norris, M. (1996). Advance prediction of hypotension at cesarean delivery under spinal anesthesia. *International Journal of Obstetric Anesthesia*, 5(1):3–7.
- [96] Klapholz, M. (2009). β -Blocker Use for the Stages of Heart Failure. *Mayo Clinic Proceedings*, 84(8):718–729.
- [97] Kunz, V. C., Borges, E. N., Coelho, R. C., Gubolino, L. A., Martins, L. E., and Silva, E. (2012). Linear and nonlinear analysis of heart rate variability in healthy subjects and after acute myocardial infarction in patients. *Braz J Med Biol Res*, 45(5):450–458.
- [98] Kuo, T. B. J., Lin, T., Yang, C. C. H., Li, C.-L., Chen, C.-F., and Chou, P. (1999). Effect of aging on gender differences in neural control of heart rate. *American Journal of Physiology - Heart and Circulatory Physiology*, 277(6).
- [99] Kyokong, O., Charuluxananan, S., Sriprajittichai, P., Poomseetong, T., and Nakorn, P. (2006). The incidence and risk factors of hypotension and bradycardia associated with spinal anesthesia. *Journal of the Medical Association of Thailand = Chotmaihet thangphaet*, 89 Suppl 3:S58–64.
- [100] Landry, D. P., Bennett, F. M., and Oriol, N. E. (1994). Analysis of heart rate dynamics as a measure of autonomic tone in obstetrical patients undergoing epidural or spinal anesthesia. *Regional anesthesia*, 19(3):189–95.
- [101] Laurent, S., Cockcroft, J., Van Bortel, L., Boutouyrie, P., Giannattasio, C., Hayoz, D., Pannier, B., Vlachopoulos, C., Wilkinson, I., Struijker-Boudier, H., and European Network for Non-invasive Investigation of Large Arteries (2006). Expert consensus document on arterial stiffness: methodological issues and clinical applications. *European heart journal*, 27(21):2588–605.

- [102] Lázaro, J., Alcaine, A., Romero, D., Gil, E., Laguna, P., Pueyo, E., and Bailón, R. (2014a). Electrocardiogram derived respiratory rate from QRS slopes and R-wave angle. *Annals of biomedical engineering*, 42(10):2072–83.
- [103] Lázaro, J., Gil, E., Vergara, M., and Laguna, P. (2014b). Pulse Rate Variability Analysis for Discrimination of Sleep-Apnea-Related Decreases in the Amplitude Fluctuations of Pulse Photoplethysmographic Signal in Children. *IEEE JOURNAL OF BIOMEDICAL AND HEALTH INFORMATICS*, 18(1).
- [104] Lee, J. A. and Verleysen, M., editors (2007). *Nonlinear Dimensionality Reduction*. Information Science and Statistics. Springer New York, New York, NY.
- [105] Lempel, A. and Ziv, J. (1976). On the Complexity of Finite Sequences. *IEEE Transactions on Information Theory*, 22(1):75–81.
- [106] Liu, C., Liu, C., Shao, P., Li, L., Sun, X., Wang, X., and Liu, F. (2011). Comparison of different threshold values r for approximate entropy: application to investigate the heart rate variability between heart failure and healthy control groups. *Physiological measurement*, 32(2):167–80.
- [107] Liu, G., Wang, L., Wang, Q., Zhou, G., Wang, Y., and Jiang, Q. (2014). A new approach to detect congestive heart failure using short-term heart rate variability measures. *PloS one*, 9(4):e93399.
- [108] López-Sendó, J., Swedberg, K., McMurray, J., Tamargo, J., Maggioni, A. P., Dargie, H., Tendera, M., Waagstein, F., Kjekshus, J., Lechat, P., Pedersen, C. T., Priori, S. G., Alonso García, M. A., Blanc, J.-J., Budaj, A., Cowie, M., Dean, V., Deckers, J., Fernandez Burgos, E., Lekakis, J., Lindahl, B., Mazzotta, G., McGregor, K., Morais, J., Oto, A., Smiseth, O. A., Alonso García, M. A., Ardiissino, D., Avendano, C., Lundqvist, C. B., Ment, D. C., Drexler, H., Ferrari, R., Fox, K. A., Julian, D., Kearney, P., Klein, W., Ber, L. K., Mancia, G., Nieminen, M., Ruzylo, W., Simoons, M., Thygesen, K., Tognoni, G., Tritto, I., and Wallentin, L. (2004). Expert consensus document on β -adrenergic receptor blockers: The Task Force on Beta-Blockers of the European Society of Cardiology. *European Heart Journal*, 25(15):1341–1362.
- [109] Lorenz, E. N. (1963). Deterministic Nonperiodic Flow. *Journal of the Atmospheric Sciences*, 20(2):130–141.
- [110] Lu, S., Chen, X., Kanters, J. K., Solomon, I. C., and Chon, K. H. (2008). Automatic Selection of the Threshold Value r for Approximate Entropy. *IEEE Trans. Biomed. Eng.*, 55(8):1966–1972.
- [111] Maayan-Metzger, A., Schushan-Eisen, I., Todris, L., Etchin, A., and Kuint, J. (2010). Maternal hypotension during elective cesarean section and short-term neonatal outcome. *American journal of obstetrics and gynecology*, 202(1):56.e1–5.
- [112] Maestri, R., Pinna, G. D., Accardo, A., Allegrini, P., Balocchi, R., D'Addio, G., Ferrario, M., Menicucci, D., Porta, A., Sassi, R., Signorini, M. G., La Rovere, M. T., and Cerutti, S. (2007). Nonlinear indices of heart rate variability in chronic heart failure patients: Redundancy and comparative clinical value. *Journal of Cardiovascular Electrophysiology*, 18(4):425–433.
- [113] Martin, S. L.-O., Carek, A. M., Kim, C.-S., Ashouri, H., Inan, O. T., Hahn, J.-O., and Mukkamala, R. (2016). Weighing Scale-Based Pulse Transit Time is a Superior Marker of Blood Pressure than Conventional Pulse Arrival Time. *Scientific Reports*, 6(1):39273.
- [114] Martínez, J. P., Almeida, R., Olmos, S., Rocha, A. P., and Laguna, P. (2004). A Wavelet-Based ECG Delineator Evaluation on Standard Databases. *IEEE Trans. Biomed. Eng.*, 51(4):570–581.

- [115] Mateo, J. and Laguna, P. (2000). Improved Heart Rate Variability Signal Analysis from the Beat Occurrence Times According to the IPFM Model. *IEEE Trans. Biomed. Eng.*, 47(8):985–996.
- [116] Mateo, J. and Laguna, P. (2003). Analysis of Heart Rate Variability in the Presence of Ectopic Beats Using the Heart Timing Signal. *IEEE Trans. Biomed. Eng.*, 50(3):334–343.
- [117] Mayer, C., Bachler, M., Holzinger, A., Stein, P., and Wassertheurer, S. (2016). The Effect of Threshold Values and Weighting Factors on the Association between Entropy Measures and Mortality after Myocardial Infarction in the Cardiac Arrhythmia Suppression Trial (CAST). *Entropy*, 18(4):129.
- [118] Mayer, C. C., Bachler, M., Hörtenhuber, M., Stocker, C., Holzinger, A., and Wassertheurer, S. (2014). Selection of entropy-measure parameters for knowledge discovery in heart rate variability data. *BMC Bioinformatics*, 15(Suppl 6):S2.
- [119] Melillo, P., Bracale, M., and Pecchia, L. (2011). Nonlinear Heart Rate Variability features for real-life stress detection. Case study: students under stress due to university examination. *Biomedical Engineering Online*, 10(96):1–13.
- [120] Merri, M., Farden, D., Mottley, J., and Titlebaum, E. (1990). Sampling frequency of the electrocardiogram for spectral analysis of the heart rate variability. *IEEE Trans. Biomed. Eng.*, 37(1):99–106.
- [121] Meste, O., Khaddoumi, B., Blain, G., and Bermon, S. (2005). Time-varying analysis methods and models for the respiratory and cardiac system coupling in graded exercise. *IEEE Trans. Biomed. Eng.*, 52(11):1921–1930.
- [122] Migliorini, M., Mendez, M. O., and Bianchi, A. M. (2011). Study of Heart Rate Variability in Bipolar Disorder: Linear and Non-Linear Parameters during Sleep. *Frontiers in neuroengineering*, 4:22.
- [123] Monfredi, O., Lyashkov, A. E., Johnsen, A., Inada, S., Schneider, H., Wang, R., Nirmalan, M., Wisloff, U., Maltsev, V. A., Lakatta, E. G., Zhang, H., and Boyett, M. R. (2014). Biophysical characterization of the underappreciated and important relationship between heart rate variability and heart rate. *Hypertension*, 64(6):1334–1343.
- [124] Moon, E., Lee, S.-H., Kim, D.-H., and Hwang, B. (2013). Comparative Study of Heart Rate Variability in Patients with Schizophrenia, Bipolar Disorder, Post-traumatic Stress Disorder, or Major Depressive Disorder. *Clinical psychopharmacology and neuroscience : the official scientific journal of the Korean College of Neuropsychopharmacology*, 11(3):137–43.
- [125] Moorman, J. R. (2000). Physiological time-series analysis using approximate entropy and sample entropy. *AM J Physiol-Heart C*, 278(6):2039–2049.
- [126] Muehlsteff, J., Aubert, X., and Schuett, M. (2006). Cuffless Estimation of Systolic Blood Pressure for Short Effort Bicycle Tests: The Prominent Role of the Pre-Ejection Period. In *2006 International Conference of the IEEE Engineering in Medicine and Biology Society*, pages 5088–5092. IEEE.
- [127] Mukkamala, R., Hahn, J.-O., Inan, O. T., Mestha, L. K., Kim, C.-S., Töreyin, H., and Kyal, S. (2015). Toward Ubiquitous Blood Pressure Monitoring via Pulse Transit Time: Theory and Practice. *IEEE Trans. Biomed. Eng.*, 62(8):1879–901.
- [128] Musialik-Łydka, A., Sredniawa, B., and Paszk, S. (2003). Heart rate variability in heart failure. *Kardiologia polska*, 58(1):10–6.

- [129] Naughton, M. T. and Bradley, T. D. (1998). Sleep apnea in congestive heart failure. *Clinics in Chest Medicine*, 19(1):99–113.
- [130] Navarro-Verdugo, A. L., Goycoolea, F. M., Romero-Meléndez, G., Higuera-Ciapara, I., and Argüelles-Monal, W. (2011). A modified Boltzmann sigmoidal model for the phase transition of smart gels. *Soft Matter*, 7(12):5847.
- [131] Ngan Kee, W. D. (2010). Prevention of maternal hypotension after regional anaesthesia for caesarean section. *Current opinion in anaesthesiology*, 23(3):304–9.
- [132] Okamoto, Y., Imai, R., Yoshida, H., Taeka, K., and Kuramoto, C. (2011). Relationships among frequency domain and non-linear parameters from heart rate variability. *Rinsho Byori*, 59(8):770–773.
- [133] Orbach-Zinger, S., Ginosar, Y., Elliston, J., Fadon, C., Abu-Lil, M., Raz, A., Goshen-Gottstein, Y., and Eidelman, L. A. (2012). Influence of preoperative anxiety on hypotension after spinal anaesthesia in women undergoing Caesarean delivery. *British journal of anaesthesia*, 109(6):943–9.
- [134] Orini, M., Bailón, R., Mainardi, L. T., and Laguna, P. (2012). Synthesis of HRV signals characterized by predetermined time-frequency structure by means of time-varying ARMA models. *Biomedical signal processing and control*, 7:141–150.
- [135] Osaka, M., Saitoh, H., Atarashi, H., and Hayakawa, H. (1993). Correlation dimension of heart rate variability: a new index of human autonomic function. *Frontiers of medical and biological engineering : the international journal of the Japan Society of Medical Electronics and Biological Engineering*, 5(4):289–300.
- [136] Pagani, M. (2000). Heart rate variability and autonomic diabetic neuropathy. *Diabetes, nutrition & metabolism*, 13(6):341–6.
- [137] Penttilä, J., Helminen, A., Jartti, T., Kuusela, T., Huikuri, H. V., Tulppo, M. P., and Scheinin, H. (2003). Effect of cardiac vagal outflow on complexity and fractal correlation properties of heart rate dynamics. *Autonomic and Autacoid Pharmacology*, 23(3):173–179.
- [138] Pepine, C. J., Hill, J. A., Imperi, G. A., and Norvell, N. (1988). Beta-adrenergic blockers in silent myocardial ischemia. *The American journal of cardiology*, 61(3):18B–21B.
- [139] Peter, L., Noury, N., and Cerny, M. (2014). A review of methods for non-invasive and continuous blood pressure monitoring: Pulse transit time method is promising? *IRBM*, 35(5):271–282.
- [140] Pincus, S. (1995). Approximate entropy (ApEn) as a complexity measure. *Chaos (Woodbury, N.Y.)*, 5(1):110–117.
- [141] Pincus, S. and Goldberger, A. (1994a). Physiological time-series analysis: What does regularity quantify? *The American Journal of Physiology*, 266(4 Pt 2):H1643–H1656.
- [142] Pincus, S. and Singer, B. H. (1996). Randomness and degrees of irregularity. *Proceedings of the National Academy of Sciences of the United States of America*, 93(5):2083–2088.
- [143] Pincus, S. M., Cummins, T. R., and Haddad, G. G. (1993). Heart rate control in normal and aborted-SIDS infants. *The American journal of physiology*, 264(3 Pt 2):R638–46.
- [144] Pincus, S. M., Gladstone, I. M., and Ehrenkranz, R. A. (1991). A regularity statistic for medical data analysis. *J Clin Monitor*, 7(4):335–345.

- [145] Pincus, S. M. and Goldberger, A. L. (1994b). Physiological time-series analysis: what does regularity quantify? *The American journal of physiology*, 266(4 Pt 2):H1643–56.
- [146] Platisa, M. M. and Gal, V. (2006). Reflection of heart rate regulation on linear and nonlinear heart rate variability measures. *Physiol. Meas.*, 27(2):145–154.
- [147] Ponikowski, P., Chua, T. P., Amadi, A. A., Piepoli, M., Harrington, D., Volterrani, M., Colombo, R., Mazzuero, G., Giordano, A., and Coats, A. J. (1996). Detection and significance of a discrete very low frequency rhythm in RR interval variability in chronic congestive heart failure. *The American journal of cardiology*, 77(15):1320–6.
- [148] Porta, A., Gnechi-Ruscone, T., Tobaldini, E., Guzzetti, S., Furlan, R., and Montano, N. (2007a). Progressive decrease of heart period variability entropy-based complexity during graded head-up tilt. *J Appl Physiol*, 103:1143–1149.
- [149] Porta, A., Guzzetti, S., Furlan, R., Gnechi-Ruscone, T., Montano, N., and Malliani, A. (2007b). Complexity and nonlinearity in short-term heart period variability: comparison of methods based on local nonlinear prediction. *IEEE Trans. Biomed. Eng.*, 54(1):94–106.
- [150] Pradhapan, P., Tarvainen, M. P., Nieminen, T., Lehtinen, R., Nikus, K., LehtimÄki, T., Kähönen, M., and Viik, J. (2014). Effect of heart rate correction on pre- and post-exercise heart rate variability to predict risk of mortality – an experimental study on the FINCAVAS cohort. *Frontiers in Physiology*, 5:208.
- [151] Pueyo, E., Smetana, P., Caminal, P., de Luna, A. B., Malik, M., and Laguna, P. (2004). Characterization of QT interval adaptation to RR interval changes and its use as a risk-stratifier of arrhythmic mortality in amiodarone-treated survivors of acute myocardial infarction. *IEEE Trans. Biomed. Eng.*, 51(9):1511–1520.
- [152] Radhakrishna, R. K., Dutt, D. N., and Yeragani, V. K. (2000). Nonlinear measures of heart rate time series: influence of posture and controlled breathing. *Auton. Neurosci.*, 83(3):148–158.
- [153] Rajendra Acharya, U., Faust, O., Adib Kadri, N., Suri, J. S., and Yu, W. (2013). Automated identification of normal and diabetes heart rate signals using nonlinear measures. *Computers in biology and medicine*, 43(10):1523–9.
- [154] Reardon, M. and Malik, M. (1996). Changes in heart rate variability with age. *Pacing and clinical electrophysiology : PACE*, 19(11 Pt 2):1863–6.
- [155] Restrepo, J. F., Schlotthauer, G., and Torres, M. E. (2014). Maximum approximate entropy and r threshold: A new approach for regularity changes detection. *Physica A: Statistical Mechanics and its Applications*, 409:97–109.
- [156] Rigaut, J. P. (1994). An empirical formulation relating boundary lengths to resolution in specimens showing "non-ideally fractal" dimensions. *Journal of Microscopy*, 133(1):41–54.
- [157] Roberts, S. W., Leveno, K. J., Sidawi, J. E., Lucas, M. J., and Kelly, M. A. (1995). Fetal acidemia associated with regional anesthesia for elective cesarean delivery. *Obstetrics and gynecology*, 85(1):79–83.
- [158] Sabeti, M., Katebi, S., and Boostani, R. (2009). Entropy and complexity measures for EEG signal classification of schizophrenic and control participants. *Artificial Intelligence in Medicine*, 47(3):263–274.
- [159] Sacha, J. (2014). Interaction between heart rate and heart rate variability. *Annals of Noninvasive Electrocardiology*, 19(3):207–216.

- [160] Sakata, K., Yoshimura, N., Tanabe, K., Kito, K., Nagase, K., and Iida, H. (2016). Prediction of hypotension during spinal anesthesia for elective cesarean section by altered heart rate variability induced by postural change. *International Journal of Obstetric Anesthesia*.
- [161] Sassi, R., Cerutti, S., Lombardi, F., Malik, M., Huikuri, H. V., Peng, C. K., Schmidt, G., and Yamamoto, Y. (2015). Advances in heart rate variability signal analysis: Joint position statement by the e-Cardiology ESC Working Group and the European Heart Rhythm Association co-endorsed by the Asia Pacific Heart Rhythm Society. *Europace*, 17(9):1341–1353.
- [162] Saul, J. P., Berger, R. D., Albrecht, P., Stein, S. P., Chen, M. H., and Cohen, R. J. (1991). Transfer function analysis of the circulation: unique insights into cardiovascular regulation. *The American journal of physiology*, 261(4 Pt 2):H1231–H1245.
- [163] Schroeder, E. B., Liao, D., Chambless, L. E., Prineas, R. J., Evans, G. W., and Heiss, G. (2003). Hypertension, Blood Pressure, and Heart Rate Variability: The Atherosclerosis Risk in Communities (ARIC) Study. *Hypertension*, 42(6):1106–1111.
- [164] Schuckers, S. A. (1998). Use of approximate entropy measurements to classify ventricular tachycardia and fibrillation. *Journal of electrocardiology*, 31 Suppl:101–5.
- [165] Shaffer, F., McCraty, R., and Zerr, C. L. (2014). A healthy heart is not a metronome: an integrative review of the heart’s anatomy and heart rate variability. *Frontiers in Psychology*, 5:1040.
- [166] Sharwood-Smith, G., Bruce, J., and Drummond, G. (2006). Assessment of pulse transit time to indicate cardiovascular changes during obstetric spinal anaesthesia. *British journal of anaesthesia*, 96(1):100–5.
- [167] Signorini, M. G. (2004). Nonlinear analysis of heart rate variability signal: physiological knowledge and diagnostic indications. In *Proceedings of the Annual International Conference of the IEEE Engineering in Medicine and Biology Society, EMBS*, volume 7 of *Annual International Conference of the IEEE*, pages 5407–5410.
- [168] Signorini, M. G., Ferrario, M., Cerutti, S., and Magenes, G. (2011). Advances in monitoring cardiovascular signals. Contribution of nonlinear signal processing. In *Proceedings of the Annual International Conference of the IEEE Engineering in Medicine and Biology Society, EMBS*, Annual International Conference of the IEEE, pages 6568–6571.
- [169] Silke, B., Guy, S., and Riddell, J. G. (1997). Effects of beta-adrenoceptor agonists and antagonists on heart-rate variability in normal subjects assessed using summary statistics and nonlinear procedures. *Journal of cardiovascular pharmacology*, 30(6):817–23.
- [170] Silva, L. E. V., Lataro, R. M., Castania, J. A., da Silva, C. A. A., Valencia, J. F., Murta, L. O., Salgado, H. C., Fazan, R., and Porta, A. (2016). Multiscale entropy analysis of heart rate variability in heart failure, hypertensive, and sinoaortic-denervated rats: classical and refined approaches. *American Journal of Physiology - Regulatory, Integrative and Comparative Physiology*, 311(1):R150–R156.
- [171] Singh, A., Saini, B. S., and Singh, D. (2016). An adaptive technique for multiscale approximate entropy (MAEbin) threshold (r) selection: application to heart rate variability (HRV) and systolic blood pressure variability (SBPV) under postural stress. *Australasian Physical & Engineering Sciences in Medicine*, 39(2):557–569.
- [172] Sipinková, I., Hahn, G., Meyer, M., Tadlánek, M., and Hájek, J. (1997). Effect of respiration and posture on heart rate variability. *Physiol. Res.*, 46(3):173–179.

- [173] Skinner, J. E., Meyer, M., Nester, B. A., Geary, U., Taggart, P., Mangione, A., Ramalanjaona, G., Terregino, C., and Dalsey, W. C. (2009). Comparison of linear-stochastic and nonlinear-deterministic algorithms in the analysis of 15-minute clinical ECGs to predict risk of arrhythmic death. *Therapeutics and clinical risk management*, 5(3):671–82.
- [174] Smetana, P., Pueyo, E., Hnatkova, K., Batchvarov, V., Laguna, P., and Malik, M. (2004). Individual patterns of dynamic QT/RR relationship in survivors of acute myocardial infarction and their relationship to antiarrhythmic efficacy of amiodarone. *Journal of Cardiovascular Electrophysiology*, pages 1147–1154.
- [175] Sobh, J. F., Risk, M., Barbieri, R., and Saul, J. P. (1995). Database for ECG, arterial blood pressure, and respiration signal analysis: feature extraction, spectral estimation, and parameter quantification. In *Proc. of the Ann. Int. Conf. IEEE Engineering Medical Biology Society*, Annual International Conference of the IEEE, pages 955–956.
- [176] Srinivasan, V., Eswaran, C., and Sriraam, N. (2007). Approximate entropy-based epileptic EEG detection using artificial neural networks. *IEEE transactions on information technology in biomedicine : a publication of the IEEE Engineering in Medicine and Biology Society*, 11(3):288–95.
- [177] Storella, R. J., Wood, H. W., Mills, K. M., Kanters, J. K., Højgaard, M. V., and Holstein-Rathlou, N. H. (1998). Approximate entropy and point correlation dimension of heart rate variability in healthy subjects. *Integrative physiological and behavioral science : the official journal of the Pavlovian Society*, 33(4):315–20.
- [178] Takens, F. (1981). Detecting strange attractors in turbulence. In Rand, D. and Young, L.-S., editors, *Dynamical Systems and Turbulence, Warwick 1980*, volume 898, pages 366–381. Springer Berlin Heidelberg.
- [179] Task Force of the ESC-NASPE (1996). Heart Rate Variability: Standards of Measurement, Physiological Interpretation, and Clinical Use. *Circulation*, 93(1):1043–1065.
- [180] Theiler, J. (1990). Estimating fractal dimension. *Journal of the Optical Society of America A*, 7(6):1055–1073.
- [181] Truccolo, W., Eden, U. T., Fellows, M. R., Donoghue, J. P., and Brown, E. N. (2005). A point process framework for relating neural spiking activity to spiking history, neural ensemble, and extrinsic covariate effects. *Journal of neurophysiology*, 93(2):1074–89.
- [182] Tulppo, M. P., Mäkkitalo, T. H., Takala, T. E., Seppänen, T., and Huikuri, H. V. (1996). Quantitative beat-to-beat analysis of heart rate dynamics during exercise. *Am. J. Physiol.*, 271(1 Pt 2):H244–52.
- [183] Valencia, J. F., Porta, A., Vallverdú, M., Clarià, F., Baranowski, R., Orłowska-Baranowska, E., and Caminal, P. (2009). Refined multiscale entropy: application to 24-h Holter recordings of heart period variability in healthy and aortic stenosis subjects. *IEEE transactions on bio-medical engineering*, 56(9):2202–13.
- [184] Valenza, G., Citi, L., and Barbieri, R. (2013). Instantaneous nonlinear assessment of complex cardiovascular dynamics by laguerre-volterra point process models. In *Proceedings of the Annual International Conference of the IEEE Engineering in Medicine and Biology Society, EMBS*, volume 2013, pages 6131–6134. IEEE.
- [185] Valenza, G., Citi, L., Garcia, R. G., Taylor, J. N., Toschi, N., and Barbieri, R. (2017). Complexity Variability Assessment of Nonlinear Time-Varying Cardiovascular Control. *Scientific reports*, 7:42779.

- [186] van de Borne, P., Montano, N., Pagani, M., Oren, R., and Somers, V. K. (1997). Absence of Low-Frequency Variability of Sympathetic Nerve Activity in Severe Heart Failure. *Circulation*, 95(6).
- [187] Voss, A., Schulz, S., Schroeder, R., Baumert, M., and Caminal, P. (2009). Methods derived from nonlinear dynamics for analyzing heart rate variability. *Phil. Trans. R. Soc. A*, 367(1887):277–296.
- [188] Weippert, M., Behrens, K., Rieger, A., Stoll, R., and Kreuzfeld, S. (2013). Heart rate variability and blood pressure during dynamic and static exercise at similar heart rate levels. *Plos one*, 8(12):e83690.
- [189] Weltman, G., Sullivan, G., and Bredon, D. (1964). The continuous measurement of arterial pulse wave velocity. *Medical Electronics & Biological Engineering*, 2(2):145–154.
- [190] Widman, G., Lehnertz, K., Jansen, P., Meyer, W., Burr, W., and Elger, C. E. (1998). A fast general purpose algorithm for the computation of auto- and cross-correlation integrals from single channel data. *Physica D*, 121(1-2):65–74.
- [191] Wolf, A., Swift, J. B., Swinney, H. L., and Vastano, J. A. (1985). Determining Lyapunov Exponents from a Time-Series. *Physica D*, 16(3):285–317.
- [192] Wu, H.-T., Lee, C.-Y., Liu, C.-C., Liu, A.-B., Wu, H.-T., Lee, C.-Y., Liu, C.-C., and Liu, A.-B. (2013). Multiscale Cross-Approximate Entropy Analysis as a Measurement of Complexity between ECG R-R Interval and PPG Pulse Amplitude Series among the Normal and Diabetic Subjects. *Computational and Mathematical Methods in Medicine*, 2013:1–7.
- [193] Yamamoto, Y. and Hughson, R. L. (1994). On the fractal nature of heart rate variability in humans: effects of data length and beta-adrenergic blockade. *Am. J. Physiol.*, 266(1 Pt 2):R40–9.
- [194] Yaniv, Y., Ahmet, I., Liu, J., Lyashkov, A. E., Guiriba, T.-R., Okamoto, Y., Ziman, B. D., and Lakatta, E. G. (2014a). Synchronization of sinoatrial node pacemaker cell clocks and its autonomic modulation impart complexity to heart beating intervals. *Heart rhythm : the official journal of the Heart Rhythm Society*, 11(7):1210–9.
- [195] Yaniv, Y., Lyashkov, A. E., Sirenko, S., Okamoto, Y., Guiriba, T.-R., Ziman, B. D., Morrell, C. H., and Lakatta, E. G. (2014b). Stochasticity intrinsic to coupled-clock mechanisms underlies beat-to-beat variability of spontaneous action potential firing in sinoatrial node pacemaker cells. *Journal of molecular and cellular cardiology*, 77:1–10.
- [196] Yentes, J. M., Hunt, N., Schmid, K. K., Kaipust, J. P., McGrath, D., and Stergiou, N. (2013). The appropriate use of approximate entropy and sample entropy with short data sets. *Annals of Biomedical Engineering*, 41(2):349–365.
- [197] Yeragani, V. K., Nadella, R., Hinze, B., Yeragani, S., and Jampala, V. C. (2000). Nonlinear measures of heart period variability: decreased measures of symbolic dynamics in patients with panic disorder. *Depression and anxiety*, 12(2):67–77.
- [198] Yeragani, V. K., Srinivasan, K., Vempati, S., Pohl, R., and Balon, R. (1993). Fractal dimension of heart rate time series: an effective measure of autonomic function. *Journal of applied physiology (Bethesda, Md. : 1985)*, 75(6):2429–38.
- [199] Yokose, M., Mihara, T., Sugawara, Y., and Goto, T. (2015). The predictive ability of non-invasive haemodynamic parameters for hypotension during caesarean section: a prospective observational study. *Anaesthesia*, 70(5):555–62.

- [200] Young, H. and Benton, D. (2015). We should be using nonlinear indices when relating heart-rate dynamics to cognition and mood. *Scientific Reports*, 5(1):16619.
- [201] Yuan, Q., Zhou, W., Li, S., and Cai, D. (2011). Epileptic EEG classification based on extreme learning machine and nonlinear features. *Epilepsy Research*, 96(1):29–38.
- [202] Zaza, A. and Lombardi, F. (2001). Autonomic indexes based on the analysis of heart rate variability: a view from the sinus node. *Cardiovascular research*, 50(3):434–42.
- [203] Zhe Chen, Brown, E. N., and Barbieri, R. (2008). A study of probabilistic models for characterizing human heart beat dynamics in autonomic blockade control. In *Proc. of the Int. Conf. IEEE Acoustics, Speech and Signal Processing*, pages 481–484. IEEE.
- [204] Zhe Chen, Z., Brown, E. N., and Barbieri, R. (2010). Characterizing Nonlinear Heartbeat Dynamics Within a Point Process Framework. *IEEE Transactions on Biomedical Engineering*, 57(6):1335–1347.
- [205] Zurek, S., Guzik, P., Pawlak, S., Kosmider, M., and Piskorski, J. (2012). On the relation between correlation dimension, approximate entropy and sample entropy parameters, and a fast algorithm for their calculation. *Physica A*, 391(24):6601–6610.

